

**MASS SPECTROMETRY AT POINT-OF-CARE: SIMPLE YET
POWERFUL SOLUTIONS FOR BETTER HEALTH**

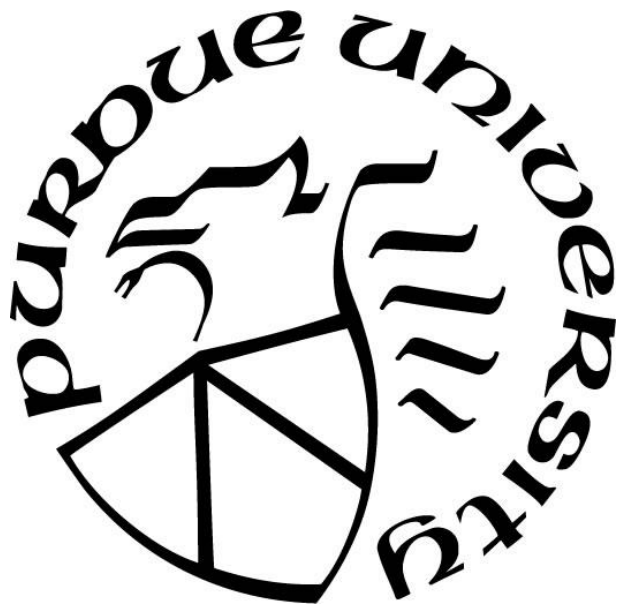
by
Fan Pu

A Dissertation

Submitted to the Faculty of Purdue University

In Partial Fulfillment of the Requirements for the degree of

Doctor of Philosophy



Department of Chemistry

West Lafayette, Indiana

December 2019

**THE PURDUE UNIVERSITY GRADUATE SCHOOL
STATEMENT OF COMMITTEE APPROVAL**

Dr. R. Graham Cooks, Co-Chair

Department of Chemistry

Dr. Zheng Ouyang, Co-Chair

Weldon School of Biomedical Engineering

Dr. Scott A. McLuckey

Department of Chemistry

Dr. Jianguo Mei

Department of Chemistry

Approved by:

Dr. Christine Hrycyna

To my dear parents and wife, who are always there for me

ACKNOWLEDGMENTS

It would not be possible for me to come this far in my graduate career if not for the help I get from numerous people. First and foremost, I would like to thank Prof. R. Graham Cooks and Prof. Zheng Ouyang, they provided me with the opportunities to perform cutting edge research and trained me to become an independent researcher. It is a great honor and luck to have them guide me through my Ph.D. study. I would also like to thank Prof. Scott A. McLuckey and Prof. Jianguo Mei to kindly serve as my committee members.

I want to give special thanks to Dr. Wenpeng Zhang and Dr. Xiao Wang, they taught me a lot on mass spectrometry and beyond. They are outstanding scientists and teachers. I would also like to express my thanks to Dr. Karen Yannell, Dr. Zhenwei Wei, Dr. Linfan Li, Dr. Yuan Su, Dr. Chengan Guo, Dr. Ran Zou and Dr. Yue Ren for the tremendous help and trainings I received from them.

I was lucky to work with several brilliant group members: Hannah Brown, Dr. Clint Alfaro, Dr. Valentina Pirro, Dr. Patrick Fedick, Nicolas Morato, Sangeeta Pandey, Zhuoer Xie, Dr. Zhenwei Wei, Spencer Chiang, Dr. Adam Hollerbach and Tsdale Mehari. It was a great pleasure to work with them. Other group members are also acknowledged for their help and meaningful discussions: Robert Schrader, Lucas Szalwinski, Dalton Snyder, Rong Chen, Yangjie Li, Pei Su, Pengqing Yu, Dr. Hong Zhang, Dr. Honggang Nie and Dr. Tianyang Guo. Several Tsinghua University students are acknowledged for their help when I visited China: Xinwei Liu, Manqing Kang, Zishuai Li, Wenbo Cao and Yuchen Wang.

Experts from PURSPEC Technologies have provided me with important technical support, especially Dr. Jiexun Bu and Dr. Binglin Qiu. I thank them for all the help and discussions.

My research projects involve lots of collaborations, the projects are simply not possible without them. I would like take this chance to thank my collaborators: Dr. Chao Han from Wenzhou Entry-Exit Inspection and Quarantine Bureau of P.R.C; Dr. Yong Liu, Dr. Kevin P. Bateman and Dr. Roy Helmy from Merck & Co; Dr. Scott A. Shapiro, Dr. Aaron A. Cohen-Gadol, Dr. Mahua Dey, Dr. James Miller and Dr. Mitesh Shah from Goodman Campbell Brain and Spine; Lane Bushman and Prof. Peter Anderson from University of Colorado Denver.

Finally, I want to thank my parents and my wife Yu Li, they are always there for me and they are the reasons why I will never give up.

Words alone cannot express how grateful I am to these people; I wish all of them well in their future endeavors.

TABLE OF CONTENTS

LIST OF TABLES	9
LIST OF FIGURES	10
LIST OF ABBREVIATIONS.....	14
ABSTRACT.....	16
CHAPTER 1. INTRODUCTION	17
1.1 Overview.....	17
1.2 Ambient ionization mass spectrometry.....	17
1.3 Miniaturization of mass spectrometer.....	21
CHAPTER 2. PRECLINICAL PHARMACOKINETICS STUDY WITH MINIATURE MASS SPECTROMETER	29
2.1 Introduction.....	29
2.2 Experimental	34
2.2.1 Equipment and chemicals	34
2.2.2 Animal Studies.....	34
2.3 Results and discussion	35
2.3.1 MS/MS methods on Mini 12	36
2.3.2 Quantitative analysis using SFME.....	38
2.3.3 PK analysis with Culex ABS.....	43
2.4 Conclusions and Future Perspectives.....	46
CHAPTER 3. RAPID DETERMINATION OF ISOCITRATE DEHYDROGENASE MUTATION STATUS OF HUMAN GLIOMAS BY EXTRACTION NANO-ELECTROSPRAY USING A MINIATURE MASS SPECTROMETER.....	47
3.1 Introduction.....	47
3.2 Experimental	51
3.2.1 Tissue Samples	51
3.2.2 Chemicals and Materials.....	51
3.2.3 Fabrication of Nanotips	51
3.2.4 Extraction nESI.....	51
3.2.5 MS Analysis.....	52

3.2.6 Calculation of IDH Mutation Score.....	52
3.2.7 Statistical Analysis and Software	52
3.2.8 Compliance with Ethical Standards.....	53
3.3 Results and Discussion	53
3.3.1 Extraction nESI for Brain Tissue.....	53
3.3.2 Analysis of Tissue Sections	57
3.3.3 Analysis of Bulk Tissues	59
3.4 Conclusions.....	65
CHAPTER 4. INTRAOPERATIVE DIAGNOSIS OF IDH MUTATION IN HUMAN GLIOMAS WITH MINI MS	71
4.1 Introduction.....	71
4.2 Experimental	73
4.2.1 Adaptation of Mini β for Deployment in Operating Room	73
4.2.2 Protocol for Intraoperative 2-HG Detection	75
4.2.3 Validation with Benchtop Instrument.....	76
4.2.4 Data Analysis.....	77
4.2.5 Compliance with Ethical Standards.....	77
4.3 Results and Discussion	77
4.4 Conclusions and future perspectives.....	81
CHAPTER 5. FAST QUANTITATION OF PYRAZOLE FUNGICIDES IN WINE BY PAPER CAPILLARY SPRAY MASS SPECTROMETRY	82
5.1 Introduction.....	82
5.2 Experimental	85
5.3 Results and Discussions.....	86
5.3.1 Setup of paper capillary spray	86
5.3.2 Matrix effect	88
5.3.3 Effect of the distance between capillary and MS inlet	89
5.3.4 Effect of heated capillary temperature and spray voltage	90
5.3.5 Determination of the MRM parameters.....	92
5.3.6 Quantitation with Paper Capillary Spray	94
5.3.7 Quantitation using paper spray as a comparison	97

5.3.8 Comparison with Other Methods.....	98
5.4 Conclusions and future perspectives.....	99
CHAPTER 6. DIRECT QUANTITATION OF TENOFOVIR DIPHOSPHATE IN HUMAN WHOLE BLOOD FOR ADHERENCE MONITORING.....	100
6.1 Introduction.....	100
6.2 Experimental.....	101
6.2.1 Materials and chemicals.....	101
6.2.2 Plasma separation with membranes.....	102
6.2.3 MS analysis.....	103
6.3 Results and discussions.....	104
6.3.1 Considerations for direct MS analysis of TDP.....	104
6.3.2 Direct analysis of TDP by plasma separation with membranes.....	106
6.3.3 Direct quantitation of simulated whole blood samples by plasma separation using VPM	110
6.3.4 Method validation with human subject samples.....	112
6.4 Conclusions and future perspectives.....	114
REFERENCES.....	116
VITA.....	125
PUBLICATIONS.....	126

LIST OF TABLES

Table 1.1 Comparison of recent generations of Mini MS developed at Purdue.....	26
Table 2.1. Results of quality control experiments. n = 3.	42
Table 2.2. PK parameters calculated for IMB in rats.	45
Table 3.1 Chemical structures and MS/MS transitions of GLU and 2-HG.	50
Table 3.2 IDH mutation scores of tissue sections.	66
Table 4.1 Pathology results, IDH mutation scores from intraoperative Mini MS experiments and post-operative TSQ experiments.	80
Table 5.1. MRM parameters.	93
Table 5.2. Analytical performance of paper capillary spray for the analysis of fungicides	95
Table 5.3. Quality control data, paper capillary spray, n=3.....	96
Table 5.4 Quality control data, paper spray, n=3*	98
Table 6.1 MRM transitions used for quantitation.	104
Table 6.2 Concentrations of patient samples	113

LIST OF FIGURES

Figure 1.1 Illustrations of (a) PSI (reprinted with permission ⁷ , copyright 2010 Wiley-VCH), (b) PCS (reprinted with permission ²⁶ , copyright 2016 Springer), (c) extraction nESI (reprinted with permission ²⁷ , copyright 2013 RSC) and (d) SFME (reprinted with permission ¹³ , copyright 2014 Wiley-VCH).....	20
Figure 1.2 Development of the concept of RIT (reprinted with permission, copyright 2004 ACS).	23
Figure 1.3 (a) DAPI fitted to a Mini MS; b) pressure curve inside a DAPI fitted vacuum manifold (reprinted with permission ³⁸ , copyright 2008 ACS).....	24
Figure 1.4 Mini MS developed at Purdue University. (a) Mini 10 (Reprinted with permission ³⁹ , copyright 2006 ACS); (b) Mini 11(Reprinted with permission ⁴⁰ , copyright 2008 ACS); (c) Mini 12 (Reprinted with permission ⁴¹ , copyright 2014 ACS) and (d) Mini S (Reprinted with permission ⁴² , copyright 2014 ACS).	25
Figure 2.1. (A) SFME (reprinted with permission ¹³ , copyright 2014 Wiley-VCH);(B) SFME for bulk sample analysis (reprinted with permission ⁶⁹ , copyright 2019 ACS); (C) three phase SFME (reprinted with permission ⁶⁸ , copyright 2018 Elsevier); (D) polymer coating transfer enrichment (reprinted with permission ⁷⁰ , copyright 2019 Wiley-VCH).	32
Figure 2.2. Chemical structures of the drug compounds used in the study.	33
Figure 2.3. Workflow of the PK study, Mini 12 and Culex ABS are coupled using offline SFME. Reprinted with permission.	35
Figure 2.4. MS/MS spectra of (a) STG, (b) STG-d4, (c) IMB and (d) IMB-d8 by nanoESI-Mini 12.	37
Figure 2.5. Principle of off-line SFME nanoESI with Mini 12.	39
Figure 2.6. Calibration curves of (a) STG and (b) IMB.	40
Figure 2.7. Whole blood concentration profile of STG	44

Figure 2.8. Whole blood concentration profile of IMB.	45
Figure 3.1. MS/MS product ion spectra recorded using Mini MS (a) GLU; (b) 2-HG.	54
Figure 3.2. Extraction nanoelectrospray of brain tissue.	55
Figure 3.3 MS/MS spectra recorded using Mini MS (a) IDH mutant glioma and (b) IDH wildtype glioma. Note that peak at m/z 129 only occurs in IDH mutant tissue.	56
Figure 3.4 IDH mutation scores of tissue sections. 29 IDH wildtype, 10 IDH mutant (1 low TCP, 3 medium TCP and 6 high TCP).	57
Figure 3.5 Correlation between concentration of 2-HG determined by triple quad MS analysis ¹⁰⁰ and IDH mutation scores determined using the Mini MS [this work] from an adjacent tissue section.	59
Figure 3.6 MS/MS spectra, IDH wildtype, low TCP.	60
Figure 3.7 MS/MS spectra, IDH wildtype, high TCP.	61
Figure 3.8 MS/MS spectra, IDH mutant, low TCP.	61
Figure 3.9 MS/MS spectra, IDH mutant, high TCP.	62
Figure 3.10 IDH mutation scores of tissue biopsies. 16 were IDH Wildtype, 28 were IDH mutant (12 low TCP, 5 medium TCP and 11 high TCP).	63
Figure 3.11 Comparison of IDH mutation scores of IDH wildtype (16 samples) and IDH mutant with high TCP (11 samples).	64
Figure 4.1 Setup of Mini MS in operating room.	73
Figure 4.2 Extraction nESI mount for Mini MS.	74
Figure 4.3 Full MS spectrum of calibration standard.	75
Figure 4.4 IDH mutation scores calculated from intraoperative Mini MS data.	78
Figure 4.5 IDH mutation scores calculated from post-operative TSQ data. Note that the y-axis is on log scale.	79
Figure 5.1 Chemical structures of five pyrazole fungicides.	83

Figure 5.2 Photo and dimensions of a paper capillary spray device.....	87
Figure 5.3 MS/MS spectra of (a) PEN and (b) BIX obtained using LTQ. m/z 256.3, m/z 300.3 in (a) and m/z 302.3 in (b) were from background.....	89
Figure 5.4 The effect of wine matrix on paper capillary spray. The matrices are (a) methanol, (b) wine 1, (c) wine 2 and (d) wine3. Insets are spectra of blank matrices.....	89
Figure 5.5 The effect of distance between capillary and the MS inlet. a) Product ion signals for PEN and BIX and b) their ratio as functions of the distance between the capillary tip and MS inlet.....	90
Figure 5.6 (a) Effect of heated capillary temperature on ion intensity. (b) Effect of high voltage on paper capillary spray and paper spray.	91
Figure 5.7 MS/MS spectra of (a) PEN, (b) ISO, (c) FLU, (d) PYRA and (e) BIX.	93
Figure 5.8 Calibration curves of (a) PEN, (b) ISO, (c) FLU and (d) PYRA with paper capillary spray mass spectrometry.....	94
Figure 5.9 Calibration curves of (a) PEN, (b) ISO, (c) FLU and (d) PYRA with paper spray mass spectrometry.	97
Figure 6.1 Chemical structures of TDP and stable isotope labeled ¹³ C-TDP.....	102
Figure 6.2 Direct analysis of TDP in whole blood by filtration of plasma with VPM.....	103
Figure 6.3 Full MS of TDP solution nanosprayed in negative mode.	105
Figure 6.4 Effect of added NaCl on TDP in nESI. Repeated twice under each condition.	106
Figure 6.5 Plasma separation with VPM.	108
Figure 6.6 Ion suppression from blood samples (intensities are on log scales).....	109
Figure 6.7 Comparison of total ion chromatograms.	110
Figure 6.8 Calibration curve with VPM for plasma separation, n=4. Red line: 350 fmol/punch; yellow line: 700 fmol/punch; green line: 1250 fmol/punch.	111
Figure 6.9 Stability test for storage conditions of VPM blood spots.....	112

Figure 6.10 Correlation of quantitative results from direct MS analysis using VPM with quantitative results from established LC-MS/MS method. 114

LIST OF ABBREVIATIONS

2-HG	2-hydroxyglutarate
AUC	Area under the curve
BIX	Bixafen
CAPI	Continuous atmospheric pressure interface
CBS	Coated blade spray
CID	Collision induced dissociation
CIT	Cylindrical ion trap
DAPI	Discontinuous atmospheric pressure interface
DART	Direct analysis in real time
DBDI	Dielectric barrier discharge ionization
DBS	Dried blood spot
DESI	Desorption electrospray ionization
EA	Ethyl acetate
ESI	Electrospray
FLU	Fluxapyroxad
FTC-TDF	Emtricitabine and tenofovir disoproxil fumarate
GC	Gas chromatography
GLU	Glutamic acid
IDH	Isocitrate dehydrogenase
IMB	Imatinib
iMRI	intraoperative magnetic resonance imaging
IS	Internal standard
ISO	Isopyrazam
LC	Liquid chromatography
LIT	Linear ion trap
LOD	Limit of detection
LOQ	Limit of quantitation
LTP	Low temperature plasma

MRL	Maximum residue level
MRM	Multiple reaction monitoring
MS	Mass spectrometry
NAA	N-acetyl aspartic acid
nanoDESI	nanospray desorption electrospray ionization
NCA	Non-compartmental analysis
nESI	nanoelectrospray
OR	Operating room
PCS	Paper capillary spray
PEN	Penflufen
PK	Pharmacokinetics
POC	Point-of-care
PrEP	Pre-exposure prophylaxis
PSI	Paper spray ionization
PYRA	Pyraclostrobin
QoIs	Quinone outside inhibitor
RBC	Red blood cell
REIMS	Rapid evaporative ionization MS
RIT	Rectilinear ion trap
RSD	Relative standard deviation
SDHI	Succinate dehydrogenase inhibitor
SFME	Slug-flow microextraction
SPE	Solid phase extraction
SPME	Solid phase microextraction
STG	Sitagliptin
TCP	Tumor cell percentage
TDM	Therapeutic drug monitoring
TDP	Tenofovir diphosphate
VPM	Vivid plasma membrane

ABSTRACT

The superior sensitivity and selectivity obtained with mass spectrometry (MS) is hardly matched by other analytical technologies, therefore it is an indispensable tool for modern society. Traditionally, MS is coupled with chromatography separation and performed in centralized analytical laboratories, which often requires extensive sample preparation and expensive instrumentation. With the advancements in the field of ambient MS and miniature MS, MS analysis at point-of-care (POC) has become a reality. Ambient MS includes a variety of methods for sampling and ionization, but they all share a common feature: they require little to no sample preparation. This has made rapid analysis of untreated sample possible and speed of MS analysis is significantly improved. Miniature MS, on the other hand, shrinks down the sizes of conventional benchtop instruments so they become portable or fieldable. In this dissertation, I documented the developments of ambient MS methods and applications of miniature MS for a variety of health-related topics, which include preclinical pharmacokinetics, intraoperative diagnosis, drug adherence monitoring and food safety.

CHAPTER 1. INTRODUCTION

1.1 Overview

Mass spectrometry (MS) is an indispensable tool for modern society. The performance of mass spectrometers has been constantly improving. Huge progresses have also been made in sample preparation and separation science. These advancements help tackled many analytical challenges that were not possible before. As MS instrumentation, methodology and data analysis become more and more complex, however, going to the opposite direction could also be beneficial: simple instrumentation, simple sampling/ionization and simple data analysis. MS technologies with these features could be applied to a broader range of applications and even deployed in field for use by non-analytical scientists with minimal training.

This dissertation describes efforts into developing simple yet powerful MS-based methodologies to solve practical problems that could help improve human health: pre-clinical pharmacokinetics study that could be performed in near real-time (Chapter 2), rapid diagnosis of isocitrate dehydrogenase (IDH) mutation in human gliomas and its intraoperative implementation (Chapter 3 and 4), analysis of fungicides residues in wines with ambient ionization MS (Chapter 5) and direct analysis of tenofovir diphosphate (TDP) in human whole blood for adherence monitoring (Chapter 6). These topics involve the use of ambient ionization MS and in many cases miniature mass spectrometers (Mini MS).

1.2 Ambient ionization mass spectrometry

By definition, ambient ionization refers to ionization methods that require no sample preparation or separation.¹ Desorption electrospray ionization (DESI)² and direct analysis in real time (DART)³ are the first two reported ambient ionization methods. Following these concepts, many

new ambient ionization methods were developed. Such as dielectric barrier discharge ionization (DBDI)⁴, low temperature plasma probe (LTP)⁵, paper spray ionization (PSI)^{6, 7} and nanospray desorption electrospray ionization (nanoDESI)⁸. Most of ambient ionization methods have been summarized in several review articles⁹⁻¹¹.

For biological samples, complex matrices are often present. Therefore, some sample preparation may be required to achieve desired performance for some analytes. This sample preparation, however, does not need to be extensive. Fast and simple sample preparation may be involved where ionization is carried out under ambient conditions.¹² Examples include slug-flow microextraction (SFME)¹³ and coated blade spray (CBS)¹⁴, where rapid sample preparation under ambient conditions could significantly improve quantitative performance for biofluid analysis.

Ambient MS techniques can be useful for both quantitative and non-quantitative applications. Quantitative studies seek to quantify analytes in complex matrix, such as blood, urine or saliva. Taking therapeutic drug monitoring (TDM) for example, by measuring concentrations of therapeutic drugs present in patients' blood, dosage can be adjusted to each patient's unique condition, achieving reduced toxicity and optimized efficacy. The measurement can be easily carried out with PSI, which can be used in conjunction with widely applied dried blood spots (DBS)¹⁵. Quantitation of drugs on DBS with DESI has also been demonstrated: faster screening speed was achieved although sensitivity was somewhat compromised¹⁶. Lower limits of detection (LODs) have been achieved with rapid sample extraction or preconcentration using SFME¹³, CBS¹⁴ or solid phase microextraction (SPME)^{17, 18}. Modification of paper matrix has also been shown to significantly improve sensitivity. A recent study achieved sub-ppt level detection limits with polystyrene microsphere coated PSI¹⁹.

Important information could also be obtained from applications of non-quantitative ambient ionization MS. MS imaging can provide detailed molecular information compared with conventional medical imaging techniques, spatial distribution of different analytes can be mapped. Performing MS imaging under ambient conditions is even more advantageous because untreated sample can be used²⁰. Ambient MS imaging could be applied to study molecular features of cancerous tissue samples and identify tumor margins²¹. For example, DESI-MS has been used to differentiate white matter, grey matter and glioma base on lipid and metabolite profiles²². For some applications, obtaining a MS image is too time-consuming and may not be necessary. Rapid profiling could provide sufficient information on tumor margins by DESI analysis of tissue smears, which made it possible to carry out the analysis intraoperatively and could potentially be used to guide tumor resection²³. Tissue identification has also been realized *in vivo* with rapid evaporative ionization MS (REIMS)²⁴ and MasSpec Pen²⁵. REIMS utilizes electrosurgical devices to generate aerosols that can be transferred to mass spectrometers for analysis; whereas MasSpec Pen is a home-made probe that delivers water droplets to tissue surface for analytes extraction in a non-destructive fashion.

Established methods that have been used in this dissertation research include PSI^{6, 7}, paper capillary spray (PCS)²⁶, extraction nanoelectrospray (extraction nESI)²⁷ and SFME¹³, these methods are all ESI-based and illustrated in Figure 1.1.

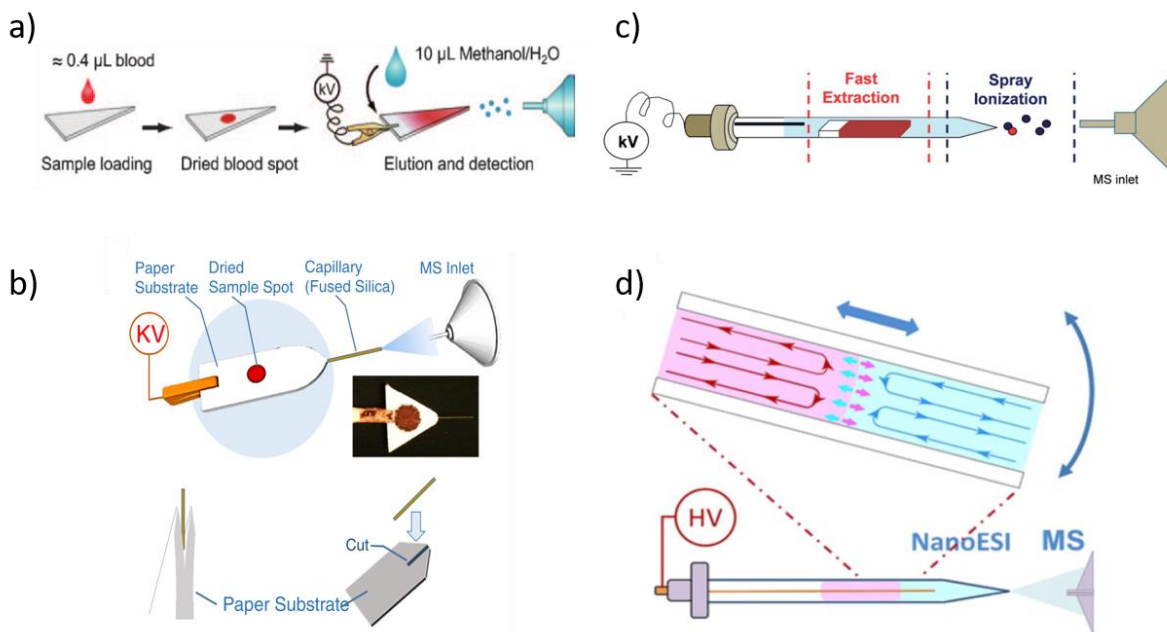


Figure 1.1 Illustrations of (a) PSI (reprinted with permission⁷, copyright 2010 Wiley-VCH), (b) PCS (reprinted with permission²⁶, copyright 2016 Springer), (c) extraction nESI (reprinted with permission²⁷, copyright 2013 RSC) and (d) SFME (reprinted with permission¹³, copyright 2014 Wiley-VCH).

The device for PSI is very simple: a filter paper (or some porous materials) cut into a small triangle with a sharp point for ESI. Sample and small amount of solvent (usually 10 μL) are applied on paper, then a high voltage (usually 3.5 kV) is applied to the back of the paper to generate ESI. PSI is probably the simplest form of ambient ionization, hence has been adopted for a wide range of applications in just a few years. A few pioneering examples include using PSI for tissue analysis²⁸, quantitation of therapeutic drugs in DBS²⁹, quantitation of contaminants in foodstuffs³⁰. PCS is developed base on PSI. To make the spray device, a short piece of fused silica capillary is inserted into a trimmed filter paper. The emitter is less susceptible to damage compared to paper tip in PSI. Both PSI and PCS have been commercialized: PSI was first commercialized by Prosolia Inc. as Velox 360 system, later by Thermo as VeriSpray; PCS was commercialized by Purspec Inc. as MS Mate and PCS cartridge.

As for extraction nESI, a thin paper strip is used to absorb several microliters of biofluid, then inserted into pulled nanotip to perform nESI. The extraction happens on-line during nESI, the low extraction solvent volume (usually 10 μ L) makes the extracted solution relatively concentrated, which improves sensitivity. As will be discussed in this dissertation, this method could also be used to sample from wet tissue.

SFME is a novel liquid-liquid extraction method. Microliters of aqueous biofluids and immiscible organic solvent are loaded into thin borosilicate glass capillary to form contacting plugs, back-and-forth motions are introduced to the plugs by a pipette gun or tilting the capillary. The turbulence formed at the interface will extract analytes from sample to extraction solvent. More analytes can be extracted to extraction solvent with more cycles of plug movements until equilibrium is achieved. Then the extraction solvent is transferred to a pulled nanotip for nESI. Online extraction could also be performed in pulled nanotip, although the plug movement may be more difficult to introduce.

1.3 Miniaturization of mass spectrometer

Development of simple sampling and ionization method is only part of the story, a complete solution to everyday analytical problems also requires availability of mass spectrometers. In typical procedures, samples need to be sent to analytical labs for sample preparation and MS analysis by benchtop instruments. By miniaturizing mass spectrometer, they become portable or fieldable, hence can be deployed to virtually anywhere instead of stationed only in analytical labs. Besides the obvious compact size, other benefits of miniaturized mass spectrometers include lower power consumption, lower cost and relatively simple instrumentation. Early developments of miniature mass spectrometer and some commercial systems have been reviewed^{31, 32}. Here the discussion is focused on recent generations of Mini MS, especially the ones developed at Purdue.

Miniaturization of virtually all types of mass analyzers have been reported^{31, 32}. Ion traps are of special interest due to its relatively high operating pressure, thus easier to achieve with small pumps; and they are capable of tandem MS, MS^n can be performed in a single ion trap³³. Cylindrical ion traps (CIT) are simple to construct comparing with hyperbolic ion traps, they have been miniaturized and built into miniature mass spectrometer systems^{34, 35}. Despite the simplicity achieved with CIT, space charge effects are quite significant and limit the trapping capacity of CIT. To overcome this limitation while still maintain a simple construction, rectilinear ion traps (RIT) were introduced³³. RIT borrows the idea of linear ion traps (LIT), trapping efficiency of LITs are much improved when compared with 3D ion traps^{36, 37}. Meanwhile, the geometry in RIT is simplified from LIT, making it easier to build. This relationship is clearly illustrated in Figure 1.2. RITs were adopted as the mass analyzers of the recent generations of miniature mass spectrometers developed at Purdue.

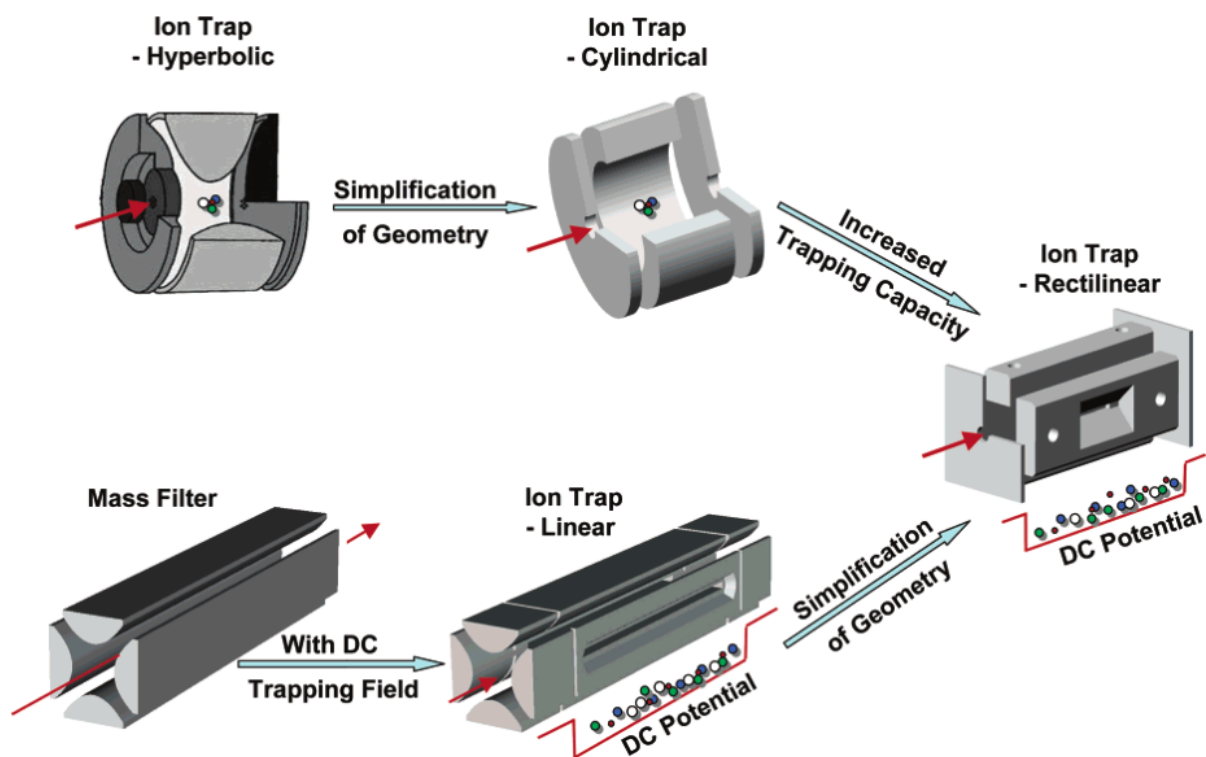


Figure 1.2 Development of the concept of RIT (reprinted with permission, copyright 2004 ACS).

One of the many challenges in miniaturization of mass spectrometers is to overcome the pumping barrier. In a conventional benchtop instrument, the rough pump itself can be as big as a Mini MS. Much smaller pumps are therefore utilized in Mini MS, which usually have limited pumping capacity. To overcome this barrier, discontinuous atmospheric pressure interface (DAPI) was introduced in 2008³⁸. The vacuum chamber of mass spectrometer is interfaced with atmosphere via a silicone tubing inserted into a normally closed pinch valve (Figure 1.3 (a)). Since DAPI is closed all the time except open briefly during ion injection, pressure as low as 10^{-5} Torr can be achieved with a combination of small diaphragm pump and small turbomolecular pump (10 L/s pumping speed). During ion introduction, the pinch valve briefly opens for several milliseconds to let ions and air in, pressure inside the vacuum chamber will also rise to about 10^{-1} Torr and gradually fall back to 10^{-5} Torr, thus generating a characteristic pressure curve (Figure

1.3 (b)). The air introduced during ion introduction can also serve as collision gas, therefore no external gas tank is needed. One need to be aware of the pressure curve when develop scan functions on mass spectrometers with DAPI, as ion isolation, collision induced dissociation (CID) and scan out could all be affected by the changing pressure, optimization is usually required.

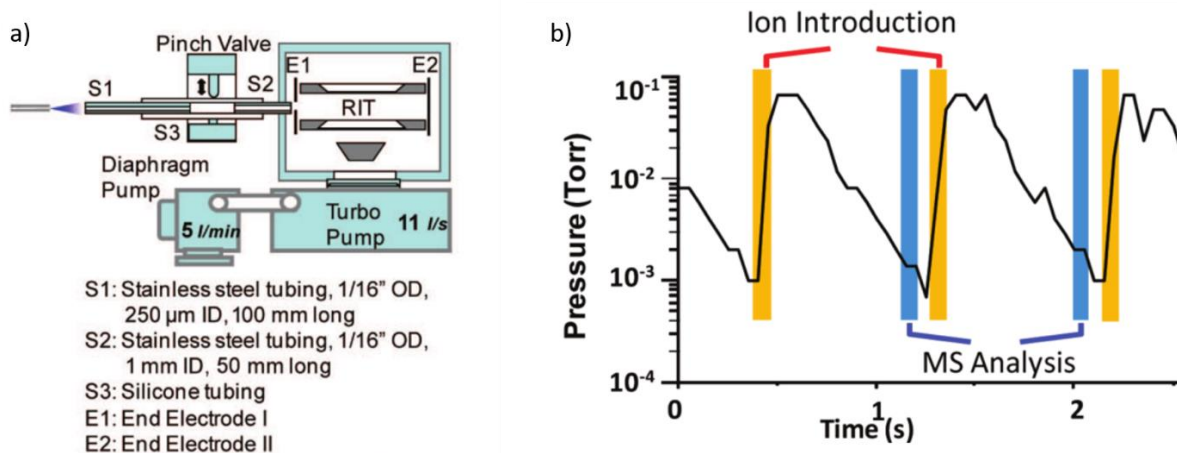


Figure 1.3 (a) DAPI fitted to a Mini MS; b) pressure curve inside a DAPI fitted vacuum manifold (reprinted with permission³⁸, copyright 2008 ACS).

The concept of recent generations of Mini MS from Purdue has been relatively consistent: simple yet robust construction, all-in-one standalone system, easy to use interface, light weight. Mini 10³⁹, Mini 11⁴⁰, Mini 12⁴¹ and Mini S⁴² all feature RIT as mass analyzer. These Mini MS are shown in Figure 1.4. Although initial report of Mini 10 utilized a membrane inlet system, DAPI was later implemented as sample inlet, as were all other Mini MS. Performances of Mini MS have been constantly improving, some key features are summarized in Table 1.1 along with Mini β , the commercialized version of this series of Mini MS.

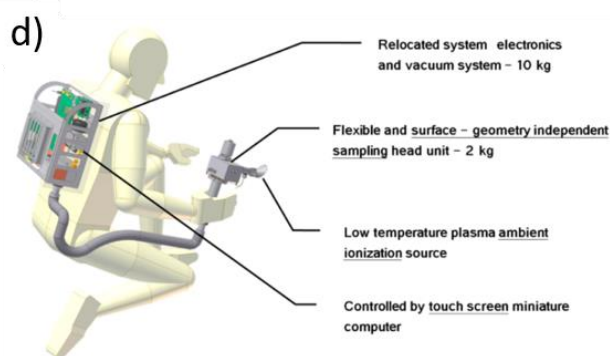
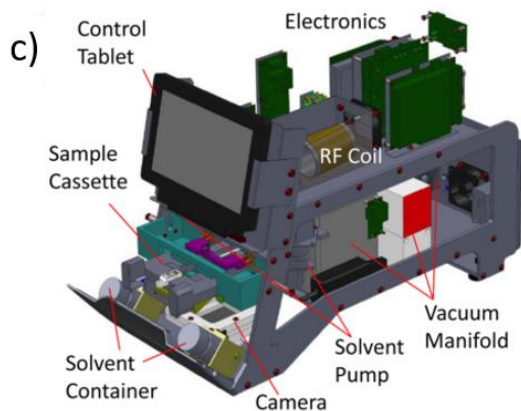


Figure 1.4 Mini MS developed at Purdue University. (a) Mini 10 (Reprinted with permission³⁹, copyright 2006 ACS); (b) Mini 11 (Reprinted with permission⁴⁰, copyright 2008 ACS); (c) Mini 12 (Reprinted with permission⁴¹, copyright 2014 ACS) and (d) Mini S (Reprinted with permission⁴², copyright 2014 ACS).

Table 1.1 Comparison of recent generations of Mini MS developed at Purdue.

	Mini 10	Mini 11	Mini 12	Mini S	Mini β
Size (LxWxH, cm)	32x22x19	22x12x18	50x56x42	30.5x29.5x12.5 (backpack portion)	55x24x31
Weight	10 kg with battery	4.95 kg with battery	25 kg	10 kg (backpack portion)	22 kg
Mass analyzer	RIT	RIT	RIT	RIT	Single LIT, Dual LIT
Sample inlet	Membrane sample inlet, DAPI	Membrane sample inlet, DAPI	DAPI	DAPI	DAPI
Ion source	Electron impact, Glow discharge	Glow discharge electron impact, external source such as DESI	External source such as paper spray	LTP	External source such as paper capillary spray
Mass range	m/z 60-520	Up to m/z 650, can be extended to m/z 1500	Up to m/z 850	Up to m/z 925	Up to m/z 2000
Mass resolution	Unit at m/z 91 and 92	180 ($m/\Delta m$, FWHM definition) at m/z 1422	0.6 FWHM at m/z 277	0.6 FWHM at m/z 226	0.4 FWHM at m/z 277
Detection limit	50 ppb, naphthalene in water	150 ppb, naphthalene	<10 ppb, verapamil in DBS	2 $\mu\text{g}/\text{cm}^2$ cocaine from human fingers	sub-ppb, verapamil in methanol
Power consumption	30-70 W	35 W	<100W	65W	70-100 W
Power source	Battery	Battery or plug in	Battery or plug in	Battery	Plug in
Polarity	Positive	Positive	Positive/Negative	Positive/Negative	Positive/Negative
Reference	Gao <i>et al.</i> ³⁹	Gao <i>et al.</i> ⁴⁰	Li <i>et al.</i> ⁴¹	Hendricks <i>et al.</i> ⁴²	Wang ⁴³

Mini 12 and Mini β have been used for this dissertation research. These are Mini MS systems designed for point-of-care (POC) applications, with Mini β commercialized by Purspec Technologies. The idea behind the systems has not been changed in its evolution into commercial instrument: simplified MS analysis that could be performed by everyone. Specialized sample cartridges are designed for specific applications (*e.g.* TDM), users are trained only at sample loading (including dispense sample/solvent to cartridge, insert cartridge to instrument) and perform this task, with a push of button the rest is carried out in a black box fashion where users will only see reports. What happens behind the scene is: after the user push “start”, the instrument will scan the barcode on cartridge and fetch the corresponding method from database, carry out MS or tandem MS scans and data analysis, then generate report.⁴¹ One significant difference between Mini 12 and Mini β is the later uses LIT instead of RIT. Although single LIT instrument was used for this dissertation, dual LIT version of the instrument has been constructed and shown to be capable of multiple reaction monitoring (MRM) and precursor ion scan⁴⁴. Precursor ion scan and neutral loss scan have been implemented on Mini 12 using unconventional AC frequency scan⁴⁵. The mass range of Mini 12 has been extended to above m/z 2000 using inverse Mathieu q scan⁴⁶. These new scan modes made available on Mini MS could significantly expand the applications of Mini MS.

Another way of approaching miniature ion trap mass spectrometer is through continuous atmospheric pressure interface (CAPI), which was realized by differential pumping⁴⁷. In this case the LIT operates in a much higher pressure (mTorr level), which limits ion transfer efficiency and achieving good sensitivity was challenging. In order to improve the performance of this Mini MS system, the same group reported the use of new ion ejection method⁴⁸ and integration of ion funnels

to first vacuum stage^{49, 50}. In their most recent work, the incorporation of a hybrid ion funnel has improved the LOD to 1 ng/mL (reserpine)⁴⁹.

A broad range of applications have been reported for miniature mass spectrometers. Examples include food safety control^{51, 52}, chemical reaction monitoring⁵³, tissue analysis⁵⁴, TDM⁴¹, discrimination of bacteria⁵⁵, quantitation of drugs of abuse⁵⁶, *etc.* These applications suggest that miniature mass spectrometers are truly versatile. With more commercialized systems becoming available on the market (*e.g.* MALDImini-1 from Shimadzu, 908MX from 908 Devices), more and more routine analysis could be carried out with Mini MS.

CHAPTER 2. PRECLINICAL PHARMACOKINETICS STUDY WITH MINIATURE MASS SPECTROMETER

A version of this chapter has been published by *Bioanalysis*. Reprinted with permission from Fan Pu, Wenpeng Zhang, Kevin P. Bateman, Yong Liu, Roy Helmy and Zheng Ouyang. Using miniature MS system with automatic blood sampler for preclinical pharmacokinetics study. *Bioanalysis*. 2017, 9, 1633.⁵⁷ Copyright 2017 Future Science.

2.1 Introduction

Preclinical pharmacokinetics (PK) study is an essential part of modern drug discovery. By performing preclinical PK studies, candidate compounds with improper PK properties are to be dropped and excluded from the later costly clinical studies⁵⁸. Many new approaches have been explored to improve the throughput of preclinical PK studies, including the recent use of dried blood spots (DBS)⁵⁹, which provides faster sample collection with low sample volumes and easier sample storage. New strategies, such as cassette dosing⁶⁰ and snapshot PK,⁶¹ were also suggested and have attracted many follow-up work. In cassette dosing, multiple compounds are given to one animal, whereas in conventional methods only one compound used. For cassette dosing full PK data are collected while for snapshot PK only partial PK data are collected for a quick decision. These strategies can help to save animal resources as well as shrink analysis time, at an expense of the comprehensiveness of the PK data.

The sample collection in animal labs can be automated. It has been demonstrated that automatic blood samplers can be used for collection of samples for PK study. With animals moving freely inside the cage while blood samples being taken, it is believed that the PK study results could be more reliable.^{62, 63} It has been demonstrated that the catheterization created initial stress to the rats but quickly recovered after surgery, during the blood draws such autosampler would not induce corticosterone release in blood.⁶⁴ The most common practice for blood sample analysis is

to use liquid chromatography mass spectrometry (LC-MS) or LC-MS/MS.⁶⁵ This analytical method can produce high-quality data; however, when used for screening large amount of drug candidates, high workload is demanded for sample preparation. In a modern analytical lab, the entire analysis process can be automated. Although the sample collection at the animal lab and the chemical analysis in the analytical be both be highly automated, the sample transfer between the labs, however, involves additional logistics that slows down the entire process of the animal studies.

The recent development of miniature mass spectrometry analytical systems has an important implication on the future means of conducting the PK studies, which could enable the performing of MS analysis in real time at the point of sample collection. In this study, a miniature MS system was used with a Culex auto-sampler (Culex ABS, BASi Inc., West Lafayette, IN, USA) for a demonstration in PK study. Two key components in the application of miniaturization of MS systems are 1) the use of ambient ionization to simplify the sample preparation process and 2) the development of the miniature mass spectrometers that can be readily used on site. The most important feature of ambient ionization is that it does not require sample preparation, thus direct analysis of raw samples such as whole blood, urine or tissues can be performed. Ambient ionization methods have quickly found their applications such as illicit drugs detection⁶⁶ and therapeutic drug monitoring.²⁹ Among many of these methods, the paper spray or paper capillary spray have been proven to be very effective in the quantitative analysis of drugs in biofluids including whole blood, serum and raw urine.^{6, 7, 26, 67} Coated blade spray combines the sample collection using solid-phase microextraction (SPME) and ambient ionization, with quantitative analysis of urine and plasma samples demonstrated.¹⁴

Slug-flow microextraction (SFME) was developed for direct analysis of biofluid samples in liquid forms (Figure 2.1).¹³ This is a single-step in-capillary microextraction method, two adjacent plugs were formed by sequentially injecting microliters of organic solvent and biofluids. Liquid-liquid extraction can be expected, and the extraction speed can be significantly increased with the slug flows induced by the movements of the two plugs. This is a simple but very efficient technique to extract analytes from whole blood. Furthermore, three-phase SFME was recently reported, where a new phase-solvent bridge is included in between biofluid plug and extraction solvent plug, this way it is possible to use water-miscible solvent for SFME to extraction polar compounds from aqueous biofluid.⁶⁸ Another recent advancement of SFME is the application of the technique for analysis of bulk samples. Thanks to the large sample to extraction solvent ratio, the sensitivity is much improved and high precision quantitation of biofluids was demonstrated.⁶⁹ Inspired by SFME, polymer coating transfer enrichment was developed. In this novel technique, an intermediate polymer phase was coated on the wall of the capillary, repeated movement of sample plug would enrich analytes on the polymer coating which were then washed off to the elution solvent.⁷⁰

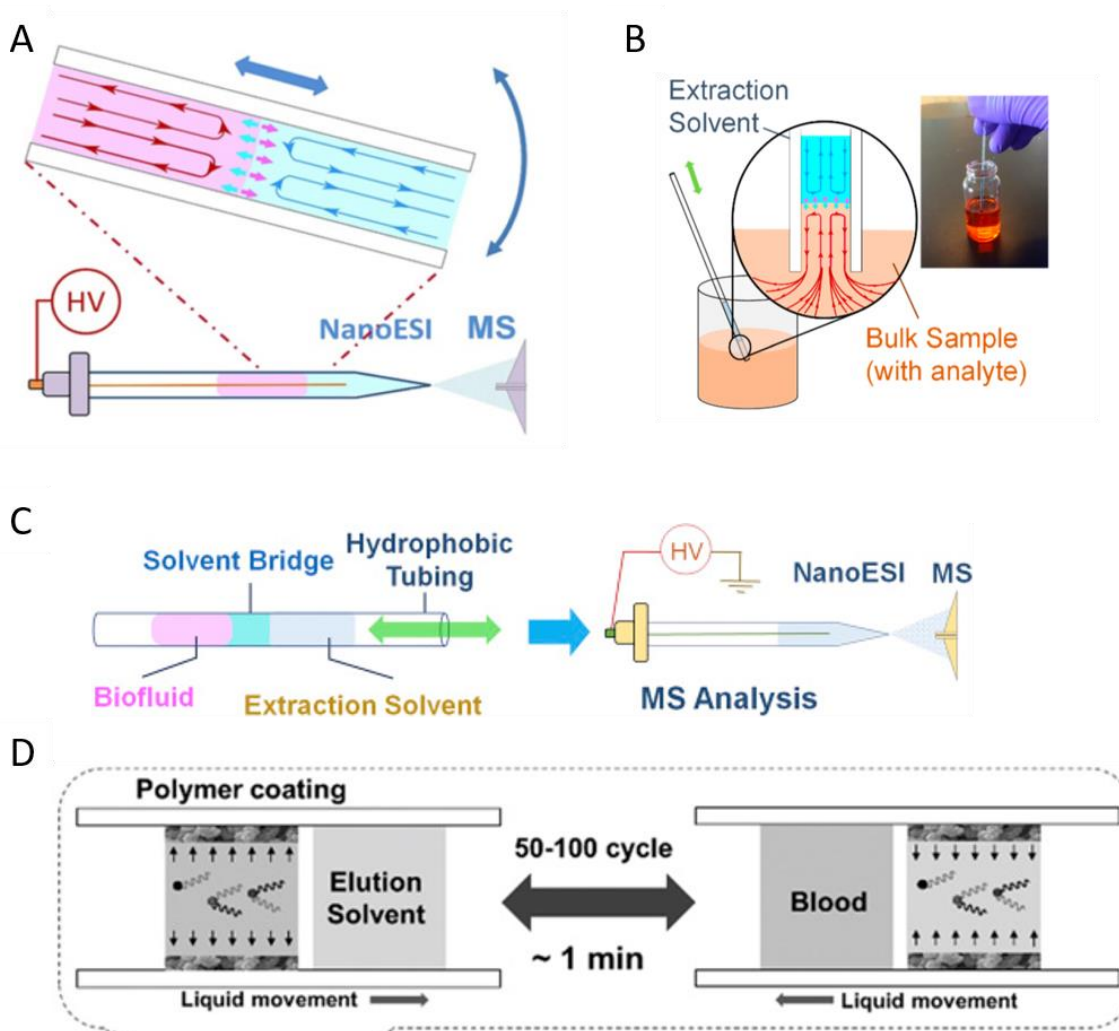


Figure 2.1. (A) SFME (reprinted with permission¹³, copyright 2014 Wiley-VCH);(B) SFME for bulk sample analysis (reprinted with permission⁶⁹, copyright 2019 ACS); (C) three phase SFME (reprinted with permission⁶⁸, copyright 2018 Elsevier); (D) polymer coating transfer enrichment (reprinted with permission⁷⁰, copyright 2019 Wiley-VCH).

In this study, the simplest two phase SFME was able to provide sufficient performance and was adopted for direct analysis of the blood samples taken by the Culex auto-sampler.

MS analysis was performed using the home built miniature mass spectrometer, Mini 12⁴¹, which could perform tandem MS analysis. Comparing with commercialized mass spectrometers with also small footprints that are mostly used as detectors for chromatography, the Mini 12 is a standalone MS system that designed for POC applications. Contrary to the conventional way of transferring the sample from an animal lab to an analytical lab, the entire PK study could now be performed onsite from sample collection (Culex autosampler) to sample preparation (SFME) and then MS analysis (Mini 12). In this study, we demonstrated this system by measuring the pharmacokinetics of two drugs in rat whole blood, sitagliptin (STG, Januvia, Merck Research Laboratories, Rahway, NJ, USA), an oral antihyperglycemic of the dipeptidyl peptidase-4 inhibitor class used for treating type II diabetes, and imatinib (IMB, Gleevec, Sigma-Aldrich, St. Louis, MI, USA), a protein-tyrosine kinase inhibitor used for treatment of leukemia. The Figure 2.2 shows the chemical structures of these two drug compounds.

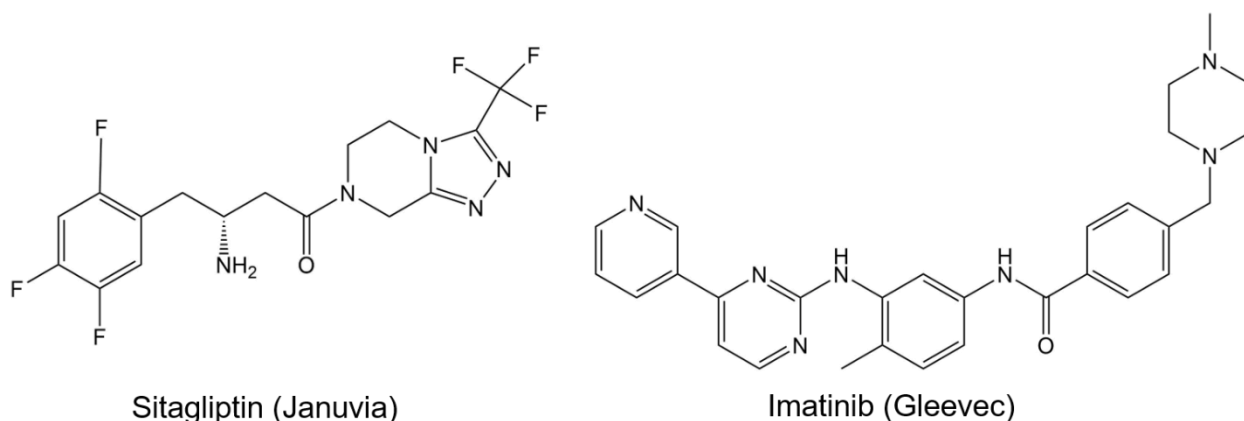


Figure 2.2. Chemical structures of the drug compounds used in the study.

2.2 Experimental

2.2.1 Equipment and chemicals

Sitagliptin phosphate and sitagliptin-d4 were provided by Merck Research Laboratories (Rahway, NJ, USA), imatinib-d8 was purchased from Alsachim (Strasbourg, France), imatinib mesylate and all other chemicals were purchased from Sigma-Aldrich (St. Louis, MI, USA).

Borosilicate glass capillaries with o.d. 1.5 mm and i.d. 0.86 mm were purchased from Sutter Instrument (Novato, CA, USA); some of them were used for SFME directly and some were made into pulled nanotips for nanoESI using a micropipette puller (model P-1000, Sutter Instrument).

A miniaturized mass spectrometer, Mini 12 was built in our lab⁴¹. Mini 12 was designed with a discontinuous atmospheric pressure interface (DAPI) suitable for ambient ionization sources and is suitable for point-of-care applications. Blood samples were taken by Culex ABS, manufactured by BASi Inc. (West Lafayette, IN, USA). Culex ABS is capable of sampling rodent blood automatically at programmed times.

2.2.2 Animal Studies

Sprague Dawley male rats were purchased from Envigo (Huntington, UK). A catheter was implanted into each rat's artery. The rats were fasted for about 15 h before oral gavage with STG or IMB. The dosing solutions were made by dissolving the drugs in de-ionized water with concentrations of 5 mg/mL for both STG and IMB. The dosage was 20 mg/kg for both STG and IMB. The STG was dosed to one rat and the IMB was dosed to four rats.

The Culex autosampler was programmed for sampling multiple times within a 24-hour period. The time points chosen were 0.5, 1, 2, 3, 6, 12, 24 h after dosing for STG, and 0.5, 1, 2, 3, 4, 6, 8, 16, 24 h after dosing for IMB. The 0-hour concentrations were set as 0 ng/mL and included in the results. At each time point, 100 μ L of whole blood was sampled from each rat and stored in vials

coated with heparin at 4 °C. PK parameters were calculated using Winnonlin Enterprise v5.3 (Pharsight Corp, Mountain View, CA, USA).

2.3 Results and discussion

The workflow used in the study is summarized in Figure 2.3. Culex ABS was used to collect whole blood samples each of 100 μL automatically from the rat. The internal standards (IS) solution was added into the blood samples post collection. For analysis, 10 μL of the sample, already mixed with IS, was transferred to a borosilicate glass capillary for SFME. After SFME, the extraction solvent was transferred to a nanoESI capillary with a pulled tip for quantitative analysis using Mini 12. The blood samples were analyzed shortly after they were collected, the sample preparation and MS analysis took about 5 minutes, so the requirements of sample transfer and storage was minimized.

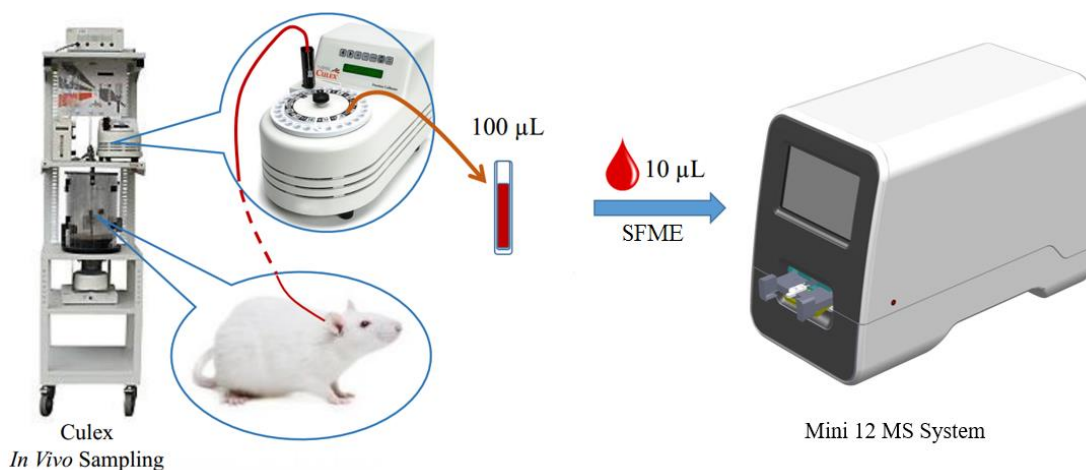


Figure 2.3. Workflow of the PK study, Mini 12 and Culex ABS are coupled using offline SFME. Reprinted with permission.

2.3.1 MS/MS methods on Mini 12

MS analysis was carried out in positive ion mode. Mini 12 mass spectrometer features a DAPI, which enables the coupling of ambient ionization sources with a miniature ion trap mass spectrometer of small pumping capacity³⁸. The mass analyzer of Mini 12 is a rectilinear ion trap (RIT)³³. MS/MS scan functions were developed and optimized using standard solutions. STG, STG-d4, IMB and IMB-d8 were diluted from high concentration stock solutions to 500 ng/mL using methanol as the solvent. These solutions were sprayed in nanotips directly to Mini 12 at a spray voltage of positive 1800 V. A DAPI open time of 15 ms and a scan out rate of 5000 Da/s was used for all analysis.

To perform MS/MS on Mini 12, a stored-waveform inverse Fourier transform (SWIFT) was used to isolate the precursor ions first, and then an AC voltage was applied to excite the ions for collision-induced dissociation (CID). The trapping RF frequency was 762 kHz and the AC frequencies for CID of STG (m/z 408), STG-d4 (m/z 412), IMB (m/z 494) and IMB-d8 (m/z 502) were 98.6 kHz, 97.3 kHz, 80.5 kHz and 78.6 kHz, respectively. The MS/MS spectra are shown in Figure 2.4. The major product ion peaks observed were at m/z 235, m/z 239, m/z 394 and m/z 394 for STG, STG-d4, IMB and IMB-d8, respectively. These MS/MS transitions were selected for subsequent quantitative analysis.

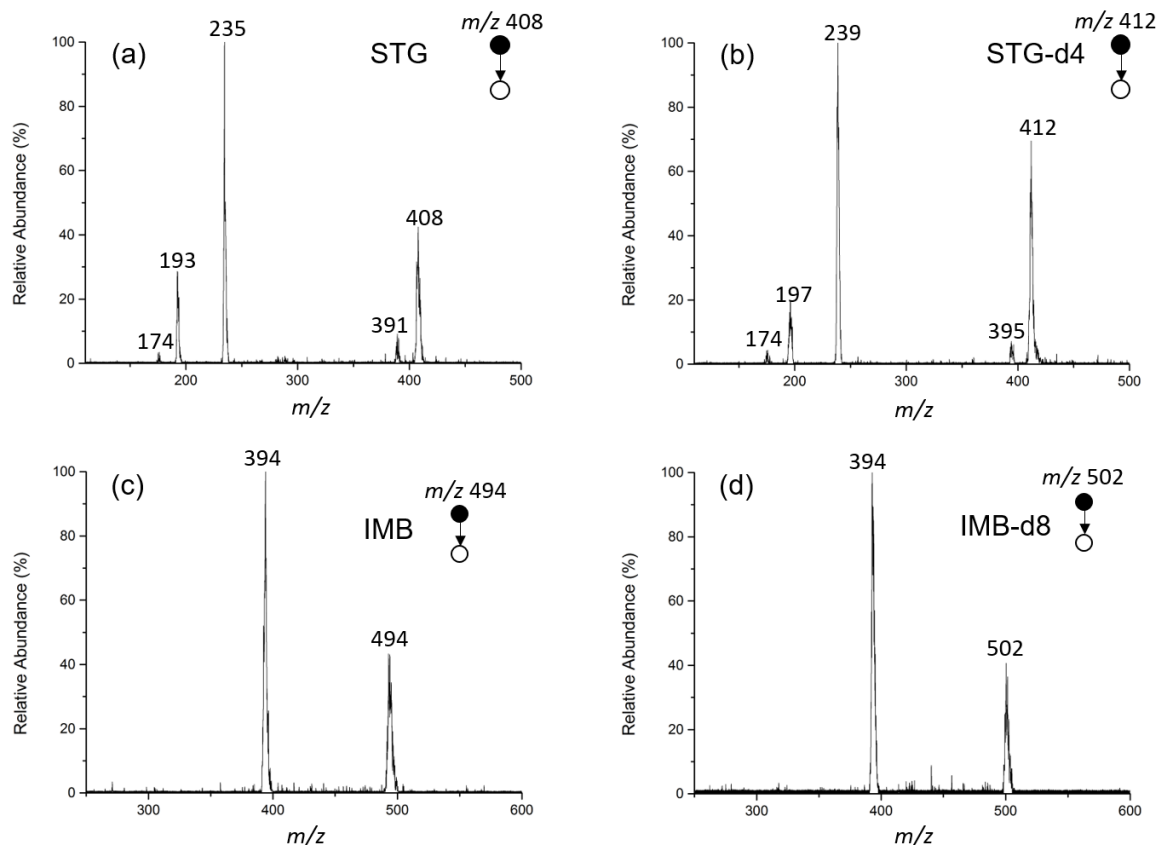


Figure 2.4. MS/MS spectra of (a) STG, (b) STG-d4, (c) IMB and (d) IMB-d8 by nanoESI-Mini 12.

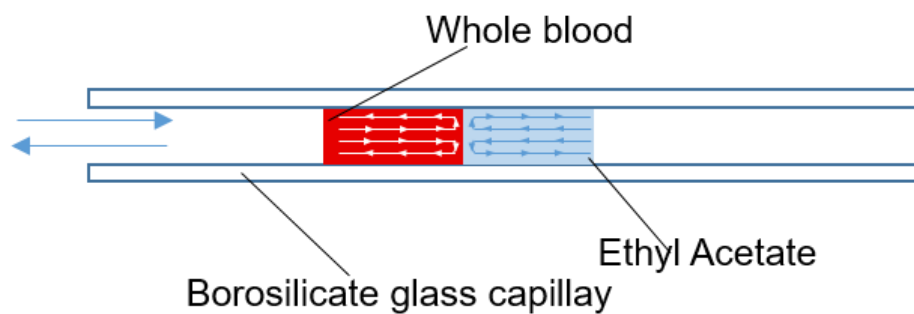
For quantitative analysis using IS, typically the product ion intensities of the analyte and IS were recorded with two adjacent MS/MS scans. In the case of STG using STG-d4 as the IS, however, their product ions are of different m/z values at 235 and 239, a single-scan method was adopted. A SWIFT with a notch window of 5 kHz centered at 165 kHz was used to isolate both STG m/z 408 and STG-d4 m/z 412; the RF amplitude was then lowered and the CID AC signal was then applied twice at two frequencies 98.6 kHz and 97.3 kHz to fragment STG and STG-d4; a spectrum was then recorded and the ratio of the intensities of the peak m/z 235 to m/z 239 (A/IS ratio, analyte to IS ratio) was hence obtained using a single scan.

For IMB and IMB-d8, the product ions were the same at m/z 394. Two scans were used to obtain the A/IS ratio. A SWIFT with a notch window of 5 kHz centered at 165 kHz was used to isolate the precursor ions; the RF amplitude was lowered and the AC signal voltage was then applied for CID, either at 80.5 kHz for IMB or 78.6 kHz for IMB-d8, to fragment them. The A/IS ratio was then calculated using the fragment ion intensities obtained from the two adjacent MS/MS scans.

2.3.2 Quantitative analysis using SFME

SFME was used in this study to extract drug molecules directly from rat whole blood samples. The working principle of off-line SFME is shown in Figure 2.5. 10 μ L of whole blood was first loaded to the borosilicate glass tube, and then 10 μ L extraction solvent was loaded to the tube, in contact with the blood sample plug. The selection of the extraction solvent is crucial¹³. The solvent needs to be immiscible with blood, has reasonable solubility for the target analytes, and could also be used for nanoESI. Ethyl acetate (EA) was used in the current work because it can meet these requirements, and both STG and IMB can be extracted from whole blood efficiently. A pipette gun was used to induce push-and-pull movements of the two plugs, which induced the turbulence inside the sample and solvent plugs, which facilitate the efficient extraction¹³. After SFME was performed, the extraction solvent was transferred to a nanotip for MS/MS analysis using Mini 12.

① SFME



② NanoESI

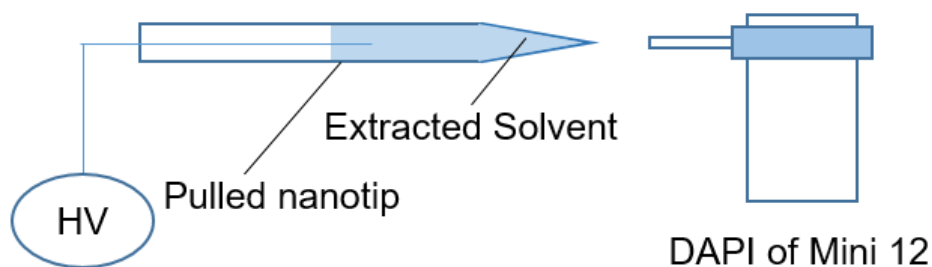


Figure 2.5. Principle of off-line SFME nanoESI with Mini 12.

In our previous research, it was found that the equilibrium of the extraction during can be reached during the SFME after a certain number of movement cycles, which can be as low as 5 cycles for extracting drug molecules from blood samples¹³. In this work, 10 cycles were used for SFME of each blood sample to ensure that the equilibrium balance was achieved. The lack of heating capacity of the DAPI inlet makes desolvation more difficult, so the spray tip cannot be placed too close to inlet; signal decrease dramatically as the spray tip is pulled away from inlet. Therefore, the distance between the nanotip and the DAPI inlet was optimized at 1 cm.

Matrix-matched calibrations were made for both STG and IMB. Calibration standards were made by diluting concentrated stock solutions with methanol to calculated concentrations, and then the diluted STG or IMB solution was added to rat whole blood together with their corresponding

diluted IS solution. The volume ratio of (drug solution): IS : (rat whole blood) was 1:1:98. For STG calibration standards, the final concentrations of STG were 50, 200, 500, 1000 and 2000 ng/mL, with the IS STG-d4 at a concentration of 200 ng/mL in all standards. For IMB calibration standards, the final concentrations of IMB were 50, 200, 500, 1000, 2000 and 5000 ng/mL, and the concentration of IMB-d8 was 500 ng/mL in all standard samples. Aliquot of 10 μ L prepared blood calibration samples was processed through SFME using 10 μ L EA. Three SFME-MS analyses were repeated for each concentration, and the average of 5 MS/MS scans was taken to calculate the A/IS ratio for each standard. The calibration curves are shown in Figure 2.6.

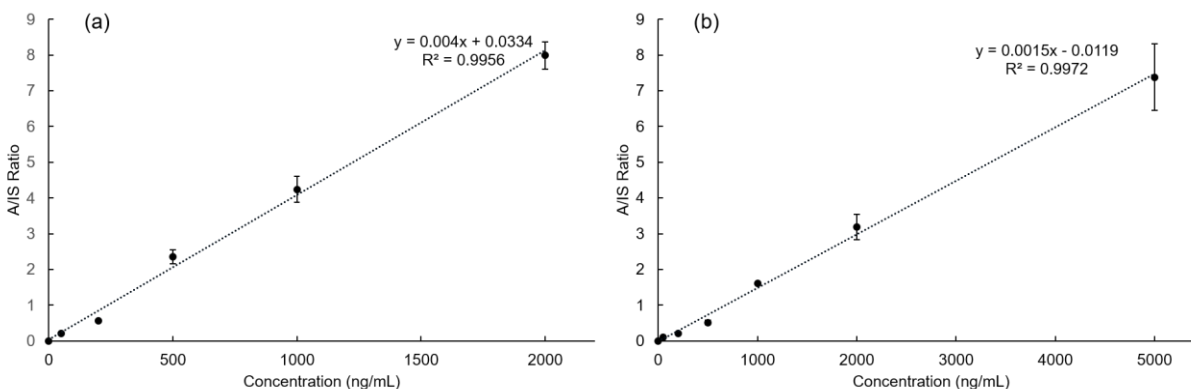


Figure 2.6. Calibration curves of (a) STG and (b) IMB.

Excellent linearity was observed for each of the calibration ranges selected, viz. 50-2000 ng/mL for STG and 50-5000 ng/mL for IMB. The limits of quantitation (LOQs) were determined to be 50 ng/mL for both STG and IMB. The linear range might be further expanded toward the higher concentration ranges, which however is considered unnecessary for the PK studies in this work.

In order to validate the method for its accuracy and precision, quality control samples were made separately and analyzed using the exact same method. These samples were made in the same

way the calibration standards were made, except that their concentrations were 50, 500, 2000 ng/mL for STG and 50, 1000, 5000 ng/mL for IMB, which represent the low, medium and high concentrations within the linear range. Both intraday and interday assays were performed, the intraday assays were carried out immediately after the calibration standards were measured, and the interday assays were performed 24 h after intraday assays using the same samples. The results are listed in Table 2.1. Satisfactory precision and accuracy were obtained, with RSD < 15% for all samples analyzed intraday or interday, and accuracy < 15 % except for LOQ, where accuracy < 20 % was obtained and considered acceptable.⁷¹ These test results indicate that the current method was reliable and could be used for PK studies.

Table 2.1. Results of quality control experiments. n = 3.

Compound	Target Concentration (ng/mL)	Concentration Found (Mean, ng/mL)	Precision (%RSD)	Accuracy (%)
STG	Intraday			
	50	41.8	13.6	83.6
	500	542.5	4.7	108.5
	2000	1978.0	6.5	98.9
	Interday			
	50	39.8	11.4	79.6
	500	497.9	9.9	99.6
	2000	1943.0	12.4	97.2
	IMB	Intraday		
50		58.6	12.2	117.3
1000		1147.9	1.3	114.8
5000		4959.3	10.1	99.2
Interday				
50		61.7	3.4	123.4
1000		1129.7	4.0	113.0
5000		4622.0	5.1	92.4

2.3.3 PK analysis with Culex ABS

As described above, whole blood samples were taken from the rats automatically using Culex autosampler at programmed time points. Each time 100 μL whole blood was taken and analyzed without performing typical in-lab sample processing or chromatographic separation. IS solution, 1 μL containing STG-d4 or IMB-d8, was spiked into the 100 μL blood samples to make a final concentration of 200 ng/mL or 500 ng/mL, respectively. Aliquots of 10 μL was then taken for analysis using SFME and Mini 12. The concentrations were calculated using the A/IS ratio obtained and the calibration curved established. As a pilot experiment, one rat was dosed with STG to establish the workflow. Figure 2.7 shows the calculated whole blood concentrations of STG plotted as a function of time after dosing. The concentration of STG in rat whole blood increased very rapidly after dosing, reaching maximum concentration of 1790 ng/mL in about 2h. After reaching maximum, the concentration began to drop rapidly, reaching an undetectable level at 24 h after dosing. Other PK parameters were calculated with non-compartmental analysis (NCA), including the area under the curve from time zero to infinity ($AUC_{0-\infty}$) as 3999 ng·mL⁻¹·h, half-life time ($t_{1/2}$) as 2.58 h, and clearance (CL/F) as 4894 mL·h⁻¹·kg⁻¹.

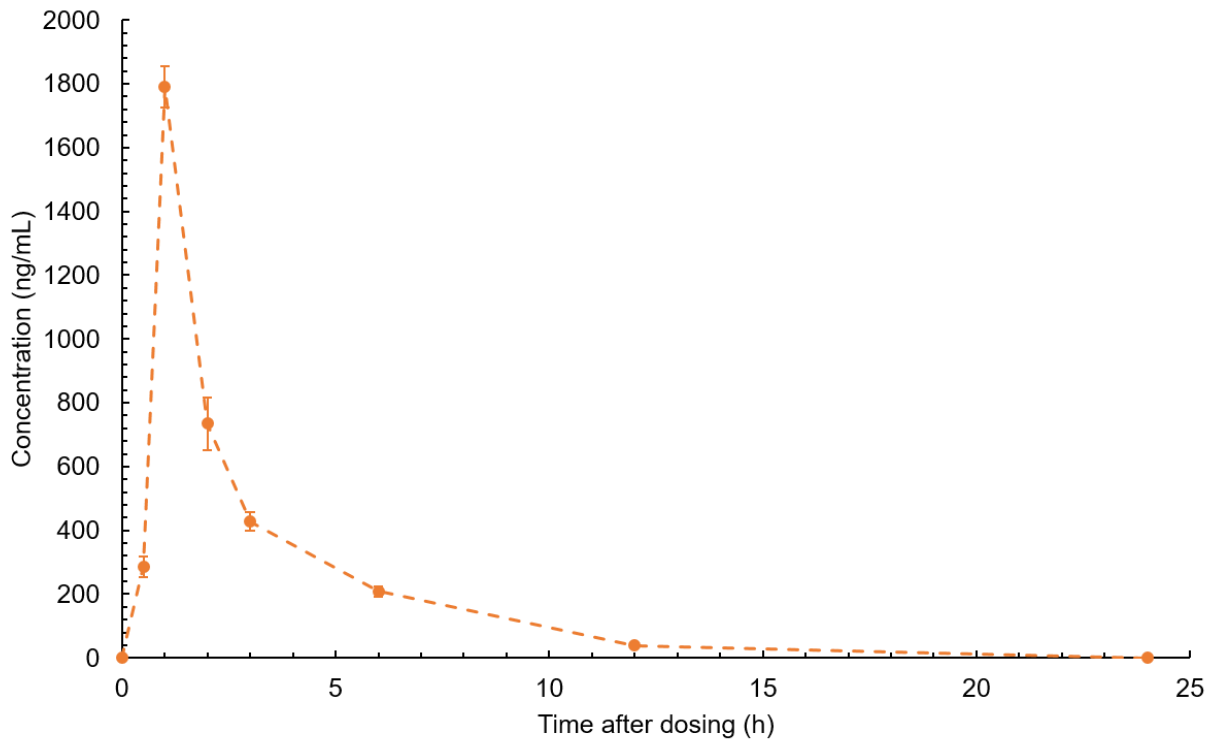


Figure 2.7. Whole blood concentration profile of STG

Figure 2.8 shows the PK data collected from four rats for IMB. Similar trends were observed for all the rats, with the concentration increasing rapidly immediately after dosing, reaching the maximum in 3-4 h and then dropping rapidly. At 24 h after dosing, there were still significant amounts of IMB presenting in the blood of all rats. Inter-individual differences among rats were observed. The PK parameters were calculated for each rat using NCA and summarized in Table 2.2.

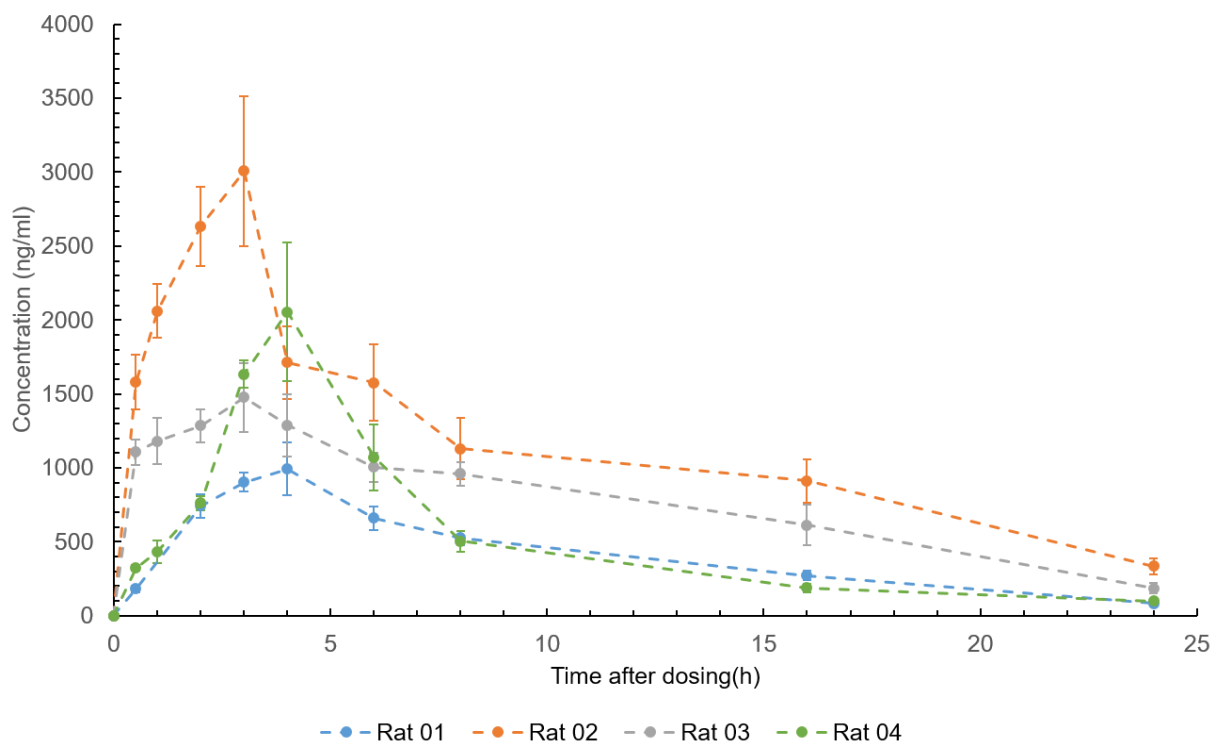


Figure 2.8. Whole blood concentration profile of IMB.

Table 2.2. PK parameters calculated for IMB in rats.

	Unit	Rat 01	Rat 02	Rat 03	Rat 04
AUC_{0-inf}	ng·mL ⁻¹ ·h	10418	31754	20129	12931
C_{max}	ng·mL ⁻¹	992.6	3006	1476	2055
T_{max}	h	4	3	3	4
t_{1/2}	h	6.01	3.24	7.37	5.26
CL/F	mL·h ⁻¹ ·kg ⁻¹	2066	728	1103	1650

2.4 Conclusions and Future Perspectives

In summary, we have demonstrated a method for preclinical PK study using a miniature ion trap mass spectrometer with an autosampler. We were able to extract target compounds from rat whole blood using SFME and perform quantitation to the liquid samples without using traditional in-lab sample preparation and chromatographic separation. With limited number of rats used in an animal study, we demonstrated the feasibility of the on-site analysis using miniature MS systems for preclinical PK studies.

An integration of the autosampler with the SFME device and the miniature mass spectrometer would be a logical next step to create an automated on-rack analytical system for preclinical study. This would certainly provide a unique and useful tool for the biologists to obtain the data readily, without the necessity of sending the samples to analytical labs. Besides PK information, more information can be extracted from the experiments when targeting different analytes, such as analysis of changes of metabolites post dosing.

CHAPTER 3. RAPID DETERMINATION OF ISOCITRATE DEHYDROGENASE MUTATION STATUS OF HUMAN GLIOMAS BY EXTRACTION NANO-ELECTROSPRAY USING A MINIATURE MASS SPECTROMETER

A version of this chapter has been published by *Analytical and Bioanalytical Chemistry*. Reprinted with permission from Fan Pu, Clint M. Alfaro, Valentina Pirro, Zhuoer Xie, Zheng Ouyang, R. Graham Cooks. Rapid determination of isocitrate dehydrogenase mutation status of human gliomas by extraction nanoelectrospray using a miniature mass spectrometer. *Analytical and Bioanalytical Chemistry*, 2019, 411, 1503.⁷² Copyright 2019 Springer.

3.1 Introduction

Gliomas represent about 27% of all primary brain and other central nervous system tumors, while accounting for about 81% of all malignant brain tumors.⁷³ Patients with high grade gliomas have poor outcomes. Glioblastoma, the most invasive form of glioma, has a five-year survival rate of just 5.5% and there are projected to be 12,760 cases in the US in 2018.⁷³ Mutations of isocitrate dehydrogenase (IDH) I and II have been found in a majority of World Health Organization (WHO) grade II and III gliomas.^{74, 75} Patients with IDH mutations have better outcomes than those with IDH wildtype.^{75, 76} Clinical studies have shown that aggressive treatment with radiotherapy and chemotherapy could benefit patients with IDH mutant gliomas.⁷⁷⁻⁷⁹ Maximal surgical resection of IDH1 mutant malignant astrocytomas was also reported to benefit patients.⁸⁰ A rapid diagnostic method for intraoperative determination of IDH mutation status is much needed and could potentially improve resection outcome.

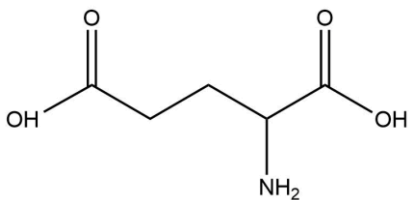
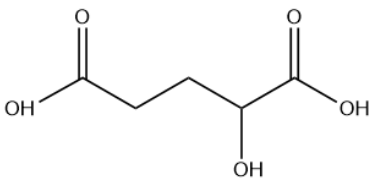
IDH 1 and IDH 2 enzymes catalyze the conversion of isocitrate to α -ketoglutarate. Mutant forms of the enzyme catalyze the further reduction of α -ketoglutarate to the oncometabolite 2-hydroxyglutarate (2-HG). The accumulation of 2-HG can reach up to 35 μmol per gram of tumor⁸¹,⁸² and the level of 2-HG in glioma can be indicative of IDH mutation status. Measurements of 2-

HG in glioma have been demonstrated using magnetic resonance spectroscopy.⁸³⁻⁸⁵ Magnetic resonance spectroscopy detection of 2-HG is non-invasive and can be performed *in vivo*. However, detection of 2-HG is challenging using conventional 1D magnetic resonance spectroscopy due to spectral overlap with glutamate (GLU) and glutamine, thus 1D-spectral editing or 2D correlation magnetic resonance spectroscopy is necessary to reduce number of false positives.⁸³

Mass spectrometry (MS) is a highly sensitive technique for qualitative or quantitative analysis of complex biological samples. MS is conventionally used in conjunction with liquid or gas chromatography although this requires tedious sample preparations and lengthy chromatographic separation. The direct MS analysis of complex samples without any sample preparation is first demonstrated with desorption electrospray ionization (DESI) MS² and direct analysis in real time (DART) MS⁸⁶. Since then, numerous new ambient ionization methods have been reported, and comprehensive reviews are available^{11, 87, 88}. DESI-MS has been applied to mapping of oncometabolites from tissue sections⁸⁹, discrimination of glioma, white matter and grey matter based on their lipid profiles²², intraoperative assessment of tumor margins during glioma resection²³ and detection of microscopic skin cancer⁹⁰. Tissue analysis has also been realized by other ambient ionization methods such as paper spray⁹¹, needle biopsy spray⁹², touch spray⁹³, swab touch spray⁹⁴, nano-DESI⁹⁵ and liquid microjunction surface sampling probe^{25, 96}. Ion trap based miniature mass spectrometer (Mini MS) systems^{31, 39-42} have been developed at Purdue and their use for therapeutic drug monitoring⁴¹, illicit drug detection⁴², and preclinical pharmacokinetics⁵⁷ have been demonstrated. These miniature MS instruments take the form of standalone systems without external pumps or gas tanks and fit easily into point-of-care settings such as an operating room. The oncometabolite 2-HG has previously been measured intraoperatively by tandem mass spectrometry using a commercial benchtop mass spectrometer.⁸⁹

⁹⁷ Here we report using of a Mini MS with extraction nanoelectrospray ionization (nESI) for 2-HG determination. The experiments were first done with banked tissue samples as a preliminary study to assess performance of a miniature MS in intraoperative identification of IDH mutation status in glioma tissue biopsies. In this application, GLU and 2-HG were simultaneously isolated and the intensities of their fragments compared to provide a *relative* measure of 2-HG in tissue. The structures of the analytes and the MS/MS transitions of interest are given in Table 3.1. Then the Mini β system was modified for deployment in OR at IU Methodist Hospital and intraoperative diagnosis of IDH mutation was performed (Chapter 4).

Table 3.1 Chemical structures and MS/MS transitions of GLU and 2-HG.

	GLU	2-HG
Chemical Structures		
<i>m/z</i> of precursor ions	146	147
(negative mode)		
<i>m/z</i> of product ions	102, 128	129
(negative mode)		

3.2 Experimental

3.2.1 Tissue Samples

Tissue sections (15 μm thickness) were prepared using a cryotome and thaw mounted on superfrost microscope slides (Thermo Fisher Scientific, Waltham, MA). IDH mutation status was determined using immunohistochemistry and genetic sequencing at Indiana University Health Molecular Pathology Laboratory. Adjacent tissue sections and smears were H&E stained using a previously published protocol²² and blindly evaluated by an expert neuropathologist to provide assessments of tumor cell percentage and diagnosis for each sample.

3.2.2 Chemicals and Materials

2-Hydroxyglutarate (2-HG), glutamic acid (GLU), methanol and Whatman 1 filter paper were purchased from Sigma-Aldrich (St. Louis, MO). Ultrapure water was obtained from a Milli-Q system (Bedford, MA). Disposable sterile acupuncture needles (0.3 mm x 40 mm) were purchased from Zhongyan Taihe (Beijing, China).

3.2.3 Fabrication of Nanotips

Borosilicate glass capillaries (o.d. 1.5mm, i.d. 0.86 mm, without filament) were purchased from Sutter Instrument (Novato, CA). Borosilicate glass capillaries were pulled into 5 μm tips using a micropipette puller (Model P-97, Sutter Instrument).

3.2.4 Extraction nESI

A narrow strip of paper (ca. 0.5 mm wide and 15 mm long) was cut from Whatman 1 filter paper. The paper strip was wiped over the tissue sample (thawed tissue section or intact tissue) to pick up small amounts of material. The sample strip was then inserted into a pulled nanotip (i.d. 0.86 mm, length about 4 cm) preloaded with 10 μL methanol/water (9:1, v/v), which act as both extraction and spray solvent. An acupuncture needle (diameter 0.3 mm, length 4 cm) was inserted into the

pulled nanotip to act as a disposable electrode to prevent cross-contamination. Negative 1.3 kV was applied to the needle to initiate nanoelectrospray. Analytes were constantly extracted during the ionization process within the nanotip.

3.2.5 MS Analysis

A linear ion trap Mini MS, Mini β mass spectrometer (PURSPEC Technologies, West Lafayette, IN), was operated in the negative ion mode. The scan function was optimized to isolate and then fragment ions of both m/z 146 and 147 simultaneously by ramping RF voltage while a fixed AC frequency was applied. Ion abundances for the transitions of interest, m/z 147- \rightarrow 129 for 2-HG and m/z 146- \rightarrow 128 for glutamate (GLU), were recorded. For each sample, 5 spectra were recorded and each spectrum was an average of three scans. Each scan takes 1.7 second, and spectra were saved manually making the total analysis time per sample ca. 1 minute. The scan rate of the Mini MS was 3200 Da/s, ejection AC frequency was 330 kHz.

3.2.6 Calculation of IDH Mutation Score

When calculating IDH mutation scores, the intensities of m/z 129 was corrected for isotopic contribution from GLU, the following formula was used to calculate the IDH mutation score:

$$IDH \text{ Mutation Score} = \frac{I_{129} - I_{128} \times 6.1\%}{I_{128}}$$

I_{129} and I_{128} are absolute intensities of m/z 129 and 128, respectively.

3.2.7 Statistical Analysis and Software

In the box and whisker plots, boxes show median, lower, and upper quartiles, and whiskers are at minimum and maximum values.

Linear regressions were applied to establish correlations of 2HG concentration in IDH mutants and their corresponding IDH mutation scores.

t-Test of two-sample assuming unequal variances was performed on IDH mutant scores between IDH mutants and IDH wildtypes, two tail p-values were reported.

Microsoft Excel was used to perform linear regressions and t-Test. OriginPro 2018b was used to plot all spectra and box and whisker plots. ChemDraw Professional 16.0 was used to draw chemical structures.

3.2.8 Compliance with Ethical Standards

Tissue samples were obtained from the Methodist Research Institute Biorepository in Indianapolis (IRB 1410015344). Tissues for bulk tissue analysis were obtained from human subjects undergoing tumor resection for suspected glioma at Indiana University Department of Neurosurgery and Goodman Campbell Brain and Spine (IRB 1410342262).

3.3 Results and Discussion

3.3.1 Extraction nESI for Brain Tissue

Extraction nESI was reported previously for therapeutic drug monitoring in whole blood^{27, 98}, and we have adapted it here to perform direct tissue analysis. In this application, deprotonated forms of GLU and 2-HG were isolated simultaneously and the intensities of their fragments compared to provide a relative measure of 2-HG in tissue. The structures of the individual compounds are shown in Table 3.1. MS/MS product ion spectra of 10 µg/mL GLU and 2-HG in methanol/water (9:1, v/v) solutions were recorded using nanoESI (Figure 3.1). Figure 3.2 illustrates tissue analysis performed using extraction nESI. On average, the time from sampling to result is ca. 5 min. Typical MS/MS spectra from tissue extracts recorded using the Mini MS are shown in Figure 3.3. The scan function for these experiments utilized a wide precursor ion isolation window covering both m/z 146 and m/z 147, which correspond to the deprotonated forms of 2-HG and GLU, and which give

product ions at m/z 129 and m/z 128, respectively. MS/MS of the extraction nESI from IDH mutant samples showed fragments from both 2-HG and GLU (Figure 3.3 (a)), whereas MS/MS of the extraction from IDH wildtype samples showed only fragments from GLU (Figure 3.3 (b)).

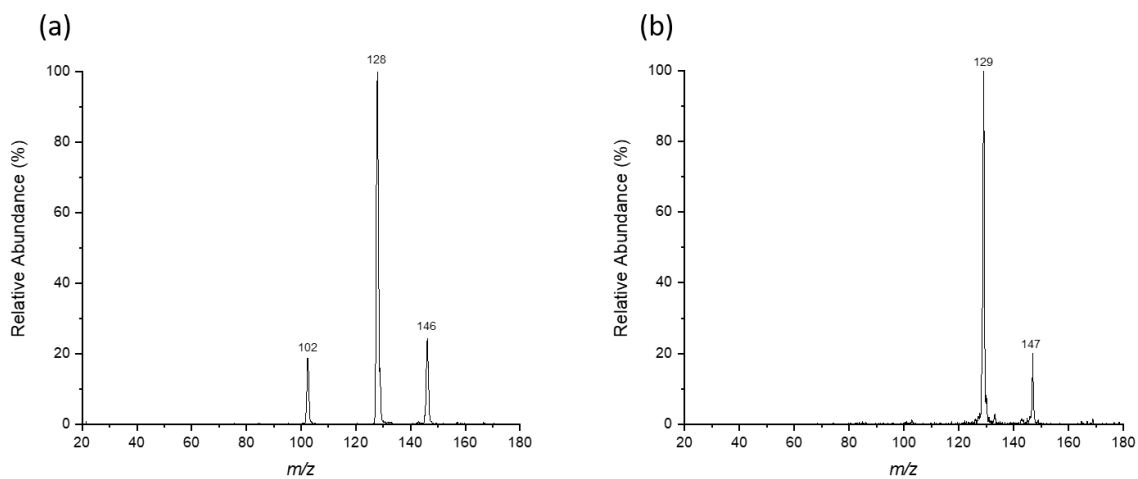
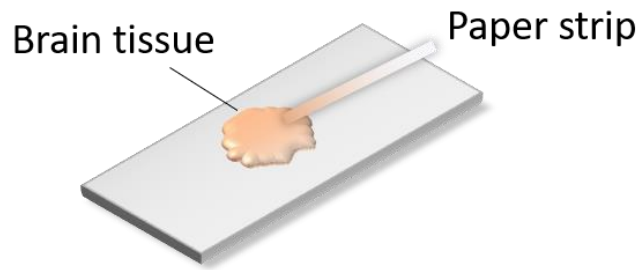


Figure 3.1. MS/MS product ion spectra recorded using Mini MS (a) GLU; (b) 2-HG.

1. Brain Tissue Sampling



2. Extraction and MS analysis

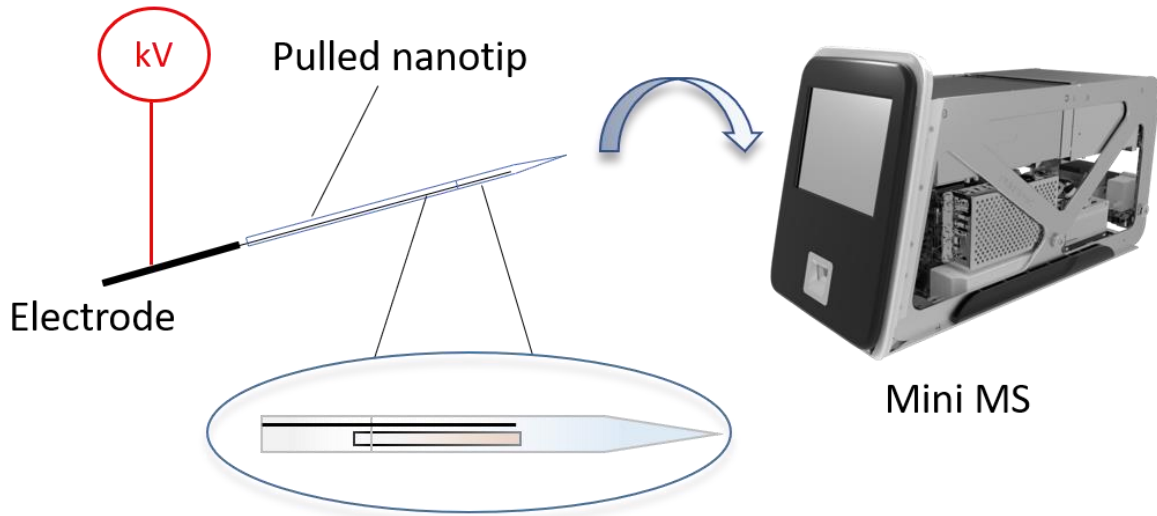


Figure 3.2. Extraction nanoelectrospray of brain tissue.

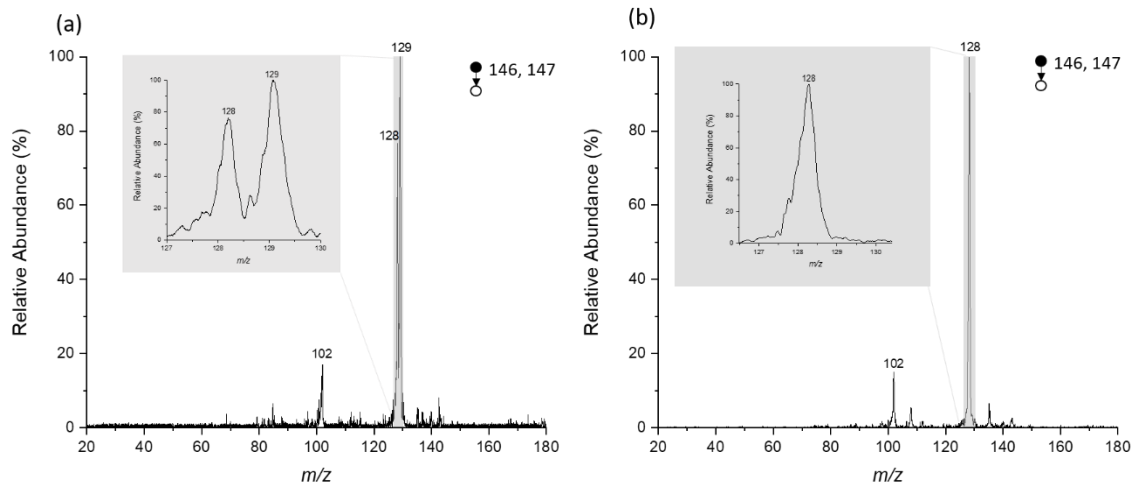


Figure 3.3 MS/MS spectra recorded using Mini MS (a) IDH mutant glioma and (b) IDH wildtype glioma. Note that peak at m/z 129 only occurs in IDH mutant tissue.

GLU is an abundant brain metabolite and has been reported⁹⁹ to have lower levels in IDH mutant gliomas compared to IDH wild-type (3.23 ± 1.27 mM in IDH mutant and 5.22 ± 1.36 mM in IDH wildtype). The combined assessment of 2-HG and GLU for IDH mutation assessment improves prediction compared to using 2-HG alone.⁹⁹ Using endogenous GLU instead of isotope labeled internal standard as a reference for 2-HG simplifies the assay.

An IDH mutation score was obtained by calculating the ratio of product ion intensities, m/z 129 intensity divided by m/z 128 intensity, with isotopic corrections for contributions of the natural C_{13} glutamate fragment ion to signal at m/z 129. A higher IDH mutation score indicates more 2-HG relative to GLU. Since IDH mutations result in accumulation of 2-HG in tissue and decreased levels of GLU, we hypothesized that a high IDH mutation score would be indicative of an IDH mutant glioma.

3.3.2 Analysis of Tissue Sections

We analyzed 39 glioma tissue cryosections (29 IDH wild-type and 10 IDH mutant) prepared from banked glioma tissues, collected from 29 human subjects, as an initial evaluation of the method. The IDH mutation scores ranged from 0.04 to 0.16 for IDH wildtype and from 0.28 to 6.83 for IDH mutant samples (Table 3.2). The distribution of IDH mutation scores was significantly higher in the IDH mutant glioma samples relative to the IDH wild-type gliomas, and the distributions were statistically different ($p=0.0025$, Figure 3.4). IDH mutant samples with low tumor cell percentage (TCP) had lower IDH mutation scores compared to IDH mutant samples with high TCP (Figure 3.4). This trend has been reported previously⁸⁹ and is recapitulated in our results.

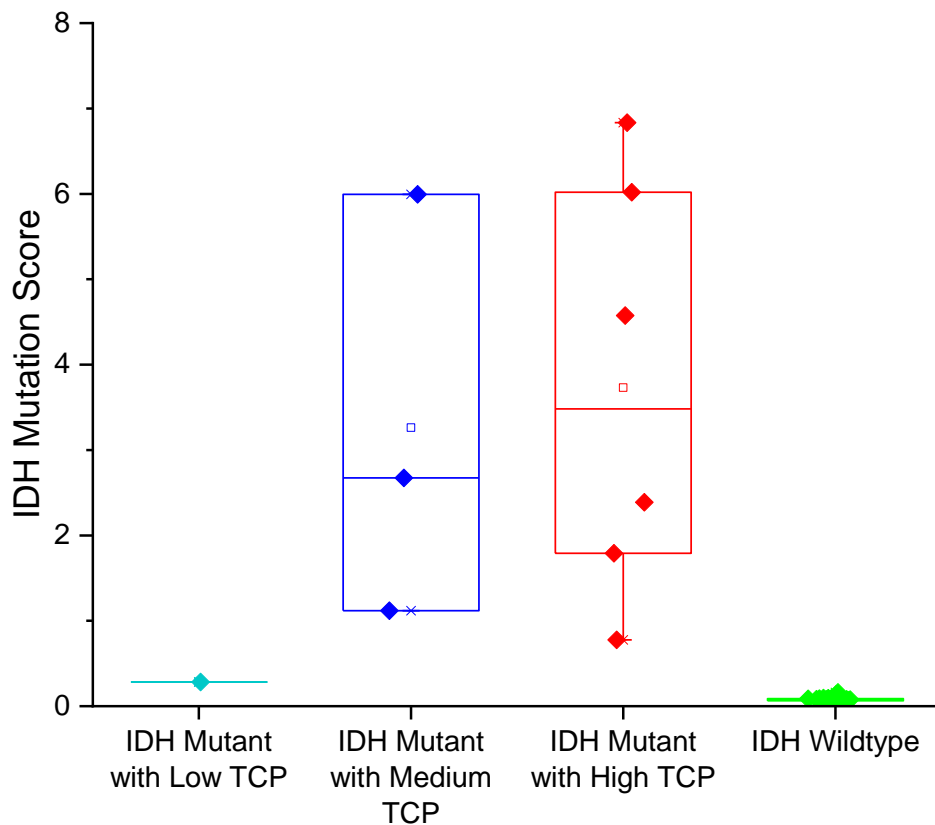


Figure 3.4 IDH mutation scores of tissue sections. 29 IDH wildtype, 10 IDH mutant (1 low TCP, 3 medium TCP and 6 high TCP).

Many of the tissue sections analyzed in this study are sections adjacent to those used in a previous study in which 2-HG was quantified using direct infusion ESI-MS/MS¹⁰⁰. The IDH mutation scores obtained from the Mini MS samples are highly correlated to the previously published quantitative results. A coefficient of determination (R^2) of 0.9229 was obtained for the five IDH mutant tissue sections, plotted as red points in Figure 3.5. Meanwhile, the 2-HG concentrations of IDH wildtypes were below limits of detection for both methods, hence the 23 blue points group at the lower left corner of the plot. The high correlation seen indicates that higher IDH mutation scores are related to higher concentrations of 2-HG in the tissue. The correlation is indicative only because the data are being compared with those of another study on adjacent tissue samples¹⁰⁰. The comparison assumes that the distribution of 2-HG is homogeneous throughout the tissue and no sample deterioration occurred on storage.

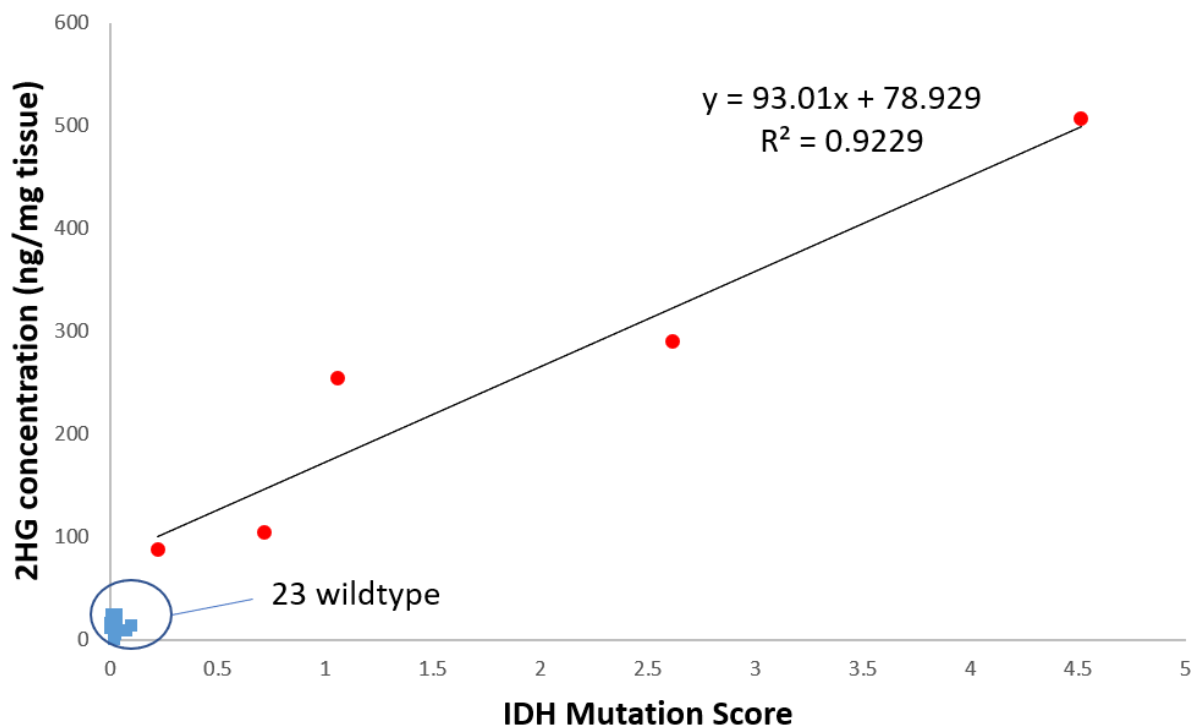


Figure 3.5 Correlation between concentration of 2-HG determined by triple quad MS analysis¹⁰⁰ and IDH mutation scores determined using the Mini MS [this work] from an adjacent tissue section.

3.3.3 Analysis of Bulk Tissues

To further evaluate the method for intraoperative diagnostic purposes, we analyzed frozen bulk tissue biopsies as an intermediate step to fresh tissue analysis. Tissue biopsies were originally collected during surgeries in 1.5 mL centrifuge tubes and kept frozen at $-80\text{ }^{\circ}\text{C}$. After thawing, each tissue piece was touched using a paper strip and analyzed with extraction nESI using the Mini MS. Reproducibility was examined by sampling three times from the same position on the same tissue biopsy. The results are presented in Table 3.3. The average relative standard deviation was $29.0 \pm 3.6\%$ for three medium or high TCP IDH mutant tissues and $24.8 \pm 11.4\%$ for five IDH wildtype tissues. Typical MS/MS spectra recorded from extraction nESI of another four different

bulk tissue biopsies are presented in Figures 3.6-3.9, insets are enlarged views of the peaks of interests.

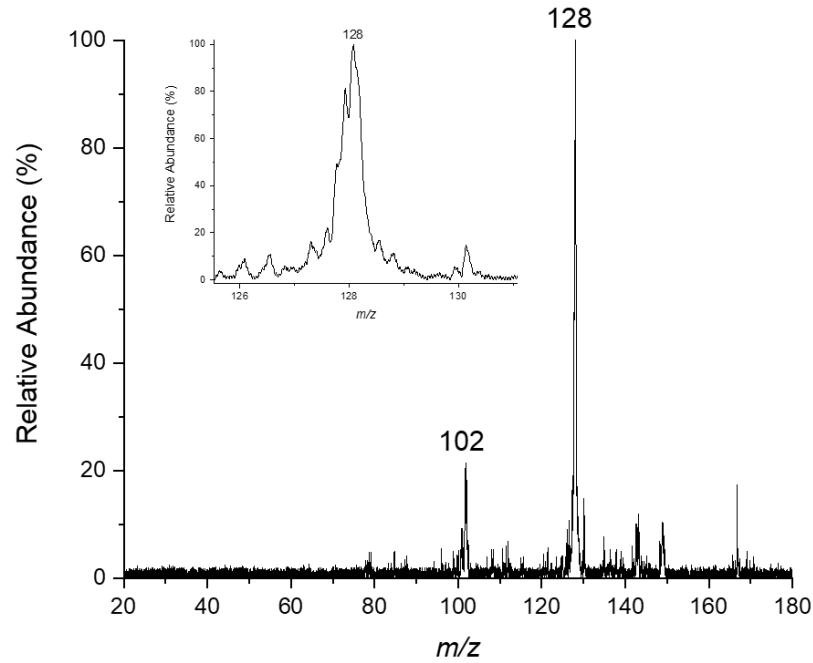


Figure 3.6 MS/MS spectra, IDH wildtype, low TCP.

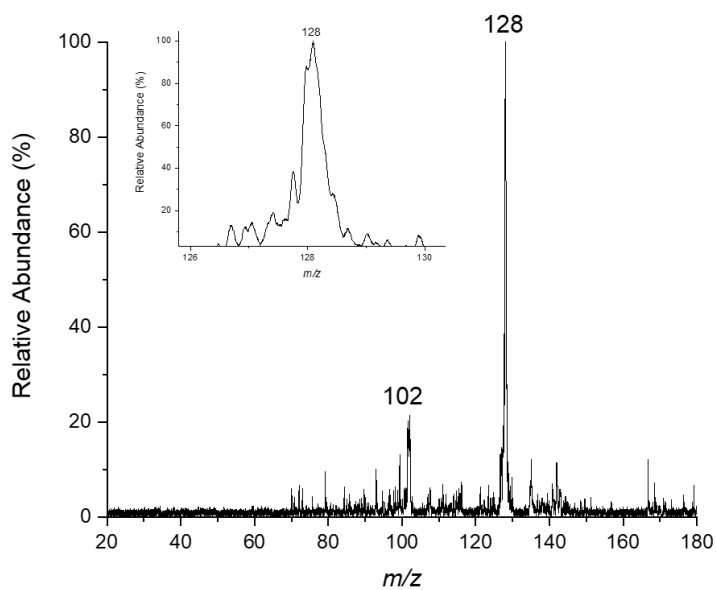


Figure 3.7 MS/MS spectra, IDH wildtype, high TCP.

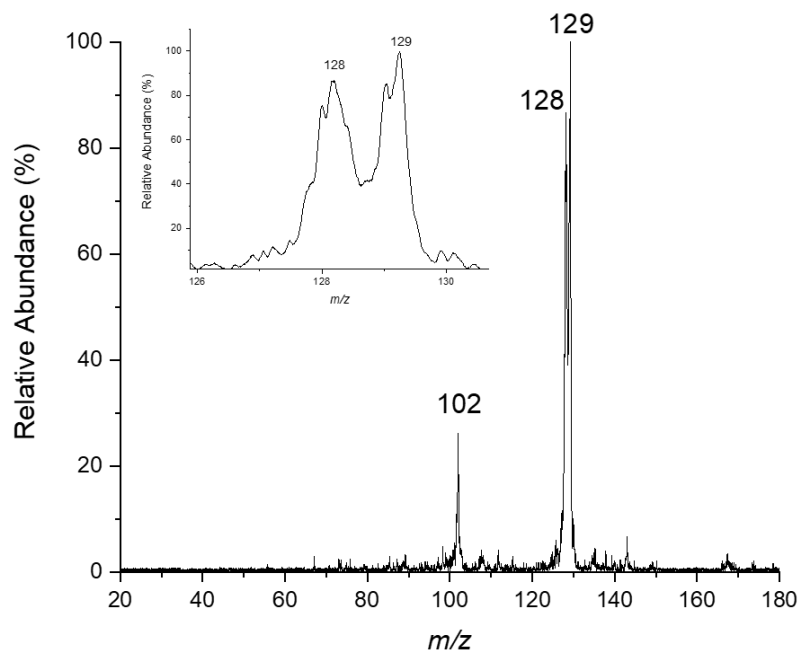


Figure 3.8 MS/MS spectra, IDH mutant, low TCP.

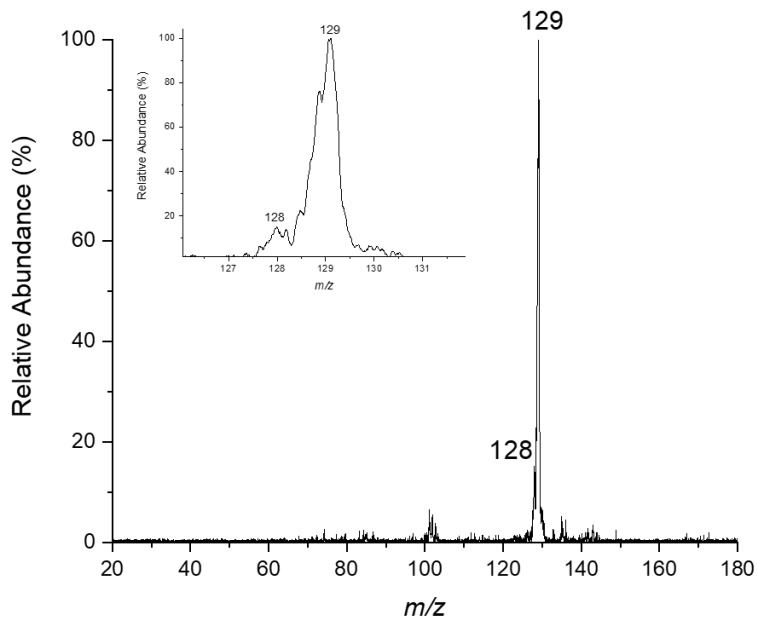


Figure 3.9 MS/MS spectra, IDH mutant, high TCP.

A total of 44 biopsies from 15 subjects were analyzed using extraction nESI with Mini MS. The IDH mutation status and IDH mutation scores are summarized in Table 3.4. The IDH wildtype tissues had IDH mutation scores below 0.15 regardless of TCP, whereas all IDH mutant samples had IDH mutation scores above 0.40 ($p = 1.06 \text{ E-}6$). Among the 28 IDH mutant tissue biopsies, 12 were low TCP tissues, 5 were medium TCP tissues and 11 were high TCP tissues. The IDH mutation scores of these samples are compared in Figure 3.10.

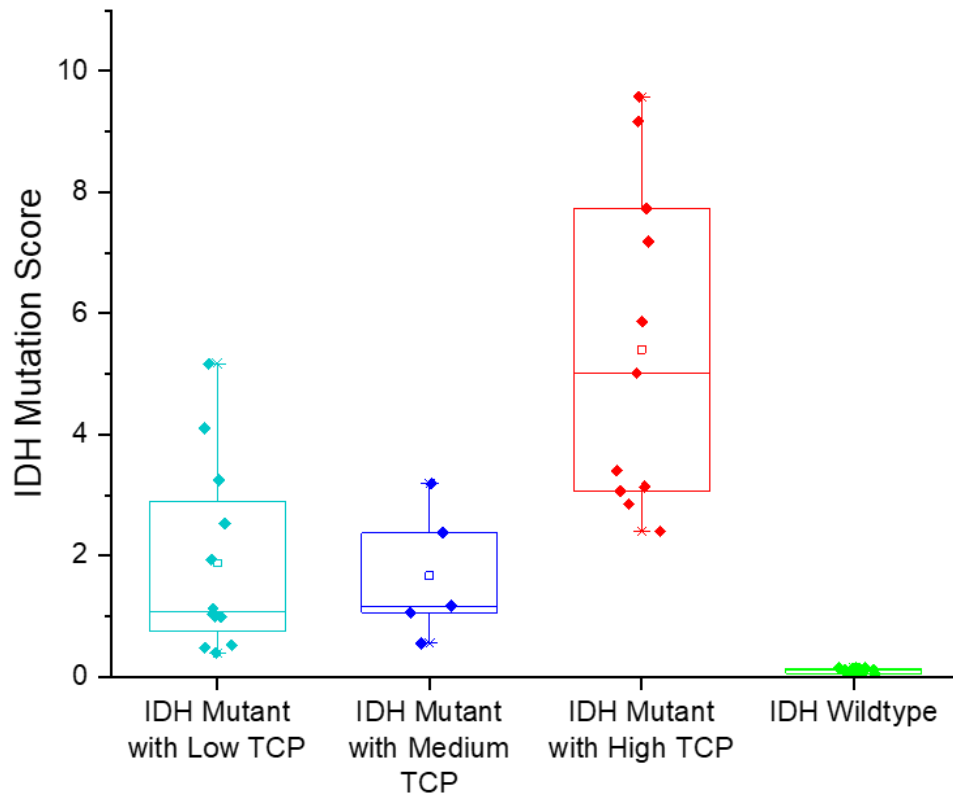


Figure 3.10 IDH mutation scores of tissue biopsies. 16 were IDH Wildtype, 28 were IDH mutant (12 low TCP, 5 medium TCP and 11 high TCP).

The TCP can significantly impact the diagnosis of IDH mutation; low TCP samples have fewer tumor cells and correspondingly lower quantities of 2-HG. In Figure 3.11, IDH mutation scores of 11 IDH mutant with high TCP and 16 IDH wildtype tissue biopsies are compared. The difference in IDH mutation scores between the highest-scored IDH wildtype and the lowest-scored IDH mutant with high TCP was 16 times (0.15 vs. 2.40). The difference in IDH mutation scores between the highest-scored IDH wildtype and the lowest-scored IDH mutant with low TCP was less than 3 times (0.15 vs. 0.40). Some low TCP samples have relatively high scores (Figure 3.10,

up to 5.17), which may reflect TCP variations in tissue. However, discrimination of IDH mutants from IDH wildtypes is achieved regardless of their TCP.

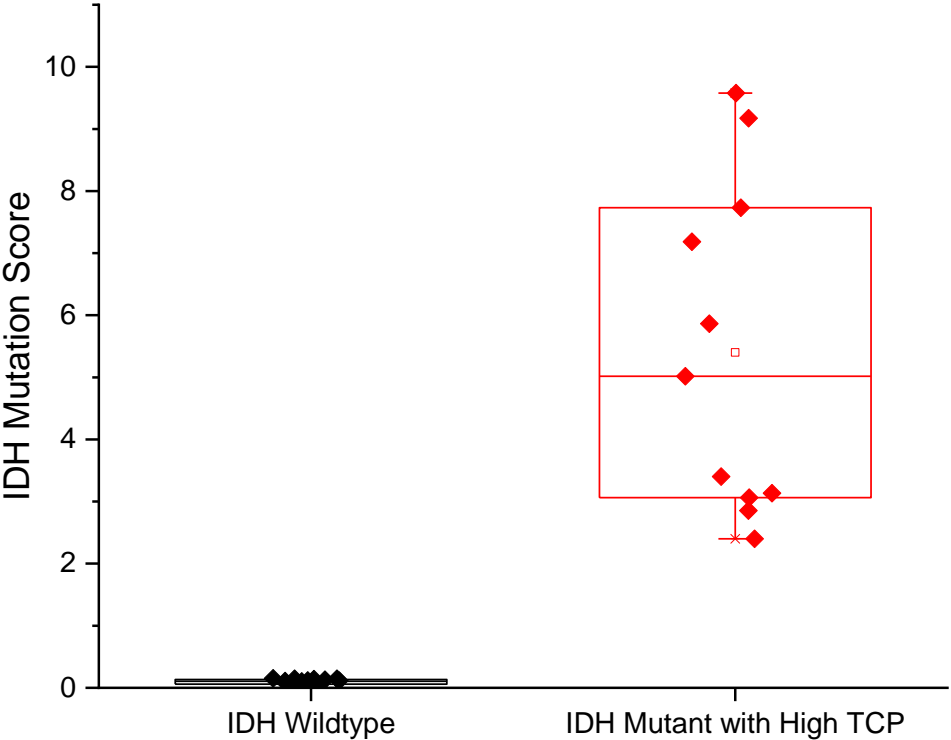


Figure 3.11 Comparison of IDH mutation scores of IDH wildtype (16 samples) and IDH mutant with high TCP (11 samples).

3.4 Conclusions

We demonstrate a method for rapid assessment of IDH mutation status of banked human gliomas samples using extraction nESI with a portable Mini MS. The Mini MS instrument used in this study provided reliable diagnostic information regarding IDH mutation status with a much smaller footprint compared to conventional bench-top mass spectrometers, thus being more suitable for an operating room. The average sampling to result time was 5 minutes. Bulk tissues of IDH wildtypes and IDH mutants with high TCP were differentiated with a 16-fold difference in IDH mutation scores. These merits suggest that the methodology could enable assessment of IDH mutation status of glioma biopsies at point-of-care during brain surgery.

Table 3.2 IDH mutation scores of tissue sections.

Subject No.	Sample No.	IDH Mutation Score	IDH Mutation Status	TCP	Diagnosis
1	1-S1	0.0634	Wildtype	Low	Normal
	1-S2	0.0846	Wildtype	Low	Normal
2	2-S1	0.0909	Wildtype	Low	Normal
	2-S2	0.0794	Wildtype	Low	Normal
3	3-S1	0.0703	Wildtype	Low	Normal
4	4-S1	0.0908	Wildtype	Low	Normal
5	5-S1	0.0934	Wildtype	Low	Infiltrated margin
6	6-S1	0.0888	Wildtype	Medium	Glioma
	6-S2	0.0668	Wildtype	Medium	Glioma
7	7-S1	0.0852	Wildtype	Low	Normal
	7-S2	0.0610	Wildtype	Low	Normal
8	8-S1	0.0760	Wildtype	Low	Infiltrated margin
9	9-S1	0.0795	Wildtype	Medium	Glioma
10	10-S1	0.0618	Wildtype	Low	Infiltrated margin
	10-S2	0.0810	Wildtype	Low	Infiltrated margin
11	11-S1	0.1370	Wildtype	High	Glioma
12	12-S1	0.0512	Wildtype	Low	Infiltrated margin
	12-S2	0.0525	Wildtype	Low	Infiltrated margin
	12-S3	0.0868	Wildtype	Low	Infiltrated margin
13	13-S1	0.0953	Wildtype	High	Glioma
14	14-S1	0.0810	Wildtype	Medium	Glioma
15	15-S1	0.1609	Wildtype	High	Glioma
16	16-S1	0.0506	Wildtype	Low	Normal

Table 3.2 Continued

17	17-S1	0.0387	Wildtype	Low	Infiltrated margin
18	18-S1	0.0625	Wildtype	Low	Infiltrated margin
19	19-S1	0.0521	Wildtype	Medium	Normal
20	20-S1	0.0888	Wildtype	Medium	Normal
21	21-S1	0.0686	Wildtype	Low	Normal
	21-S2	0.0765	Wildtype	Low	Normal
22	22-S1	0.2822	Mutant	Low	Glioma
23	23-S1	0.7763	Mutant	High	Glioma
24	24-S1	1.1191	Mutant	Medium	Glioma
25	25-S1	1.7910	Mutant	High	Glioma
26	26-S1	2.3883	Mutant	High	Glioma
27	27-S1	2.6741	Mutant	Medium	Glioma
28	28-S1	4.5745	Mutant	High	Glioma
	28-S2	6.0185	Mutant	High	Glioma
	28-S3	6.8349	Mutant	High	Glioma
29	29-S1	5.9937	Mutant	Medium	Glioma

Table 3.3. Reproducibility of extraction nESI using Mini MS, n=3.

Sample No.	IDH Mutation Score	IDH Mutation Status	RSD
M1	11.5377	Mutant	26.72%
M2	5.1516	Mutant	27.05%
M3	2.6115	Mutant	33.08%
W1	0.0699	Wildtype	25.72%
W2	0.0656	Wildtype	34.74%
W3	0.0689	Wildtype	6.32%
W4	0.0741	Wildtype	33.70%
W5	0.0842	Wildtype	23.53%

Table 3.4 IDH mutation scores of tissue biopsies.

Subject No.	Sample No.	IDH Mutation Score	IDH Mutation Status	TCP	Glioma Diagnosis
30	30-B1	0.0811	Wildtype	Low	Infiltrated white matter
	30-B2	0.1190	Wildtype	High	Glioma
	30-B3	0.1100	Wildtype	Low	Infiltrated white matter
	30-B4	0.1539	Wildtype	Low	Infiltrated white matter
	30-B5	0.1460	Wildtype	Low	Infiltrated white matter
31	31-B1	0.1394	Wildtype	High	Glioma
	31-B2	0.0900	Wildtype	High	Glioma
	31-B3	0.1012	Wildtype	High	Glioma
32	32-B1	0.0376	Wildtype	Low	Grey and white matter (80%)
	32-B2	0.0518	Wildtype	Low	White matter
	32-B3	0.1463	Wildtype	Low	White matter
33	33-B1	0.1166	Wildtype	High	Glioma
	33-B2	0.0466	Wildtype	High	Glioma
	33-B3	0.0659	Wildtype	Low	Infiltrated white matter
34	34-B1	0.1295	Wildtype	High	Tumor
35	35-B1	0.0425	Wildtype	Low	Infiltrated grey matter
36	36-B1	3.1891	Mutant	Medium	Glioma
	36-B2	2.3792	Mutant	Medium	Glioma
	36-B3	3.2451	Mutant	Low	Infiltrative margin
	36-B4	0.9918	Mutant	Low	Infiltrative margin
37	37-B1	9.5765	Mutant	High	Glioma
	37-B2	1.9356	Mutant	Low	Infiltrated white matter
	37-B3	1.1297	Mutant	Low	Infiltrated white matter
	37-B4	5.1713	Mutant	Low	Infiltrated white matter
38	38-B1	7.7310	Mutant	High	Glioma
	38-B2	9.1739	Mutant	High	Glioma

Table 3.4 Continued.

39	39-B1	0.9982	Mutant	Low	White matter
	39-B2	4.1080	Mutant	Low	Glioma
	39-B3	0.5529	Mutant	Medium	Infiltrated margin
	39-B4	1.0613	Mutant	Medium	Infiltrated white matter
40	40-B1	1.0244	Mutant	Low	Infiltrated white matter
	40-B2	0.4832	Mutant	Low	Infiltrated white matter
	40-B3	0.5211	Mutant	Low	Grey matter
41	41-B1	5.0162	Mutant	High	Tumor
	41-B2	5.8643	Mutant	High	Tumor
	41-B3	3.1335	Mutant	High	Tumor
	41-B4	7.1849	Mutant	High	Tumor
	41-B5	3.4018	Mutant	High	Tumor
42	42-B1	0.3971	Mutant	Low	Grey matter
	42-B2	1.1677	Mutant	Medium	Glioma
43	43-B1	2.8553	Mutant	High	Glioma
	43-B2	2.4004	Mutant	High	Glioma
44	44-B1	3.0641	Mutant	High	Glioma
	44-B2	2.5315	Mutant	Low	Infiltrative margin

CHAPTER 4. INTRAOPERATIVE DIAGNOSIS OF IDH MUTATION IN HUMAN GLIOMAS WITH MINI MS

A version of this chapter has been published by *Analytical and Bioanalytical Chemistry*. Reprinted with permission from Hannah M. Brown, Fan Pu, Mahua Dey, James Miller, Mitesh V. Shah, Scott A. Shapiro, Zheng Ouyang, Aaron A. Cohen-Gadol, R. Graham Cooks. Intraoperative Detection of Isocitrate Dehydrogenase Mutations in Human Gliomas using a Miniature Mass Spectrometer. *Analytical and Bioanalytical Chemistry*, 2019, ASAP. Copyright 2019 Springer.

4.1 Introduction

MS has been increasingly used for clinical applications. The simplicity and speed of ambient ionization MS has enabled its applications in intraoperative settings¹². Recent examples include DESI-MS for intraoperative assessment of tumor margins²³ and IDH mutation status⁹⁷ in human gliomas, REIMS (rapid evaporative ionization MS) for intraoperative tissue identification²⁴, and MasSpec Pen for *in vivo* cancer diagnostics²⁵. Besides its speed, one unique advantage of intraoperative MS when compared with conventional diagnostic tools is its capability of providing important molecular information. With these information, immediate feedback could be provided to surgeons to aid decision-making, which could potentially improve surgical outcomes.

We have demonstrated the use of extraction nESI to perform rapid diagnosis of IDH mutation in human gliomas (previous chapter).⁷² This methodology can be easily adapted for use in an intra-operative environment, as will be demonstrated in this chapter. Comparing with the deployment of a benchtop instrument (such as Thermo Fisher Scientific LTQ) in the OR, Mini MS has a much smaller footprint and lower noise level, therefore it is less intrusive in an OR environment to surgeons and nurses. We have performed intraoperative diagnosis for IDH mutation status with extraction nESI in several surgical cases, this proof-of-concept study has

successfully shown that important diagnostic information could be obtained with simple experiments in near real time.

4.2 Experimental

4.2.1 Adaptation of Mini β for Deployment in Operating Room

The Mini β is a stand-alone MS system that does not require external pumps or gas tanks. A hospital grade isolation transformer (Tripp Lite) was used to connect the Mini MS to a wall outlet in OR. The Mini MS has an on-board computer, but for the purpose of easy data transfer and better handling, an external laptop was connected to control the Mini MS. Everything was fitted on a small cart that measures about 18 inch x 21.5 inch x 22 inch (W x L x H), the setup is shown in Figure 4.1.



Figure 4.1 Setup of Mini MS in operating room.

The front interface of Mini β was originally designed for a sample cartridge system that is based on paper capillary spray. To accommodate the use of nESI, part of the interface was taken off and a home-made nESI mount was mounted instead. The design of the nESI mount was accomplished using Autodesk Inventor and then 3D printed using polylactic acid (Figure 4.2). The nESI mount was installed in front of Mini MS via a slide that was originally designed for aligning sampling cartridge stage. The top portion of the mount was designed to hold the acupuncture needle (act as electrode) and the nanotip, while preventing the needle from breaking the nanotip in case the nanotip falls back to the base of the acupuncture needle. The flat area in the back provide a gripping point for applying high voltage through an alligator clip.

The whole setup was inspected and tested by a hospital technician at IU Health Methodist Hospital before any experiment was conducted.

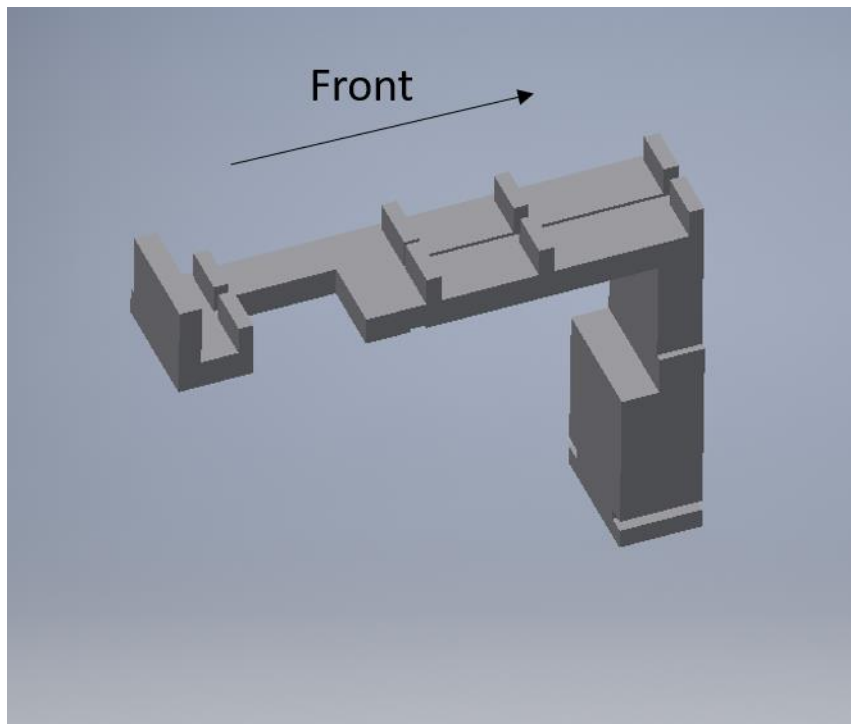


Figure 4.2 Extraction nESI mount for Mini MS.

4.2.2 Protocol for Intraoperative 2-HG Detection

Prior to the scheduled surgery, the cart with the Mini MS was rolled into the OR as soon as the patient arrived OR. The instrument was turned on after patient was anesthetized. A mass calibration was then be carried out in negative ion mode using nESI with a mixture of aspartic acid, GLU, 2-HG and N-acetyl aspartic acid, with their molecular ions found at m/z 132, 146, 147 and 174, respectively. nESI of a blank solvent was then sprayed. An example of the calibrated mass spectrum is shown in Figure 4.3. At this point the instrument was ready for sample analysis.

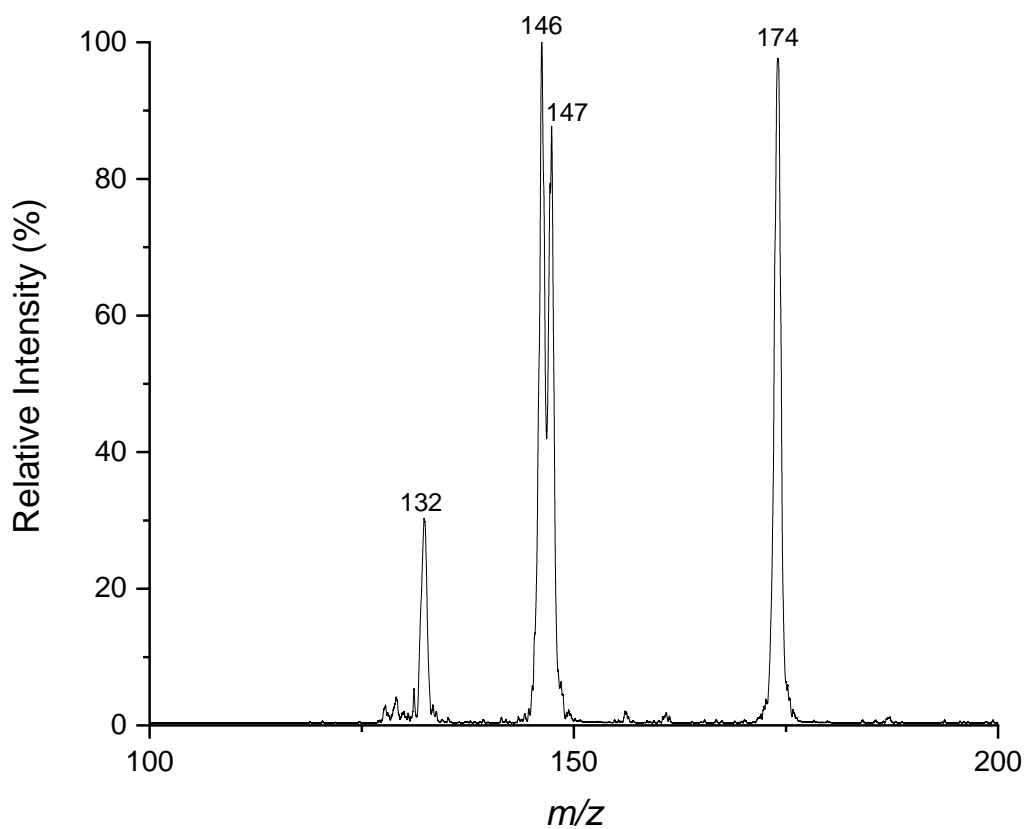


Figure 4.3 Full MS spectrum of calibration standard.

During surgery, the neurosurgeon performed tumor resection and took biopsies at his/her discretion. Our experiments did not interfere with the surgery to any extent. A small portion of the biopsies was given to us while the rest was sent to pathology. Extraction nESI was then performed on the biopsies as described in the previous chapter. Briefly, a narrow Whatman 1 paper strip was wiped over tissue biopsies, then inserted into a nanotip pre-filled with 20 μ L of 90:10 (v/v) methanol/water solution for nESI. 5 MS/MS spectra were taken for each sample, where each spectrum was an average of 3 scans. The scan function was similar to that described in the previous chapter, except some minor changes in the scan-out segment to optimize mass resolution.

After all samples were analyzed, calibration standard and blank were ran again to document any possible changes in mass calibration or carry-over effect (which we did not observe). The instrument was then turned off and moved out of the operating room after the neurosurgeon finished the surgery.

In iMRI (intraoperative magnetic resonance imaging) cases, the cart stayed outside the operating room. A trained person with all metal removed went into the operating room to obtain samples for real time analysis with Mini MS.

4.2.3 Validation with Benchtop Instrument

After each case, the samples were stored on dry ice and transport back to Purdue for analysis on Thermo TSQ using the same sampling and ionization method (extraction nESI). Data collection will be performed in MRM mode for transitions m/z 147 to m/z 129 and m/z 146 to m/z 128. A blank solvent was nanosprayed first, and the background signals were deducted in data analysis.

4.2.4 Data Analysis

Data analysis was performed in the same way as described in the previous chapter, *i.e.* IDH mutation scores were calculated based on the peak intensities of m/z 129 and m/z 128. Diagnostic information was shared with neurosurgeon during surgery to prevent any interference with standard of care.

4.2.5 Compliance with Ethical Standards

Biopsies for tissue analysis were obtained from human subjects undergoing tumor resection for suspected glioma at Indiana University Department of Neurosurgery, Goodman Campbell Brain and Spine Institute, after they had provided written informed consent to participate in the research study, following an IUSM IRB approved protocol (IRB No. 1410342262).

4.3 Results and Discussion

18 biopsies from 10 subjects have been collected and analyzed intraoperatively with Mini MS and post-operatively validated on TSQ. The results from Mini MS, TSQ and pathology are listed in Table 4.1. According to pathology base on immunohistochemistry, 4 subjects were IDH mutant and 6 subjects were IDH wildtype. The IDH mutation scores calculated based-on intraoperative Mini MS data showed a significant difference between IDH mutant and IDH wildtype (two-tail p -value = $4.16E-5$, t -test assuming unequal variances), as shown in the box chart in Figure 4.4. The lowest score of IDH mutant is 1.726 and the highest score of IDH wildtype is 0.154, which represents a 11.21 times difference.

The same biopsies were post-operatively analyzed on TSQ with extraction nESI to validate the results and similar result was obtained (Figure 4.5). Note that some of IDH wildtype samples had negative IDH mutation scores according to calculation. This is because the signal intensity of

m/z 129 is lower than that found in blank solvent, therefore these samples were assigned an IDH mutation score of zero. There is a 31.10 times difference between the IDH mutation scores of lowest IDH mutant and highest IDH wildtype (5.132 vs. 0.165). The agreement among intraoperative Mini MS analysis, post-operative TSQ analysis and pathology results strongly suggests that intraoperative detection of IDH mutation status could be readily performed with Mini MS using extraction nESI.

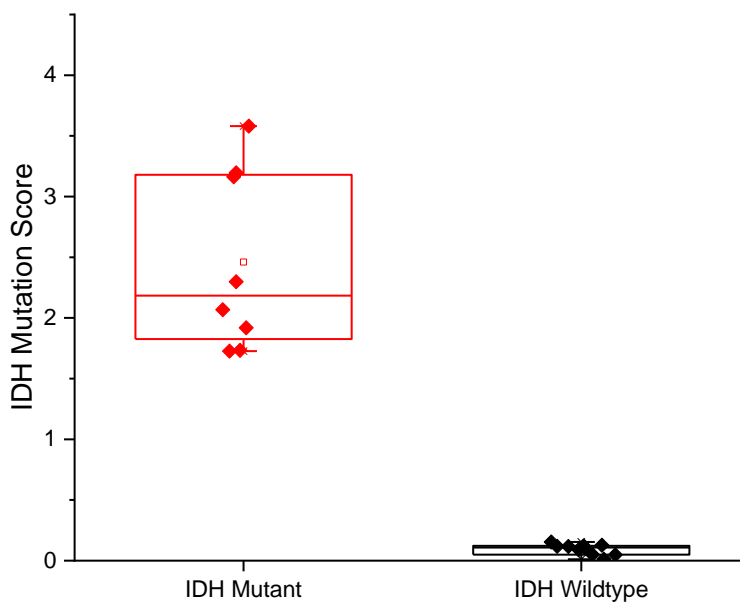


Figure 4.4 IDH mutation scores calculated from intraoperative Mini MS data.

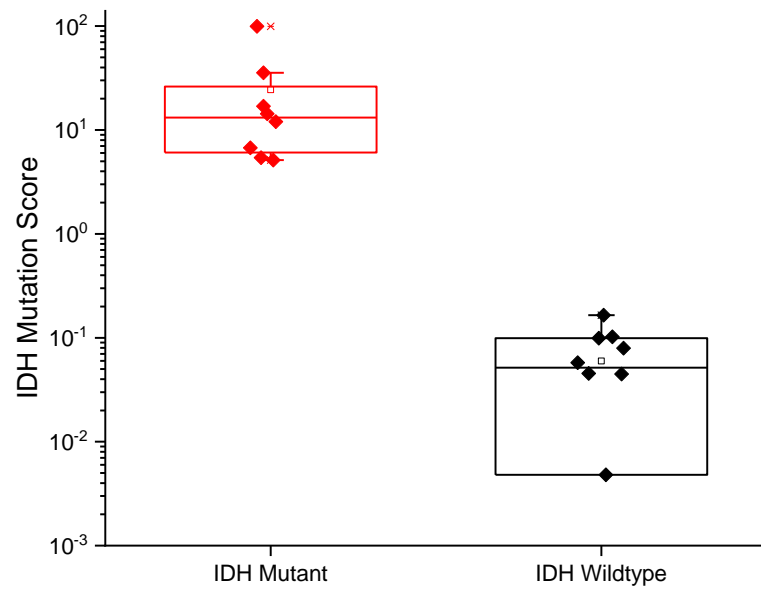


Figure 4.5 IDH mutation scores calculated from post-operative TSQ data. Note that the y-axis is on log scale.

Table 4.1 Pathology results, IDH mutation scores from intraoperative Mini MS experiments and post-operative TSQ experiments.

Subject No.	Pathology Results	Biopsy No.	IDH Mutation Score-Mini MS	IDH Mutation Score-TSQ
01	Astrocytoma, WHO grade II, IDH mutant	b1	1.919	5.132
		b2	3.581	12.020
02	Pleomorphic xanthoastrocytoma, WHO grade II, IDH wild type	b1	0.012	0.079
		b1	0.091	0.099
03	Glioblastoma, WHO Grade IV, IDH wild type	b2	0.050	0.102
		b3	0.123	0.165
		b1	0.127	0.045
04	Glioblastoma, WHO grade IV, IDH-wildtype	b2	0.117	0.045
		b1	0.154	0.000
05	Glioblastoma, WHO Grade IV, IDH wild type	b2	0.048	0.000
		b1	3.163	5.411
06	Residual/recurrent anaplastic astrocytoma, WHO Grade III, IDH-mutant	b1	3.163	5.411
07	Glioblastoma, WHO Grade IV, IDH wild type	b1	0.099	0.005
		b1	3.196	35.512
		b2	1.726	99.326
08	Glioblastoma, WHO grade IV, IDH-mutant	b3	1.733	14.342
		b1	0.119	0.058
09	Glioblastoma, WHO Grade IV, IDH wild type	b1	0.119	0.058
		b1	2.068	6.728
10	Anaplastic astrocytoma, WHO grade III, IDH-mutant	b2	2.299	16.929

4.4 Conclusions and future perspectives

We have demonstrated that Mini MS can be deployed in an OR environment for intraoperative detection of IDH mutations in human gliomas. The method is simple and fast, the average analysis time is 5 min from sampling to results.

As a proof-of-concept study, the small number of cases could not provide any statistically valid conclusion, such as establishing the diagnostic threshold for IDH mutation.

Although the current method is very simple, it may still require some training for medical personnel to perform such an analysis. Before the technology can be developed into an approved diagnostic tool and validated in a large-scale clinical study, it is necessary to improve the protocol by standardize the working procedure, develop easy-to-use sample cartridges and automate data analysis.

CHAPTER 5. FAST QUANTITATION OF PYRAZOLE FUNGICIDES IN WINE BY PAPER CAPILLARY SPRAY MASS SPECTROMETRY

A version of this chapter has been published by *Analytical Methods*. Reprinted with permission from Fan Pu, Wenpeng Zhang, Chao Han, Zheng Ouyang. Fast quantitation of pyrazole fungicides in wine by ambient ionization mass spectrometry. *Analytical Methods*, 2017, 9, 5058.¹⁰¹ Copyright 2017 Royal Society of Chemistry.

5.1 Introduction

Wine is one of the most popular beverages around the world. During the process of growing wine grapes, the attack by fungal pathogens can lead to plant diseases such as *Alternaria alternata* and *Botrytis cinerea*. Therefore, fungicides have been widely applied to control the fungal pathogens. The sterol biosynthesis inhibitors and quinone-oxidoreductase inhibitors (QoIs) are the major types of fungicides commercially available on the market.¹⁰² A relatively new type of fungicides, the succinate dehydrogenase-inhibitor (SDHI), has been increasingly used.¹⁰³ These fungicides inhibit the succinate dehydrogenase by binding strongly to the ubiquinone-binding site, which causes the disruption of cellular respiration. Most commonly used SDHI fungicides include penflufen (PEN), fluxapyroxad (FLU), isopyrazam (ISO), pyraclostrobin (PYRA) and bixafen (BIX), their structures are shown in Figure 5.1. This group of fungicides have been quickly adopted due to their high-level activities, especially for the fungi that already developed resistance to some of the commonly used fungicides such as QoIs.¹⁰² The fungicides are usually directly sprayed onto the grapes and vines and they are fairly stable in water and soil. The fungicide residues on the grape skins could certainly be carried over to the wine products. To address the concerns about their threats to human health, the maximum residue levels (MRLs) have been established. For example, the European Union (EU) residue limits are set at 0.01 mg/kg for PEN, FLU, ISO and BIX, and

0.02 mg/kg for PYRA in wine grapes.⁹⁷ To enforce the regulatory control, it is important to develop analytical methods for quantifying the fungicide residues in wines for product inspection.

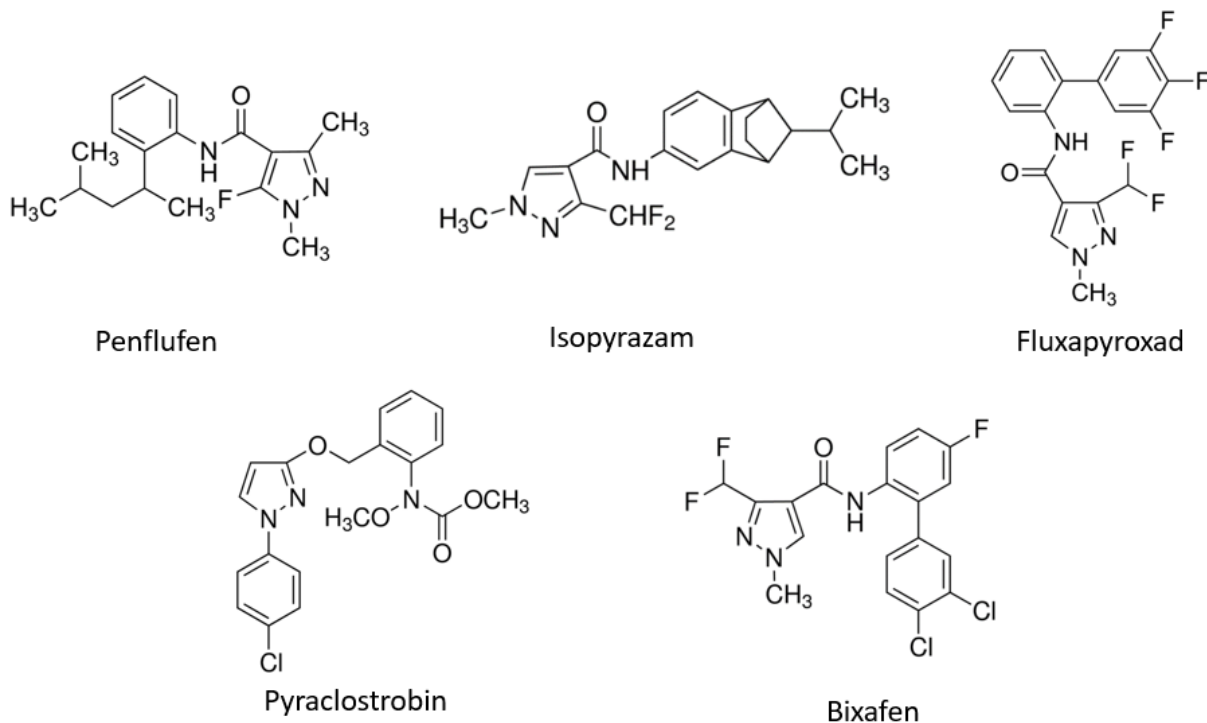


Figure 5.1 Chemical structures of five pyrazole fungicides.

Current methods for analysis of fungicides are mostly based on chromatographic separation (such as gas chromatography (GC) or liquid chromatography (LC)) coupled with tandem mass spectrometry (MS/MS). The LC-MS/MS is one of the most reliable and widely used methods for measuring agrochemical residues.^{104, 105} Modified QuEChERS (quick, easy, cheap, effective, rugged, and safe) extraction methods, followed with ultra-performance LC-MS/MS, was used to determine SDHI fungicides in fruits and vegetables.¹⁰³ In another method demonstrated, online solid phase extraction (SPE) was used for sampling, followed by LC-MS/MS method for analyzing

SDHI fungicides in surface water samples to estimate water contamination, with a limit of detection (LOD) as low as 0.1 ng/L obtained.¹⁰⁶

Despite the good analytical performance achieved by these methods, comprehensive sample preparation and separation procedures are still required, which are labor- and time-consuming and causing delays in getting results for the inspection. In the current study, we explored the use of ambient ionization method for direct analysis of the fungicides in wines, which could be of significantly improved analysis speed and extremely low cost. One of the benefits provided by ambient ionization techniques is the greatly improved throughput with the sample preparation eliminated or significantly simplified. Paper spray and its variants have been developed in recent years^{6, 107, 108}, with a series of applications developed for quantitative analysis. To perform paper spray, a piece of chromatography paper is cut to a triangle, which is then loaded with sample and extraction solvent; when a high voltage is applied to the paper, a spray is formed at the tip of the paper triangle and the analyte molecules extracted from the sample by the solvent are ionized. Paper spray has been applied to the quantitation of therapeutic drugs¹⁰⁹ and drugs of abuse⁶⁶ in biofluid samples, as well as contaminants in foodstuffs^{30, 52, 110}.

The application of ambient ionization to analysis of agrochemicals has been a hot topic since its debut. Paper spray has been applied to detection of agrochemicals and in a recent demonstration it was compared with leaf spray for fast screening.¹¹¹ Both methods showed good quantitative performance for atrazine, diuron and methomyl at ppb level. DART-MS/MS was investigated for screening of 50 residual pesticides and 12 illegal adulterants in red wine following a modified QuEChERS procedure.¹¹² LOQs obtained ranged between 1 and 100 ng/mL for pesticides and 10 and 250 ng/mL for different adulterants. Other examples include the use of paper spray for analyzing herbicides¹¹³, wooden-tip electrospray ionization (ESI) for toxic and hazardous

compounds in food samples,¹¹⁴ thermal desorption ESI for pesticide residuals in food stuff,¹¹⁵ and DESI for distribution of pesticides on the leaf surfaces.¹¹⁶ LTP was also previously used for detecting five classes of fungicides,¹¹⁷ but not including the pyrazole fungicides. LODs at ng/mL level were obtained, meeting the MRL requirement. Its capability for quantitative analysis has not been demonstrated yet.

Paper capillary spray¹¹⁸ was developed with a capillary sprayer embedded into the paper substrate for improved spray ionization. Thicker paper substrate could now be used to allow a higher load of sample and extraction solvent. More flexibility was also allowed in the selection of the paper substrate geometry for the design of disposable sample cartridges. The paper capillary spray was successfully used with mass spectrometers using an atmospheric pressure interface with curtain gases, which used to be challenging for paper spray.¹¹⁹

In this work, paper capillary spray ionization was used with a triple quadrupole mass spectrometer to perform a fast detection and quantitation of four pyrazole fungicides (PEN, ISO, PYRA, FLU) in wine samples, and compared with paper spray. No pretreatment of the samples was required, and the limits of quantitation (LOQs) were found to be 2 ng/mL for paper capillary spray. The fast speed, low cost, and adequate sensitivity of this method present its potential for fast screening of contaminants in wines.

5.2 Experimental

All the chemicals were purchased from Sigma-Aldrich (St. Louis, MO, USA) and used without further purification. Four different wines were purchased from local supermarkets: Coteaux du Languedoc, Les Belles Tours, France (wine 1, red); Merlot, Terrasses D'Azur, France (wine 2, red); Viognier, La Garelle, France (wine 3, white); Cabernet Sauvignon, Yellow Tail, Australia (wine 4, red). Grade 31ET and grade 1 chromatography papers were purchased from Whatman

(Whatman International, Maidstone, UK). Fused silica capillaries with outer diameter of 130 μm and inner diameter of 50 μm were purchased from Molex Inc. (Lisle, IL, USA).

Each of the four fungicide compounds was dissolved into methanol to make a concentrated stock solution (1000 $\mu\text{g}/\text{mL}$), which were then mixed together and subsequently diluted using the red wine to prepare samples at desired concentrations. Each calibration standard contained four fungicides at the same concentrations. BIX was spiked into all samples at a constant concentration of 200 ng/mL as the internal standard (IS). Final concentrations of fungicides in the matrix-matched calibration standards were 2, 5, 10, 20, 100, and 200 ng/mL .

MS analysis was performed using a TSQ Quantum Access Max (Thermo Scientific, San Jose, CA, USA) with a heated capillary. The capillary temperature was optimized and set at 200 $^{\circ}\text{C}$ for all quantitative studies. Multiple reaction monitoring (MRM) mode was used for quantitation, with an isolation window of m/z 1.0 and a scan time of 100 ms. A tube lens voltage of 100 V was used for all analytes without further optimization. The study of matrix effect and the effect of the distance between capillary and MS inlet were performed using a LTQ XL (Thermo Scientific, San Jose, CA, USA), with the capillary temperature set at 200 $^{\circ}\text{C}$ and the tube lens voltage at 100 V. A scan method was established to monitor the product ions of PEN and BIX consecutively, with an isolation window of m/z 2.0 for the product ions. The MS analysis was performed in positive ion mode.

5.3 Results and Discussions

5.3.1 Setup of paper capillary spray

Previously, paper spray has been extensively reported for direct, quantitative analysis. It was found that the thickness of the paper is critical for the stability of the spray off the paper tip. As an improvement of the repeatability and the ionization efficiency, paper capillary spray ionization

was developed. Thicker paper substrate can be used to hold more sample load while stable spray is maintained with the capillary tip. The use of capillary as emitter also significantly improves the robustness of the device, as a paper tip used in paper spray can be easily contaminated and damaged. A detailed study with comparison has been reported.¹¹⁸ To fabricate the spray device, grade 31ET chromatography paper (0.5 mm thickness) was first cut into a rectangular shape of 8 mm wide and 15 mm height, with the sharp corners trimmed to avoid direct sprays from the paper substrate (Figure 5.2). Without the capillary emitter inserted, the signal intensity would drop at least two orders of magnitude in full scan mode and nearly no signal would be detected under MS/MS mode. The capillary sprayers were made by cutting a fused silica capillary into short pieces of 10 mm long, which was then inserted into the 31ET paper with 5 mm in the substrate.

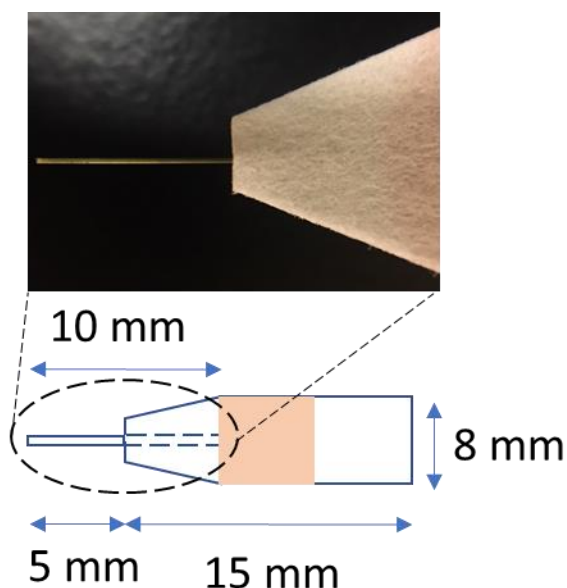


Figure 5.2 Photo and dimensions of a paper capillary spray device.

In the experiments of paper capillary spray ionization, 10 μL wine sample was deposited onto the middle of the paper substrate (Figure 5.2) and then let dry to make a dried sample spot. This

process can be expedited by using a heat gun. To analyze the dried sample spot, the paper device was held with an alligator clip and placed in front of the heated capillary of the mass spectrometer, with a distance about 1 cm between the fused silica capillary and the MS inlet. Four different pure solvents were tested, including methanol, acetonitrile, acetone and ethyl acetate. The highest intensity was obtained with pure methanol, which was subsequently adopted for all the following experiments. For MS analysis, 70 μL methanol was added to the rear end of the paper device as the elution and spray solvent, and a 2.5 kV DC high voltage was applied to the paper through the clip to initiate and sustain the spray. In the quantitative studies, the experiments were repeated three times for each sample.

5.3.2 Matrix effect

Matrix effect is a major concern of ambient ionization mass spectrometry. PEN was spiked into methanol, wine 1, wine 2 and wine 3, each at a concentration of 10 ng/mL. MS/MS spectra were recorded for analysis using paper capillary spray, as shown in Figure 5.3 for PEN (m/z 318.3). The product ion intensities of m/z 234.1 for PEN was used for comparison. The results are shown in Figure 5.4. The insets spectra show that when PEN was not spiked into these matrices, no obvious peaks can be observed at m/z 234, this confirms that the m/z 234 peaks in 10 ng/mL samples are from the spiked PEN. Good signal-to-noise ratios are observed for all matrices. No significant difference was observed due to different wine matrices. Drying the wine samples on the paper prior to the analysis was expected to minimize the matrix effect.

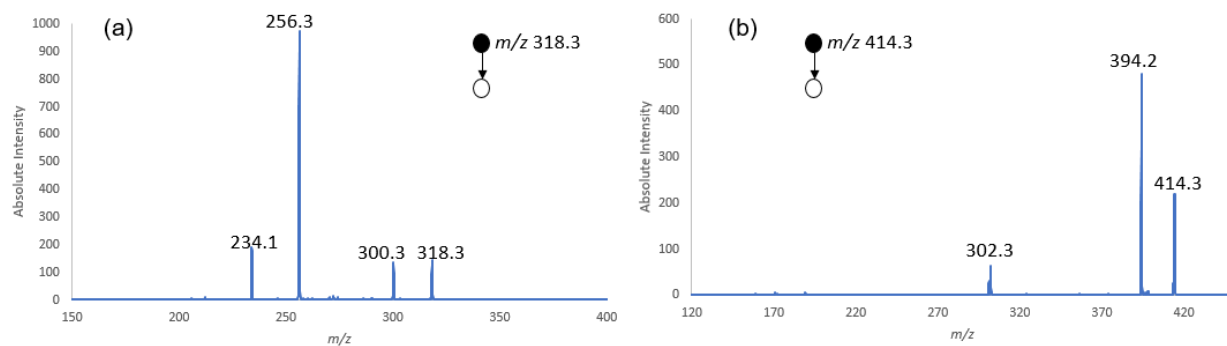


Figure 5.3 MS/MS spectra of (a) PEN and (b) BIX obtained using LTQ. m/z 256.3, m/z 300.3 in (a) and m/z 302.3 in (b) were from background.

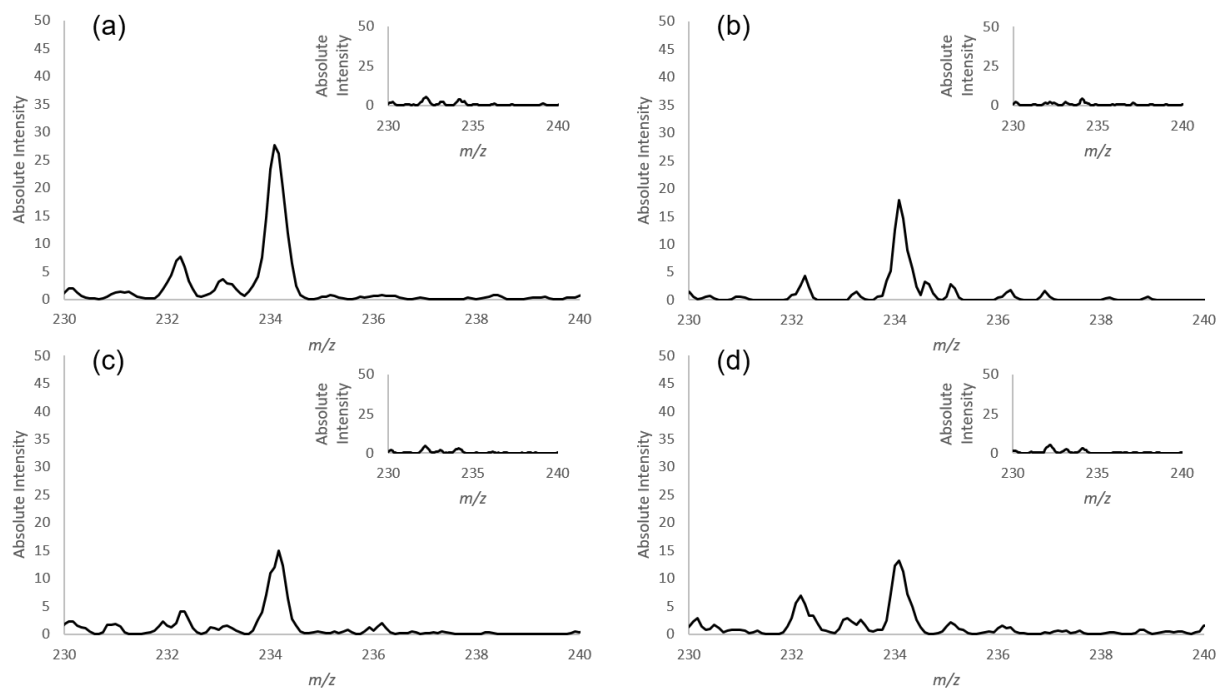


Figure 5.4 The effect of wine matrix on paper capillary spray. The matrices are (a) methanol, (b) wine 1, (c) wine 2 and (d) wine 3. Insets are spectra of blank matrices.

5.3.3 Effect of the distance between capillary and MS inlet

The distance between the capillary and the MS inlet (heated capillary) could have a strong impact on the ion signal intensity. Methanol samples spiked with 200 ng/mL PEN and BIX were analyzed

and the signal intensities of product ions m/z 234 and m/z 394 were monitored. It was found that an offset of 8 mm in radial direction at the axial distance of 5 mm could result in a complete loss of the signal. Figure 5.5 shows the results for moving the tip of the capillary away from the MS inlet, between 5 and 30 mm. A longer distance would result in a lower signal intensity. It was found that the signal can be detected even at a distance of 50 mm, although the signal was not very stable (data not shown). Despite the variation in the signal intensity, the intensity ratio between PEN and BIX was rather stable (RSD = 11.5%) as shown in Figure 5.5 (b); therefore, as long as a distance shorter than 30 mm is maintained, the quantitative performance should not be affected significantly. The optimization of this distance and keeping it consistent is crucial for achieving consistent detection limit. We used a distance of 10 mm for all quantitation experiments.

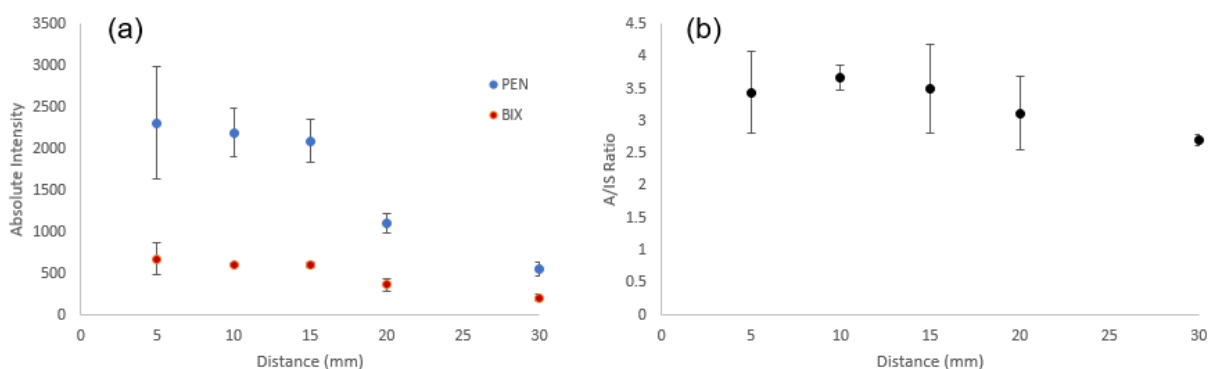


Figure 5.5 The effect of distance between capillary and the MS inlet. a) Product ion signals for PEN and BIX and b) their ratio as functions of the distance between the capillary tip and MS inlet

5.3.4 Effect of heated capillary temperature and spray voltage

The atmospheric pressure interface of the TSQ/LTQ mass spectrometer has a heated capillary, which could mitigate the potential problem of insufficient desolvation that would negatively impact the ionization efficiency¹²⁰. Studies were carried out to determine the optimal temperature

for the heated capillary, using dried sample spot prepared with 200 ng/mL PEN in pure methanol. The heated capillary temperature was adjusted between 100 °C and 300 °C, the MS analysis was performed in MRM mode where both the product ions at m/z 141.2 and m/z 234.1 of PEN were monitored. The absolute ion intensities of m/z 141.2 as a function of spray time were recorded at different temperatures. Figure 5.6 (a) shows the ion chromatograms at three temperatures of 100 °C, 200 °C and 300 °C. Higher temperatures yielded higher intensities, which could be expected due to a better evaporation of the spray solvent resulting in a more efficient formation of dry ions of the analytes. However, at a higher temperature such as 300 °C, it also appeared that the spray became relatively unstable with more fluctuation. To obtain a relatively stable spray while maintaining sufficient intensity, the heated capillary temperature was set at 200 °C for the rest of the study.

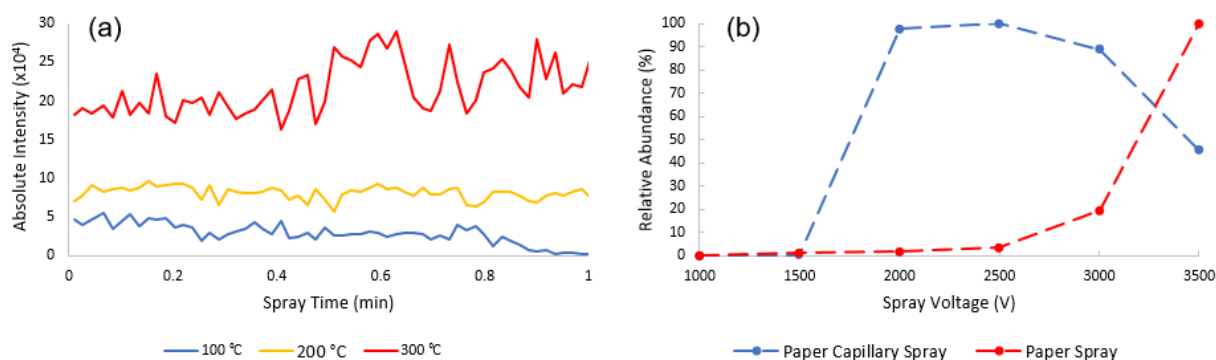


Figure 5.6 (a) Effect of heated capillary temperature on ion intensity. (b) Effect of high voltage on paper capillary spray and paper spray.

Paper capillary spray shares similar properties with paper spray in terms of using the paper substrate for a real-time sample processing. The use of the capillary sprayer, however, provided some unique flexibility for design of the sample cartridges. In the previous studies, it was found

that paper spray using 31 ET chromatography paper (0.5 mm thickness) could suffer low ionization efficiency in comparison with the grade 1 chromatography paper (0.18 mm thickness), due to the difference in the sharpness of the paper tip.¹¹⁸ The paper capillary spray provided ionization efficiency similar to the paper spray with thin paper substrate but could use thicker paper substrates for higher sample loads.¹¹⁸ In this work, we also studied the impact of the spray voltage on the paper capillary spray in comparison with paper spray, which usually requires a high voltage (3-5 kV).¹⁰⁷ Figure 5.6 (b) shows the ion intensities monitored for 200 ng/mL PEN in pure methanol analyzed using paper spray and paper capillary spray each with a spray voltage varying from 1000 V to 3500 V. Both used the 31ET chromatography paper as the substrate. A triangle shape was adopted for paper spray and the dimensions were similar to the paper capillary spray device, with the width of the base being 8 mm and the height being 15 mm. In comparison with the voltage higher than 3000V required for paper spray, an optimal spray was obtained at 2000V for paper capillary spray, which is higher than those for nanoESI but similar to ESI. For the subsequent quantitative study, a spray voltage of 2500 V was used for paper capillary spray.

5.3.5 Determination of the MRM parameters

To determine the appropriate MRM transitions for the compounds of interest, MS/MS spectra were acquired using paper capillary spray ionization in product ion scan mode. The spectra are shown in Figure 5.7 and MRM parameters are summarized in Table 5.1. The precursor ions were the protonated ions at m/z 318.0, m/z 360.0, m/z 382.0, m/z 388.0 and m/z 414.0 for PEN, ISO, FLU, PYRA and BIX, respectively. For quantitative analysis, product ions of m/z 141.2, m/z 244.2, m/z 342.1, m/z 163.3, and m/z 266.2 were selected, respectively. These were the product ions with highest intensity observed. Other product ions, such as m/z 234.1, m/z 320.2, m/z 314.1,

m/z 149.2 and m/z 374.1 were also observed with relatively high intensities for the four fungicides, respectively, thus potentially could also be used for MRM quantitation.

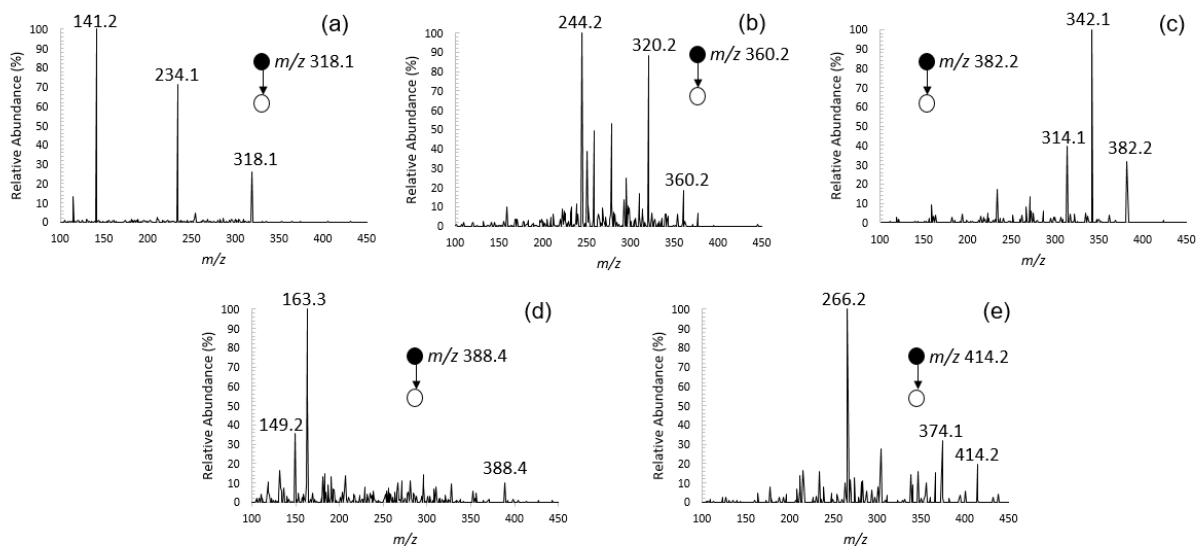


Figure 5.7 MS/MS spectra of (a) PEN, (b) ISO, (c) FLU, (d) PYRA and (e) BIX.

Table 5.1. MRM parameters.

Compounds	Molecular Weight	Precursor m/z	Product m/z
Penflufen	317.4	318.0	141.2 ^a , 234.1
Isopyrazam	359.4	360.0	244.2 ^a , 320.2
Fluxapyroxad	381.3	382.0	342.1 ^a , 314.1
Pyraclostrobin	387.8	388.0	163.3 ^a , 149.2
Bixafen	414.2	414.0	266.2 ^a , 374.1

^a Used for quantitation

5.3.6 Quantitation with Paper Capillary Spray

The quantitation was performed using MRM mode, with transitions of m/z 318.0 to 141.2, 360.0 to 244.2, 382.0 to 342.1, 388.0 to 163.3 and 414.0 to 266.2 for PEN, ISO, FLU, PYRA, and IS BIX, respectively. The fungicides were spiked into wine 4. Figure 5.8 shows the calibration curves obtained for these four fungicides using by paper capillary spray ionization mass spectrometry analysis. Table 5.2 summarizes the characteristics for the calibrations. The LOQs were determined as 2 ng/mL for all four fungicides, which were lower than the MRL levels set for these fungicides by EU⁹⁷. Good linearity was achieved in the concentration range of 2-200 ng/mL, with R^2 value above 0.99 for all four fungicides. According to the slopes of the calibration curves, FLU shows the lowest sensitivity, which is probably attributed to its poorer ionization efficiency, compared with other three fungicides.

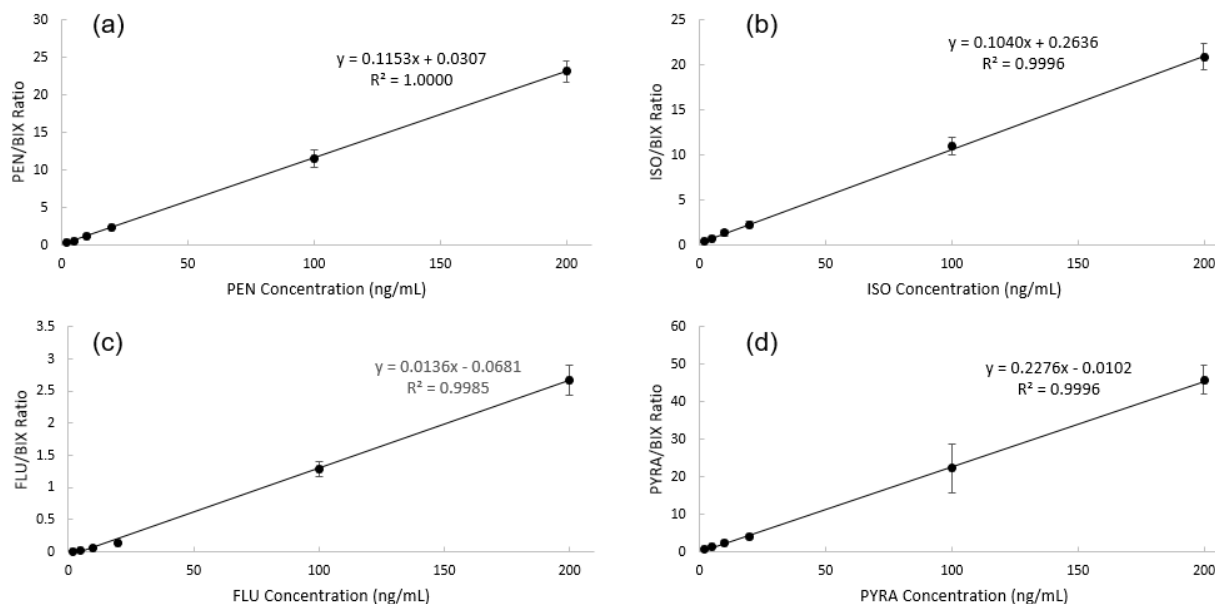


Figure 5.8 Calibration curves of (a) PEN, (b) ISO, (c) FLU and (d) PYRA with paper capillary spray mass spectrometry.

Table 5.2. Analytical performance of paper capillary spray for the analysis of fungicides

Compounds	Linearity Range (ng/mL)	LOQ (ng/mL)	Calibration Equation	Correlation Coefficient (R ²)	MRL (mg/kg)
Penflufen	2-200	2	$y = 0.1153x + 0.0307$	1.000	0.01
Isopyrazam	2-200	2	$y = 0.1040x + 0.2636$	0.9996	0.01
Fluxapyroxad	2-200	2	$y = 0.0136x + 0.0681$	0.9985	0.01
Pyraclostrobin	2-200	2	$y = 0.2276x + 0.0102$	0.9996	0.02

Quality control experiments were also performed, using samples prepared at three concentrations in the way same as the calibration standards, viz. spiking standard solutions of four fungicides simultaneously into the wine, with 200 ng/mL BIX as the internal standard. Relative standard deviations (RSDs) were calculated to evaluate the precision of the method. Quality control data are listed in Table 5.3, with the ones marked bold not meeting the recommended requirements⁷¹ (precision and accuracy within 15%, except at LOQ where $\pm 20\%$ is deemed acceptable). These results show that paper capillary spray has acceptable accuracy and precision, thus can be used as a reliable method for fungicides quantitation in wine.

Table 5.3. Quality control data, paper capillary spray, n=3

Compounds	Nominal		Precision (RSD %)
	Concentration (ng/mL)	Accuracy (%)	
Penflufen	5	111.4	8.4
	20	107.9	20.2
	100	113.3	12.7
Isopyrazam	5	94.9	10.2
	20	88.2	27.8
	100	87.0	9.7
Fluxapyroxad	5	121.7	9.1
	20	87.2	8.1
	100	88.4	9.7
Pyraclostrobin	5	112.4	5.0
	20	86.2	17.5
	100	79.5	9.6

Four different wine samples were examined with paper capillary spray mass spectrometry, and none of the four pyrazole fungicides were detected.

5.3.7 Quantitation using paper spray as a comparison

Similar quantitation experiments were performed with paper spray for comparison and validation. Grade 1 chromatography paper was cut to triangles with 8 mm base and 15 mm height. The sample load was smaller than that for paper capillary spray, at 5 μL ; and the elution and spray solvent was 40 μL . All other parameters were kept the same (distance between the sharp tip of the paper to MS inlet was kept at 10 mm). The calibration curves (Figure 5.9) and the quality control data (Table 5.4) were summarized in the supplementary information. Linear ranges were 2-200 ng/mL for PEN and ISO, and 5-200 ng/mL for FLU and PYRA, respectively, with R^2 value above 0.99 for all four fungicides. Quality control experiments showed that similar levels of accuracy and precision to paper capillary spray was achieved.

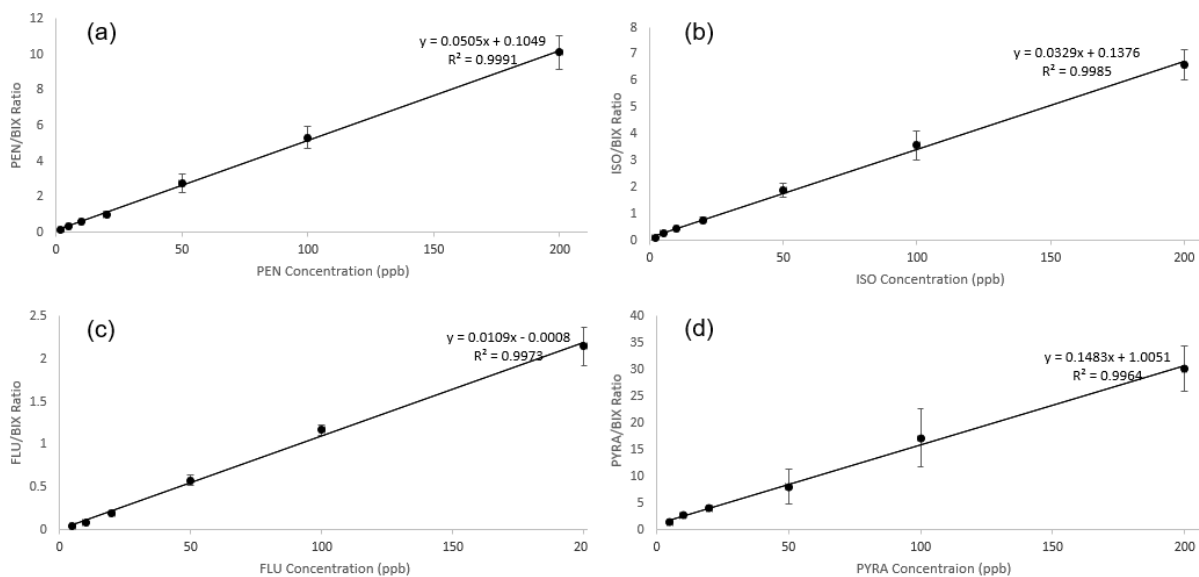


Figure 5.9 Calibration curves of (a) PEN, (b) ISO, (c) FLU and (d) PYRA with paper spray mass spectrometry.

Table 5.4 Quality control data, paper spray, n=3*

Compounds	Nominal Concentration (ng/mL)	Accuracy (%)	Precision (RSD %)
Penflufen	2	89.2	8.6
	10	115.9	3.3
	100	109.1	13.3
Isopyrazam	2	82.2	4.2
	10	112.7	6.4
	200	102.9	8.5
Fluxapyroxad	10	83.9	6.8
	50	102.2	13.1
	100	100.4	9.2
Pyraclostrobin	10	91.8	4.0
	50	108.9	31.5
	200	117.2	13.2

*Marked bold indicates not meeting the recommended requirements.

5.3.8 Comparison with Other Methods

The SPE-GC-MS method was previously demonstrated for fast screening of the fungicides with a high analytical performance.¹²¹ PYRA could be analyzed with an LOQ of 0.7 ng/mL and a linear range of 0.7-400 ng/mL; the RSDs obtained were within 5% for both intra-day and inter-day assays. This method has better sensitivity but still requires 23 minutes for analysis of one sample. Recently, a GC-MS/MS method was developed for simultaneous quantification of six pyrazole fungicides. SPE is required for sample preparation.¹²² The LOQs were 0.2 ng/g for FLU and BIX, and 0.8 ng/g for PEN and ISO, respectively. The linear range was 1-50 ng/mL. In comparison with these

methods the sampling and analysis procedure for paper capillary spray are significantly simpler and faster (shorter than 1 min), with adequate performance obtained. The amount of sample required is also significantly lower (10 μ L vs. 10 mL for SPE-GC-MS).

5.4 Conclusions and future perspectives

Paper capillary spray mass spectrometry was used with a triple quadrupole mass spectrometer for a fast quantitation of four pyrazole fungicides in wine. LOQs of 2 ng/mL were obtained for all four analytes, adequate for regulatory purposes. Study for quality control showed acceptable accuracy and precision. This method does not require any sample preparation and purification and potentially could be widely applied for high speed and high throughput analysis for product inspection.

This work was done at the early stage of my Ph.D. study, since then paper capillary spray has been developed into sample cartridges by PURSPEC Technologies. With the mass production of such simple yet powerful sample cartridges, we can envision that the adoption of such technologies could become much easier for a broad range of users. Another potential benefit of the standardization of paper capillary spray is the improvement of analytical figures of merits, especially for quantitative application where reproducibility is very important. The application of such technology is not limited to wine analysis or food safety issues, other examples may include forensics (*e.g.* drug control) and healthcare (*e.g.* therapeutic drug monitoring).

CHAPTER 6. DIRECT QUANTITATION OF TENOFOVIR DIPHOSPHATE IN HUMAN WHOLE BLOOD FOR ADHERENCE MONITORING

A version of this chapter has been submitted for publication.

6.1 Introduction

HIV remains a major threat to human health. In 2017, 1.8 million people became newly infected with HIV worldwide¹²³. Oral emtricitabine and tenofovir disoproxil fumarate (FTC-TDF) could provide protection against acquisition of HIV (preexposure chemoprophylaxis, PrEP) when the patient is adherent to a daily dosing regimen.¹²⁴ Commonly used methods for assessing adherence such as self-reporting or pill counting can be inaccurate due to human factors¹²⁵, thus direct measurement of drug concentrations in patients' blood (therapeutic drug monitoring, TDM) may be more reliable due to its objectiveness. For adherence monitoring for PrEP, the direct measurement of tenofovir can be performed, however, the result may still be biased because it only reflect the most recent dose: a patient can be non-adherence in between clinic visits and the measurement would still show he/she is adherence (“white coat” adherence).

Our collaborators at University of Colorado at Denver have identified and established concentration of tenofovir diphosphate (TDP) in red blood cells, a major metabolite of tenofovir, as an indicator of cumulative adherence.¹²⁶ It was found that TDP has a long half-life time of 17 days in red blood cells (RBC), and it will accumulate with repeated dosing. A simulated result indicates that by measuring TDP concentrations in RBCs, it is possible to differentiate dosing patterns, which suggests that the measurement of TDP concentration in RBCs could be used for monitoring of patient adherence in PrEP programs.

The current analytical method developed for the measurement of intracellular TDP involves collection of whole blood samples on dried blood spots (DBS), multiple solid-phase extractions, enzyme treatment, preconcentration and LC-MS/MS analysis^{126, 127}, making the whole process very time-consuming and expensive. Even though reliable quantitative results can be obtained, the expertise and facilities required to carry out such measurements may be a hurdle for broader adoption. In this work, we developed a method that could be potentially used to directly quantify TDP in whole blood in a significantly shortened time and at a lower cost.

6.2 Experimental

6.2.1 Materials and chemicals

Whatman 31 ET papers and 3 mm Harris Uni-Core Punch were purchased from Sigma-Aldrich. Vivid plasma membrane (VPM, Grade GF) and CytoSep membrane (Grade 1660) were purchased from Pall Corporation. TDP and stable isotope labeled ¹³C-TDP were purchased from Moravek, Inc, their chemical structures are shown in Figure 6.1. Human whole blood was purchased from Innovative Research, Inc. Borosilicate glass capillaries were purchased from Sutter Instruments and pulled into nanotips using P-97 tip puller (Sutter Instruments). All solvents and other chemicals were purchased from Fischer Scientific.

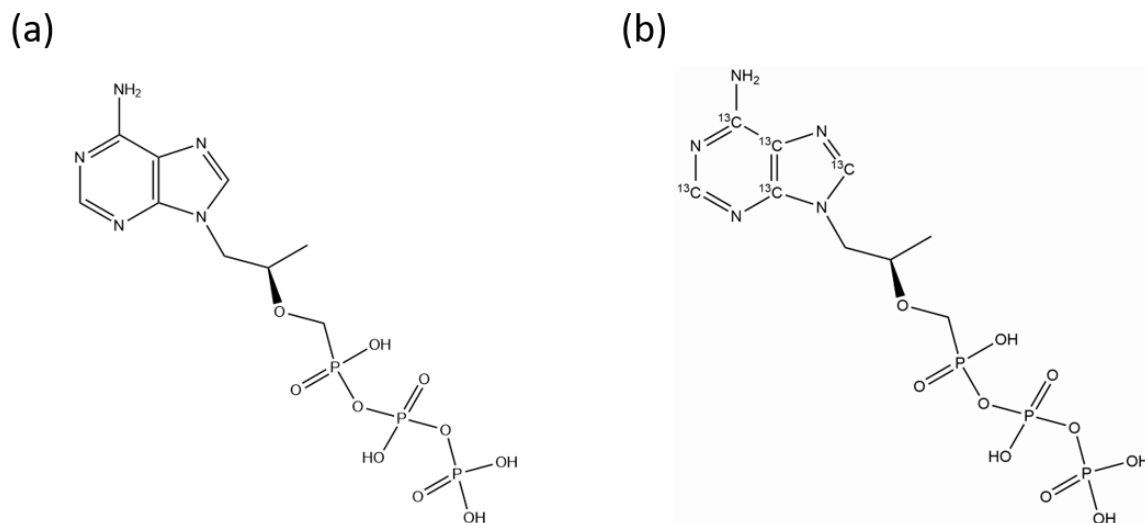


Figure 6.1 Chemical structures of TDP and stable isotope labeled ^{13}C -TDP

6.2.2 Plasma separation with membranes

The procedure for plasma separation and spiking samples are shown in Figure 6.2 (using VPM as example). For plasma separation with VPM, VPM is placed on top of another layer of 31ET with the rough side facing up. 5 μL of whole blood is then dispensed on top of the VPM, the 31ET should wick away the excess amount of plasma. A 3 mm circle is then punched from each 5 μL blood spot and spiked with 2 μL TDP in 70:30 methanol/water (v/v, abbreviated as 7M3H) at appropriate concentration. Each 3 mm circle will be placed in a 1.5 mL Eppendorf tube pre-loaded with 50 μL of solvent (for example, 70:30 acetonitrile/water, v/v, abbreviated as 7A3H) containing 90 ng/mL internal standard (^{13}C -TDP). The tubes are allowed to extract for 30 mins, which will also lyse the cells. After extraction, 3 extracts from the same sample is pooled together, then 10 μL of the pooled extract will be loaded to a nanotip for MS analysis. The pooling step can significantly improve reproducibility by reducing variations in extraction efficiency and other human errors. For plasma separation with CytoSep, the procedure is similar except that it does not require 31ET paper.

The procedure for processing real patient sample is simpler because it does not require spiking with standards. Whole blood samples will be collected on the plasma separation membrane and punched, then directly extracted in solvent for nESI.

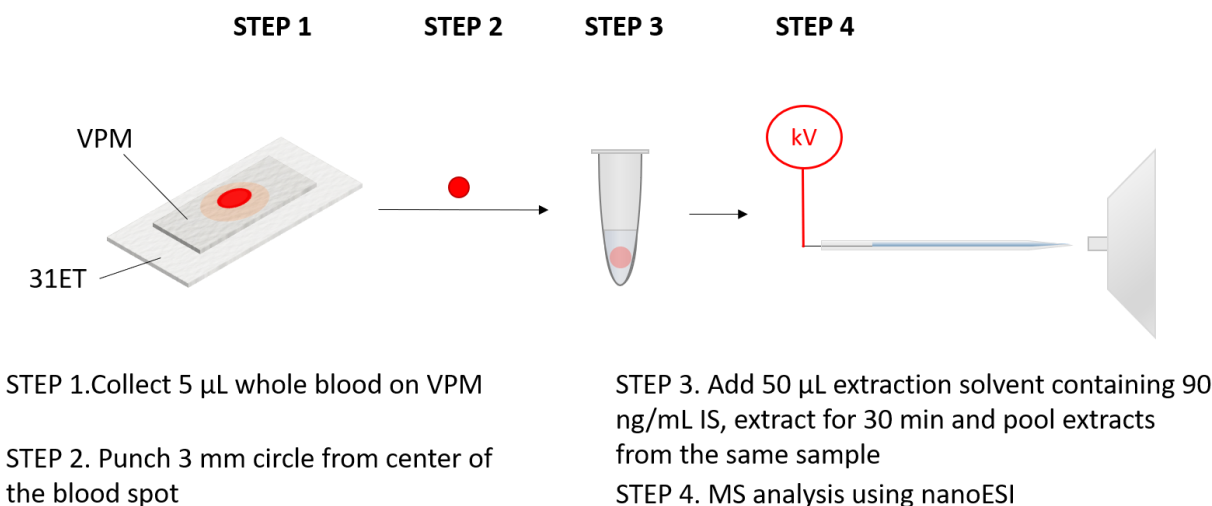


Figure 6.2 Direct analysis of TDP in whole blood by filtration of plasma with VPM.

6.2.3 MS analysis

TSQ Quantum Access Max from Thermo Fisher Scientific was used to perform all MS analysis. Standard TDP and ^{13}C -TDP solutions were nanosprayed directly to MS to perform in-software auto-optimization. MRM method was established based-on the optimized parameters. The transitions used in the MRM method were m/z 222.5 to m/z 366 and 348 for TDP and m/z 225 to m/z 371 and 353 for ^{13}C -TDP. Singly charged TDP and ^{13}C -TDP are less intensive so they are not chosen. The transitions used for quantitation are listed in Table 6.1.

Table 6.1 MRM transitions used for quantitation.

Compound	Precursor ion m/z	Product ion m/z	CE	Tube Lens
TDP	222.5 (doubly charged)	366.0	12	31
¹³C-TDP	225.0 (doubly charged)	371.0	16	31

6.3 Results and discussions

6.3.1 Considerations for direct MS analysis of TDP

nESI was performed using a rather concentrated TDP solution of 3.8 $\mu\text{g/mL}$ in 7M3H in negative mode. Full MS spectrum (range m/z 50-460) is shown in Figure 6.3. The most intense peaks are m/z 222.5 and 446, corresponding to doubly charged and singly charged TDP, respectively. This can be attributed to the multiple phosphate groups on TDP (chemical structure is shown in Figure 6.1). Although we did not find this complication to affect our quantitative performance, it is important to keep in mind that this charge state may vary depending on instrument conditions, thorough validation is necessary when transferring the method to a new instrument. In addition to the rather complexed charge state introduced by the phosphate groups, they also make the compound very hydrophilic, therefore it would be challenging to extract from blood with organic solvent due to their low partition in organic phase (negative logP).

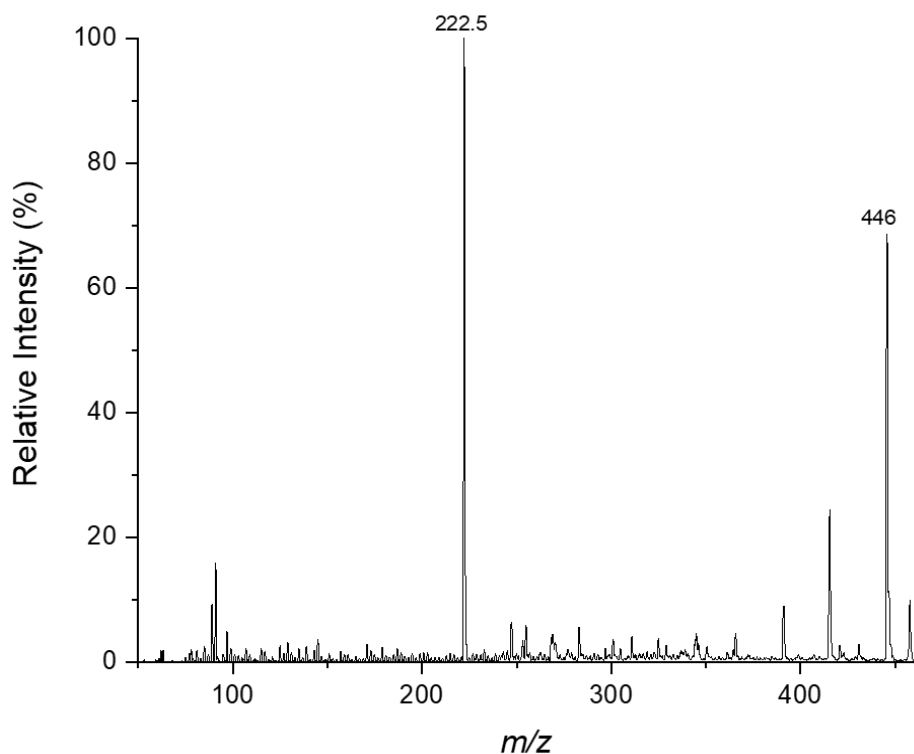


Figure 6.3 Full MS of TDP solution nanosprayed in negative mode.

Another challenge for direct analysis of TDP in whole blood is the severe matrix effect. We spiked high concentrations of TDP (ppm levels) into human whole blood and explored a variety of direct analysis methods, including extraction nESI²⁷, paper spray⁷ and SFME¹³. Although these methods have been proven to be powerful for blood analysis of many other drugs, they do not work well for TDP. Besides the possible reason of low extraction efficiency, we found that the signal intensity of TDP is very susceptible to presence of salt in the final spray solution (Figure 6.4). To illustrate this, NaCl was added to 1 $\mu\text{g/mL}$ TDP solutions (solvent: 7M3H) at 0.06% and 0.6% wt and the solutions were directly used for nESI analysis and repeated twice under each condition using different nanotips to eliminate the effect from possible defective nanotips.

MS/MS transition of m/z 222.5 to 366 was selected to compare the absolute intensities under different conditions. Without the presence of NaCl, the signal intensity reaches 10^6 levels. With addition of 0.06% NaCl, the absolute intensity dropped 3 orders of magnitudes to 10^3 levels; addition of 0.6% NaCl almost completely suppressed the signal. As whole blood is a salty matrix, this indicates that desalting will be a crucial step for direct TDP analysis.

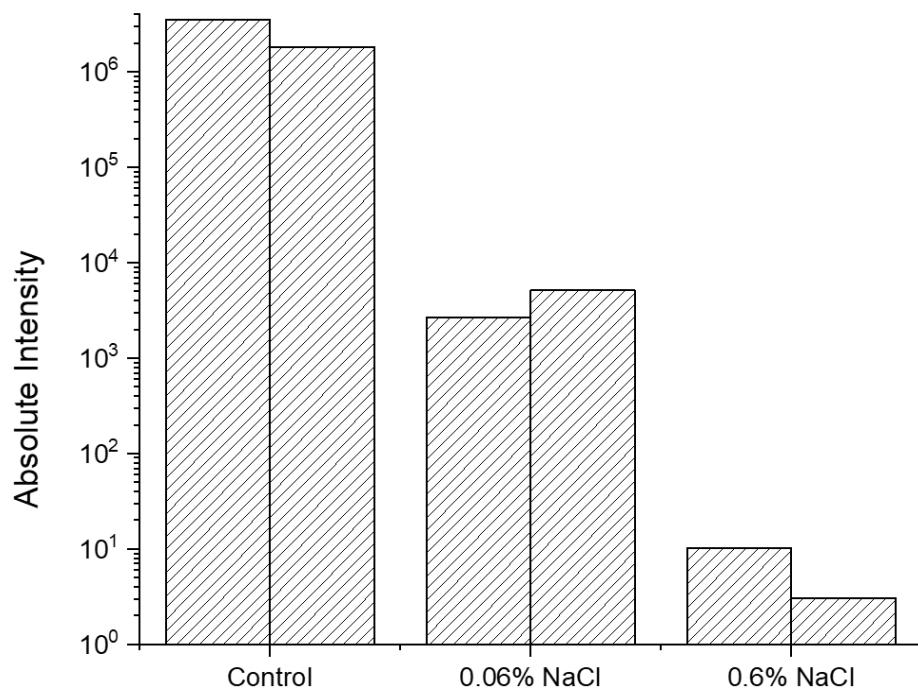


Figure 6.4 Effect of added NaCl on TDP in nESI. Repeated twice under each condition.

6.3.2 Direct analysis of TDP by plasma separation with membranes

Because long half-life TDP mainly exist in RBCs, preserving RBCs during desalting may be advantageous. Membrane filters (VPM and CytoSep) are available for separation of plasma from whole blood, these membrane filters can be easily repurposed for collection of blood cells and

filtering out plasma. As plasma dissolves most salt in whole blood, this could help clean up the sample for direct MS analysis. VPM has an asymmetric pore size distribution along the vertical direction, so blood cells will be trapped inside the pores while liquid and small molecules will pass through to the next layer (a 31ET filter paper) or spread out on the VPM. VPM is made of polysulfone, which is hydrophobic hence theoretically has low retention to TDP. CytoSep is made of a fibrous material that retains RBCs on the surface while plasma move through the matrix, some hemolysis can be expected during separation of CytoSep.

For separation with VPM, 5 μL of human whole blood was dispensed onto VPM with a layer of 31ET placed underneath, the blood would be quickly absorbed into VPM and plasma would spread out (Figure 6.5). 3 mm punches could be taken easily even without drying the blood spots. The blood cells from 5 μL whole blood occupied a circular space with a diameter slightly larger than 3mm, hence perfect for making 3mm punches without wasting blood samples. Simulated samples were made by spiking 2 μL of TDP onto 3mm punches before adding 50 μL extraction solvent. The extraction solvent contains 90 ng/mL stable isotope labeled ^{13}C -TDP as internal standard (TDP-IS). The spiking procedure is similar when using CytoSep for plasma separation.



Figure 6.5 Plasma separation with VPM.

Extraction with pure water, methanol or mixture of methanol/water turned out to be inappropriate, because blood cell debris would also be washed off the punches, rendering the extraction solution too dirty for nESI and resulting severe clogging issues. Although filtration may help alleviate the issue, this introduces an extra step while also increases the loss of analytes. Acetonitrile was found to be able to yield clean extracts, as TDP is very hydrophilic, water was mixed with acetonitrile to improve extraction efficiency; however, too much water will yield dirty extract again. The best solvent mixture was found to be 7A3H.

To investigate the signal improvement after plasma separation, one 3mm punch from DBS made on either 31ET, VPM or CytoSep was placed in 50 μL 1 $\mu\text{g}/\text{mL}$ TDP solutions and vortexed for 2 min, then 10 μL of each solution was loaded to nanotip to perform nESI. A pure TDP solution of same concentration was also analyzed as a reference. As is shown in Figure 6.6, ion suppression still exists after plasma separation. However, the signal was improved for *ca.* 5 times comparing with using 31ET alone. Total ion chromatograms shown in Figure 6.7 indicate the signal intensities were stable for at least one minute with plasma separation using CytoSep or VPM, but not stable without plasma separation in the case of 31ET. Because the possibility of hemolysis (destruction

of the RBCs) and the difficulty we experienced in cutting 3mm punches from CytoSep (due to the special material), VPM was chosen to perform the preliminary quantitative study.

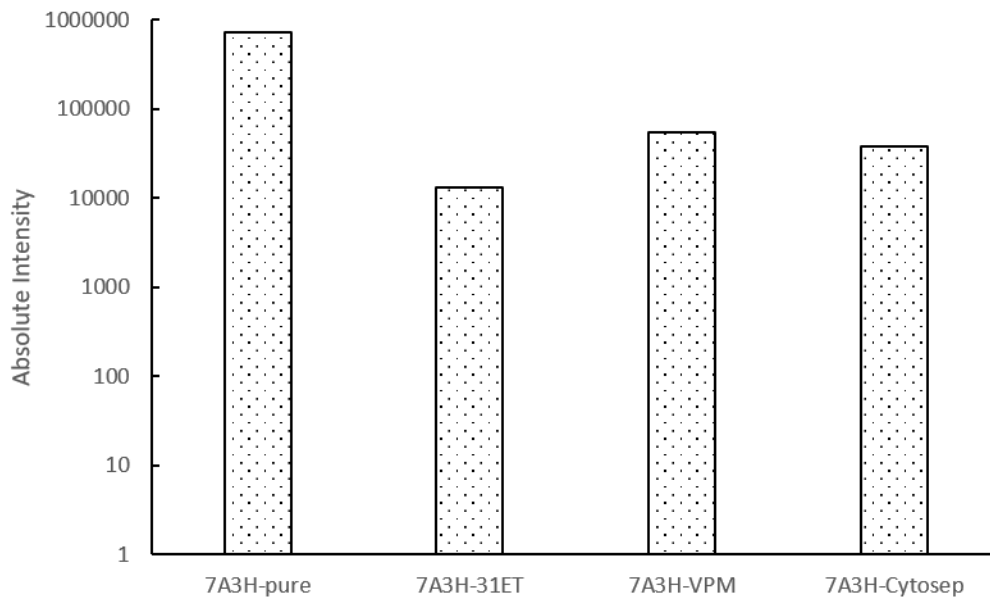


Figure 6.6 Ion suppression from blood samples (intensities are on log scales).

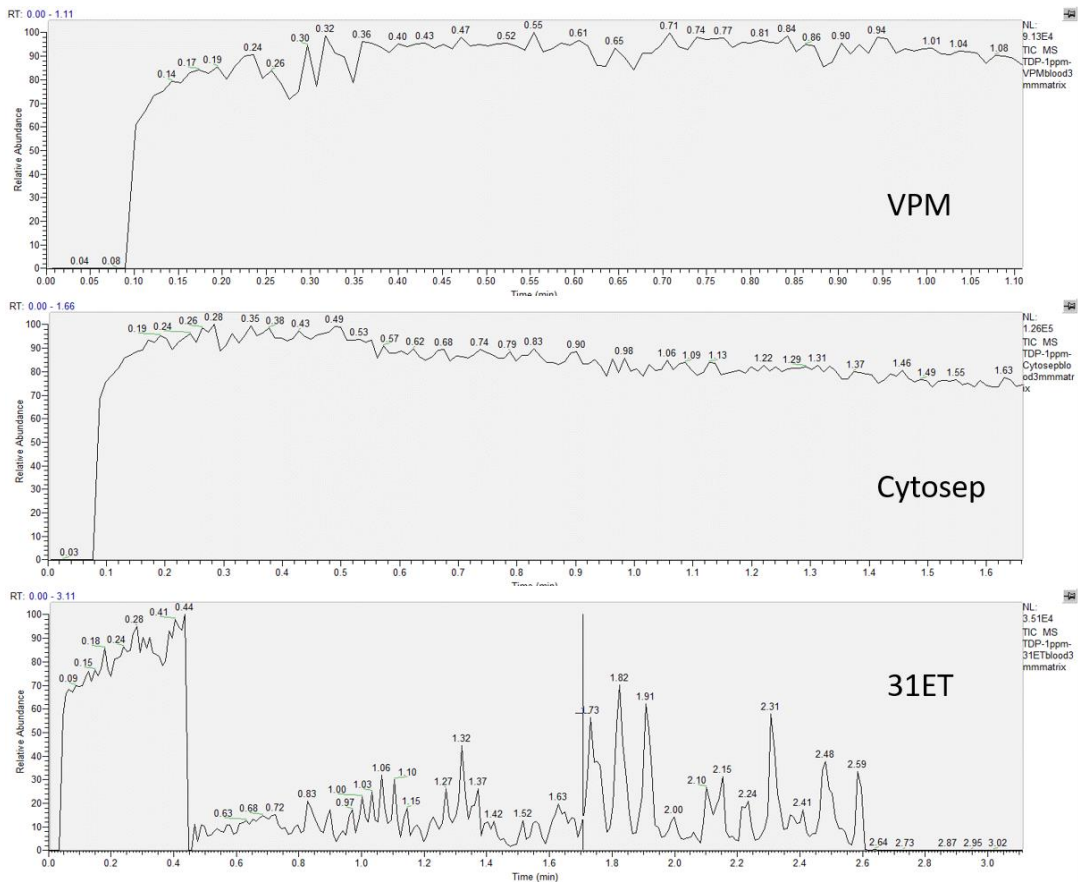


Figure 6.7 Comparison of total ion chromatograms.

6.3.3 Direct quantitation of simulated whole blood samples by plasma separation using VPM

Quantitative performance was explored by establishing a calibration curve using VPM to perform plasma separation (Figure 6.8). To establish the calibration curve, 3 different pooled samples were analyzed at each concentration. The concentration unit used here is fmol/punch to reflect the amount of TDP on each 3mm punch and facilitate the correlation with published results. The calibration standards had concentrations of 170.2 fmol/punch, 683.15 fmol/punch, 1366.3 fmol/punch and 3415.7 fmol/punch. It was reported in a simulation study that TDP concentration in DBS corresponding to adherence to daily dosing is approximately 1250 fmol/punch at steady-state (high); above 700 fmol/punch is associated with 4 or more tablets per week (medium); 350-

699 fmol/punch is associated with 2 or 3 tablets per week (low); and below detection limits or lower than 349 fmol/punch is associated with fewer than 2 tablets per week (non-adherent).¹²⁷ We draw three lines at 350 fmol/punch, 700 fmol/punch and 1250 fmol/punch in the calibration curve to show the critical thresholds. The LLOQ was estimated to be 296 fmol/punch (calculated from 10 times the area ratio of blank using calibration curve). The calibration curve covers the entire range of different doses, indicating that it can potentially be used for adherence monitoring. Two QC samples were prepared at concentrations of 341.6 fmol/punch (QC1) and 1707.9 fmol/punch (QC2), the calculated concentrations based on calibration were 421.6 fmol/punch and 1956.8 fmol/punch, respectively. This represent an accuracy of 23.4% at around LOQ and 14.6% at higher concentration. RSDs among replica (n=3) were 5.3% for QC1 and 5.2 % for QC2.

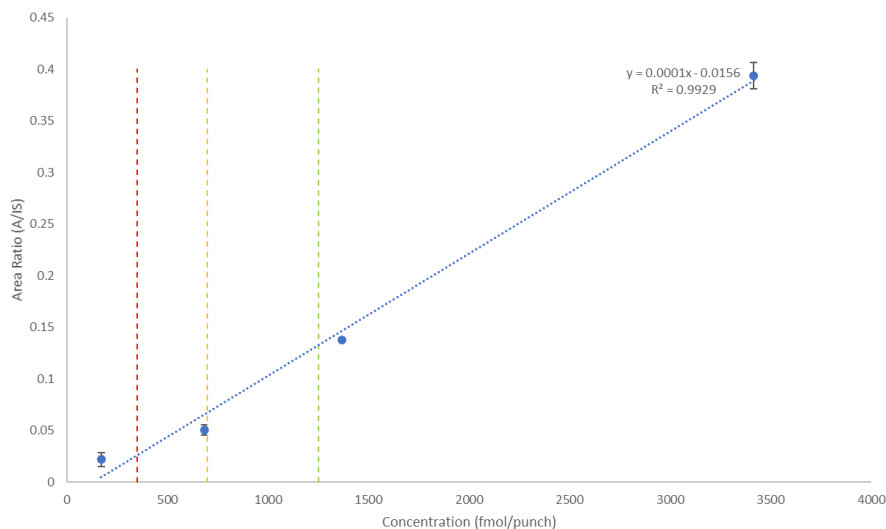


Figure 6.8 Calibration curve with VPM for plasma separation, n=4. Red line: 350 fmol/punch; yellow line: 700 fmol/punch; green line: 1250 fmol/punch.

Sample storage conditions and stability were examined. Equivalent of 3410 fmol/punch of TDP was spiked in the 3mm punches, and stored in Eppendorf tubes at different conditions for certain periods of time. These VPM blood spots were stored at room temperature (RT), 4 °C and -

20 °C. In the following days, these 3mm punches were taken out and extracted following the procedure described above, the TDP/¹³C-TDP ratios were used to assess the degradation of TDP (90 ng/mL ¹³C-TDP 7A3H solution was store at -20 °C). The results is shown in Figure 6.9. Apparently -20 °C is necessary to stablize TDP in blood spots: TDP concentration was stable at -20 °C for at least 4 days. This means dry spots need to be transported on dry ice and stored at -20 °C before analysis.

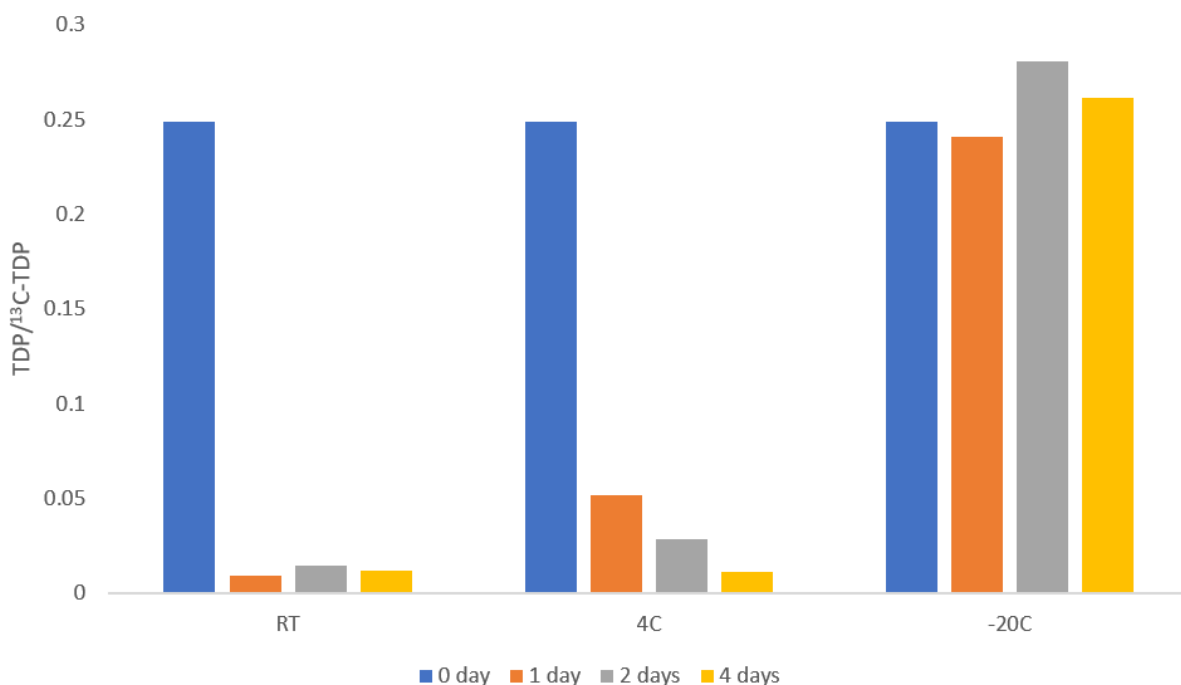


Figure 6.9 Stability test for storage conditions of VPM blood spots.

6.3.4 Method validation with human subject samples

5 human subject samples were collected on VPM at University of Colorado Denver and shipped to Purdue. The TDP concentration of these samples were determined using the established LC-MS/MS method at University of Colorado Denver and summarized in Table 6.2 as “TDP concentration”. Initial tests showed that signal from TDP can be consistently obtained, however,

the A/IS ratio has a great variability within each sample (data not presented). RSD was significantly improved by pooling extracted samples before MS analysis (below 15% for all samples, n = 4). We calculated the concentrations of these samples based on our calibration curve using our methodology, the results are listed in Table 6.2 as “calculated concentration”. Apparently the concentrations obtained using our method consistently underestimate the real concentration, which is expected by us: the calibration curve was established by spiking samples onto blood spots, which is not an accurate representation of real samples because a higher level of sample recovery can be expected from the simulated samples than real samples. We believe it is better to directly correlate the area ratios obtained using our method with LC-MS/MS data or doses for the purpose of adherence monitoring. As shown in Figure 6.10, a very good linear relationship can be established between our results and the LC-MS/MS results ($R^2 = 0.9962$).

Table 6.2 Concentrations of patient samples

Patient ID	TDP Concentration (fmol/punch)	Adherence Level	Calculated Concentration (fmol/punch)
1	1297	High	1055
2	1021	High	947
3	2977	High	2190
4	671	Medium	630
5	1754	High	1345

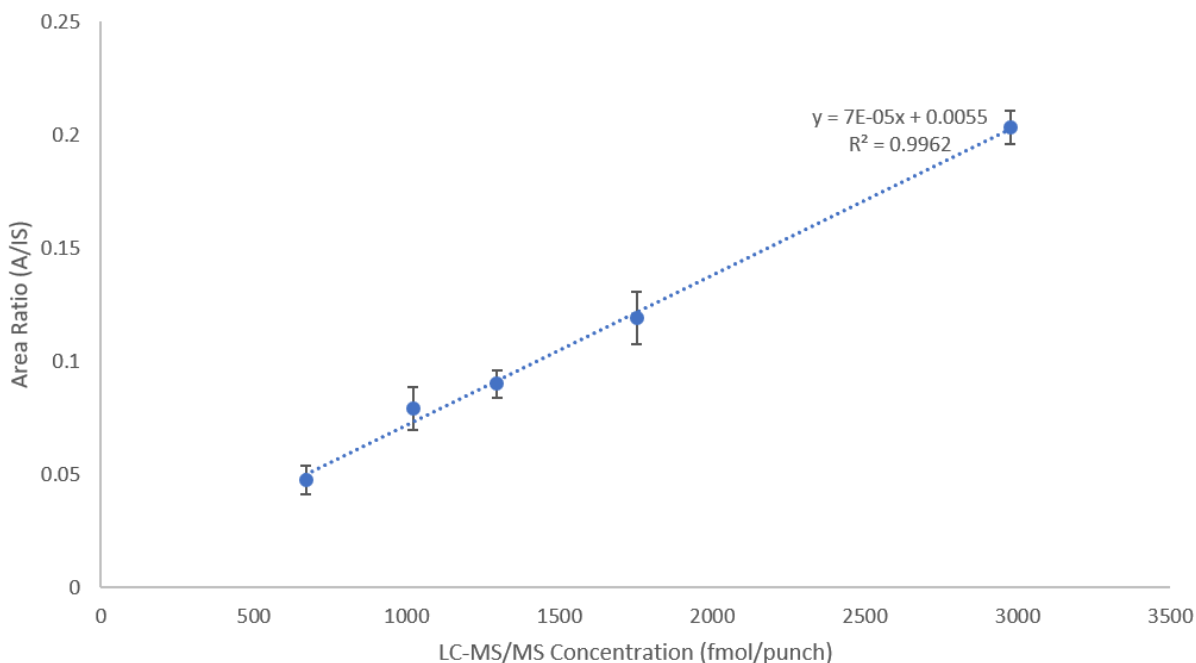


Figure 6.10 Correlation of quantitative results from direct MS analysis using VPM with quantitative results from established LC-MS/MS method.

6.4 Conclusions and future perspectives

We have developed a method for direct quantitation of TDP in whole blood. We found that TDP is sensitive to salt, therefore plasma separation was carried out to mitigate ion suppression. Plasma separation was realized using specialized membrane filters (VPM or CytoSep) and retained blood cells were lysed for direct MS analysis using nESI. With VPM, we demonstrated that the method is quantitative and could potentially be used for adherence monitoring by measuring TDP. The method is simple, fast, cost-effective and only takes microliters of whole blood for analysis, therefore fingerstick may be used for blood collection.

The assumptions of the current study with simulated samples are that blood cells are 100% lysed and no cells are lost during plasma separation. For real samples this may not be true, hence the measured concentrations are underestimated if based on calibration with simulated samples.

Considering that there could also be errors introduced during standard spiking, a preferred way of carrying out the study for the purpose of adherence assessment would be establishing a direct correlation of response levels (area ratios) to concentrations obtained using the validated method. By directly correlating the quantitation results with those obtained from LC-MS/MS method, we were able to assess patient dosage regime without the need of making calibration curves with spiked samples. To further validate the current methodology, more samples with different adherence levels need to be collected and analyzed.

Besides direct analysis of TDP, the plasma separation method developed here could also be used for fast analysis of other intracellular compounds in blood cells. such as therapeutic nucleotide analogs¹²⁸.

REFERENCES

1. R. G. Cooks, Z. Ouyang, Z. Takats and J. M. Wiseman, *Science*, 2006, **311**, 1566-1570.
2. Z. Takats, J. M. Wiseman, B. Gologan and R. G. Cooks, *Science*, 2004, **306**, 471-473.
3. R. B. Cody, J. A. Laramée and H. D. Durst, *Analytical chemistry*, 2005, **77**, 2297-2302.
4. N. Na, M. Zhao, S. Zhang, C. Yang and X. Zhang, *Journal of the American Society for Mass Spectrometry*, 2007, **18**, 1859-1862.
5. J. D. Harper, N. A. Charipar, C. C. Mulligan, X. Zhang, R. G. Cooks and Z. Ouyang, *Analytical chemistry*, 2008, **80**, 9097-9104.
6. J. Liu, H. Wang, N. E. Manicke, J. M. Lin, R. G. Cooks and Z. Ouyang, *Analytical chemistry*, 2010, **82**, 2463-2471.
7. H. Wang, J. Liu, R. G. Cooks and Z. Ouyang, *Angewandte Chemie*, 2010, **49**, 877-880.
8. P. J. Roach, J. Laskin and A. Laskin, *The Analyst*, 2010, **135**, 2233-2236.
9. G. A. Harris, A. S. Galhena and F. M. Fernandez, *Analytical chemistry*, 2011, **83**, 4508-4538.
10. C. L. Feider, A. Krieger, R. J. DeHoog and L. S. Eberlin, *Analytical chemistry*, 2019, **91**, 4266-4290.
11. M. E. Monge, G. A. Harris, P. Dwivedi and F. M. Fernandez, *Chemical reviews*, 2013, **113**, 2269-2308.
12. F. Pu, S. Chiang, W. Zhang and Z. Ouyang, *The Analyst*, 2019, **144**, 1034-1051.
13. Y. Ren, M. N. McLuckey, J. Liu and Z. Ouyang, *Angewandte Chemie*, 2014, **53**, 14124-14127.
14. G. A. Gomez-Rios and J. Pawliszyn, *Angewandte Chemie*, 2014, **53**, 14503-14507.
15. K. E. Yannell, K. R. Kesely, H. D. Chien, C. B. Kissinger and R. G. Cooks, *Analytical and bioanalytical chemistry*, 2017, **409**, 121-131.
16. J. M. Wiseman, C. A. Evans, C. L. Bowen and J. H. Kennedy, *The Analyst*, 2010, **135**, 720.
17. H. Piri-Moghadam, F. Ahmadi, G. A. Gomez-Rios, E. Boyaci, N. Reyes-Garces, A. Aghakhani, B. Bojko and J. Pawliszyn, *Angewandte Chemie*, 2016, **55**, 7510-7514.

18. G. A. Gomez-Rios, N. Reyes-Garces, B. Bojko and J. Pawliszyn, *Analytical chemistry*, 2016, **88**, 1259-1265.
19. T. Wang, Y. Zheng, X. Wang, D. E. Austin and Z. Zhang, *Analytical chemistry*, 2017, **89**, 7988-7995.
20. C. Wu, A. L. Dill, L. S. Eberlin, R. G. Cooks and D. R. Ifa, *Mass spectrometry reviews*, 2013, **32**, 218-243.
21. D. R. Ifa and L. S. Eberlin, *Clinical chemistry*, 2016, **62**, 111-123.
22. A. K. Jarmusch, V. Pirro, Z. Baird, E. M. Hattab, A. A. Cohen-Gadol and R. G. Cooks, *Proceedings of the National Academy of Sciences of the United States of America*, 2016, **113**, 1486-1491.
23. V. Pirro, C. M. Alfaro, A. K. Jarmusch, E. M. Hattab, A. A. Cohen-Gadol and R. G. Cooks, *Proceedings of the National Academy of Sciences of the United States of America*, 2017, **114**, 6700-6705.
24. J. Balog, L. Sasi-Szabo, J. Kinross, M. R. Lewis, L. J. Muirhead, K. Veselkov, R. Mirnezami, B. Dezso, L. Damjanovich, A. Darzi, J. K. Nicholson and Z. Takats, *Science translational medicine*, 2013, **5**, 194ra193.
25. J. Zhang, J. Rector, J. Q. Lin, J. H. Young, M. Sans, N. Katta, N. Giese, W. Yu, C. Nagi, J. Suliburk, J. Liu, A. Bensussan, R. J. DeHoog, K. Y. Garza, B. Ludolph, A. G. Sorace, A. Syed, A. Zahedivash, T. E. Milner and L. S. Eberlin, *Science translational medicine*, 2017, **9**.
26. Y. Ren, S. Chiang, W. Zhang, X. Wang, Z. Lin and Z. Ouyang, *Analytical and bioanalytical chemistry*, 2016, **408**, 1385-1390.
27. Y. Ren, J. Liu, L. Li, M. N. McLuckey and Z. Ouyang, *Anal Methods*, 2013, **5**.
28. H. Wang, N. E. Manicke, Q. Yang, L. Zheng, R. Shi, R. G. Cooks and Z. Ouyang, *Analytical chemistry*, 2011, **83**, 1197-1201.
29. N. E. Manicke, P. Abu-Rabie, N. Spooner, Z. Ouyang and R. G. Cooks, *Journal of the American Society for Mass Spectrometry*, 2011, **22**, 1501-1507.
30. Z. Zhang, R. G. Cooks and Z. Ouyang, *The Analyst*, 2012, **137**, 2556-2558.
31. Z. Ouyang and R. G. Cooks, *Annual review of analytical chemistry*, 2009, **2**, 187-214.
32. D. T. Snyder, C. J. Pulliam, Z. Ouyang and R. G. Cooks, *Analytical chemistry*, 2016, **88**, 2-29.
33. Z. Ouyang, G. Wu, Y. Song, H. Li, W. R. Plass and R. G. Cooks, *Analytical chemistry*, 2004, **76**, 4595-4605.

34. L. S. Riter, Y. Peng, R. J. Noll, G. E. Patterson, T. Aggerholm and R. G. Cooks, *Analytical chemistry*, 2002, **74**, 6154-6162.
35. G. E. Patterson, A. J. Guymon, L. S. Riter, M. Everly, J. Griep-Raming, B. C. Laughlin, Z. Ouyang and R. G. Cooks, *Analytical chemistry*, 2002, **74**, 6145-6153.
36. J. C. Schwartz, M. W. Senko and J. E. P. Syka, *Journal of the American Society for Mass Spectrometry*, 2002, **13**, 659-669.
37. J. W. Hager, *Rapid Communications in Mass Spectrometry*, 2002, **16**, 512-526.
38. L. Gao, R. G. Cooks and Z. Ouyang, *Analytical chemistry*, 2008, **80**, 4026-4032.
39. L. Gao, Q. Song, G. E. Patterson, R. G. Cooks and Z. Ouyang, *Analytical chemistry*, 2006, **78**, 5994-6002.
40. L. Gao, A. Sugiarto, J. D. Harper, R. G. Cooks and Z. Ouyang, *Analytical chemistry*, 2008, **80**, 7198-7205.
41. L. Li, T. C. Chen, Y. Ren, P. I. Hendricks, R. G. Cooks and Z. Ouyang, *Analytical chemistry*, 2014, **86**, 2909-2916.
42. P. I. Hendricks, J. K. Dalglish, J. T. Shelley, M. A. Kirleis, M. T. McNicholas, L. Li, T. C. Chen, C. H. Chen, J. S. Duncan, F. Boudreau, R. J. Noll, J. P. Denton, T. A. Roach, Z. Ouyang and R. G. Cooks, *Anal Chem*, 2014, **86**, 2900-2908.
43. X. Wang, Ph.D. Dissertation/Thesis, Purdue University, 2017.
44. X. Liu, X. Wang, J. Bu, X. Zhou and Z. Ouyang, *Analytical chemistry*, 2019, **91**, 1391-1398.
45. D. T. Snyder, L. J. Szalwinski, R. Hilger and R. G. Cooks, *Journal of the American Society for Mass Spectrometry*, 2018, **29**, 1355-1364.
46. D. T. Snyder, C. J. Pulliam and R. G. Cooks, *International Journal of Mass Spectrometry*, 2017, **422**, 154-161.
47. Y. Zhai, Y. Feng, Y. Wei, Y. Wang and W. Xu, *The Analyst*, 2015, **140**, 3406-3414.
48. T. Jiang, Q. Xu, H. Zhang, D. Li and W. Xu, *Analytical chemistry*, 2018, **90**, 11671-11679.
49. Y. Zhai, Q. Xu, Y. Tang, S. Liu, D. Li and W. Xu, *Analytical chemistry*, 2019, **91**, 7911-7919.
50. Y. Zhai, X. Zhang, H. Xu, Y. Zheng, T. Yuan and W. Xu, *Analytical chemistry*, 2017, **89**, 4177-4183.

51. S. Gerbig, S. Neese, A. Penner, B. Spengler and S. Schulz, *Analytical chemistry*, 2017, **89**, 10717-10725.
52. S. Soparawalla, F. K. Tadjimukhamedov, J. S. Wiley, Z. Ouyang and R. G. Cooks, *The Analyst*, 2011, **136**, 4392-4396.
53. C. J. Pulliam, R. M. Bain, H. L. Osswald, D. T. Snyder, P. W. Fedick, S. T. Ayrton, T. G. Flick and R. G. Cooks, *Analytical chemistry*, 2017, **89**, 6969-6975.
54. R. Zou, W. Cao, L. Chong, W. Hua, H. Xu, Y. Mao, J. Page, R. Shi, Y. Xia, T. Y. Hu, W. Zhang and Z. Ouyang, *Analytical chemistry*, 2019, **91**, 1157-1163.
55. C. J. Pulliam, P. Wei, D. T. Snyder, X. Wang, Z. Ouyang, R. M. Pielak and R. Graham Cooks, *The Analyst*, 2016, **141**, 1633-1636.
56. A. E. Kirby, N. M. Lafreniere, B. Seale, P. I. Hendricks, R. G. Cooks and A. R. Wheeler, *Analytical chemistry*, 2014, **86**, 6121-6129.
57. F. Pu, W. Zhang, K. P. Bateman, Y. Liu, R. Helmy and Z. Ouyang, *Bioanalysis*, 2017, **9**, 1633-1641.
58. S. S. Singh, *Current drug metabolism*, 2006, **7**, 165-182.
59. P. Beaudette and K. P. Bateman, *Journal of chromatography. B, Analytical technologies in the biomedical and life sciences*, 2004, **809**, 153-158.
60. R. E. White and P. Manitpisitkul, *Drug metabolism and disposition: the biological fate of chemicals*, 2001, **29**, 957-966.
61. B. Liu, J. Chang, W. P. Gordon, J. Isbell, Y. Zhou and T. Tuntland, *Drug discovery today*, 2008, **13**, 360-367.
62. P. C. Gunaratna, P. T. Kissinger, C. B. Kissinger and J. F. Gitzen, *Journal of Pharmacological and Toxicological Methods*, 2004, **49**, 57-64.
63. P. Wong, R. Pham, C. Whitely, M. Soto, K. Salyers, C. James and B. A. Bruenner, *Journal of pharmaceutical and biomedical analysis*, 2011, **56**, 604-608.
64. F. Royo, N. Bjork, H. Carlsson, S. Mayo and J. Hau, *Journal of Endocrinology*, 2004, **180**, 145-153.
65. W. A. Korfmacher, *Drug discovery today*, 2005, **10**, 1357-1367.
66. Y. Su, H. Wang, J. Liu, P. Wei, R. G. Cooks and Z. Ouyang, *Analyst*, 2013, **138**, 4443-4447.
67. J. Liu, R. G. Cooks and Z. Ouyang, *Analytical chemistry*, 2013, **85**, 5632-5636.

68. Y. Ren, W. Zhang, Z. Lin, L. R. Bushman, P. L. Anderson and Z. Ouyang, *Talanta*, 2018, **189**, 451-457.
69. W. Zhang, Y. Ren, Z. Lin and Z. Ouyang, *Analytical chemistry*, 2019, **91**, 6986-6990.
70. W. Zhang, S. Chiang, Z. Li, Q. Chen, Y. Xia and Z. Ouyang, *Angewandte Chemie*, 2019, **58**, 6064-6069.
71. V. P. Shah, K. K. Midha, J. W. Findlay, H. M. Hill, J. D. Hulse, I. J. McGilveray, G. McKay, K. J. Miller, R. N. Patnaik and M. L. Powell, *Pharm. Res.*, 2000, **17**, 1551-1557.
72. F. Pu, C. M. Alfaro, V. Pirro, Z. Xie, Z. Ouyang and R. G. Cooks, *Analytical and bioanalytical chemistry*, 2019, **411**, 1503-1508.
73. Q. T. Ostrom, H. Gittleman, P. Liao, T. Vecchione-Koval, Y. Wolinsky, C. Kruchko and J. S. Barnholtz-Sloan, *Neuro-oncology*, 2017, **19**, v1-v88.
74. D. N. Louis, A. Perry, G. Reifenberger, A. von Deimling, D. Figarella-Branger, W. K. Cavenee, H. Ohgaki, O. D. Wiestler, P. Kleihues and D. W. Ellison, *Acta neuropathologica*, 2016, **131**, 803-820.
75. H. Yan, D. W. Parsons, G. Jin, R. McLendon, B. A. Rasheed, W. Yuan, I. Kos, I. Batinic-Haberle, S. Jones, G. J. Riggins, H. Friedman, A. Friedman, D. Reardon, J. Herndon, K. W. Kinzler, V. E. Velculescu, B. Vogelstein and D. D. Bigner, *The New England journal of medicine*, 2009, **360**, 765-773.
76. C. Hartmann, B. Hentschel, W. Wick, D. Capper, J. Felsberg, M. Simon, M. Westphal, G. Schackert, R. Meyermann, T. Pietsch, G. Reifenberger, M. Weller, M. Loeffler and A. von Deimling, *Acta neuropathologica*, 2010, **120**, 707-718.
77. J. C. Buckner, E. G. Shaw, S. L. Pugh, A. Chakravarti, M. R. Gilbert, G. R. Barger, S. Coons, P. Ricci, D. Bullard, P. D. Brown, K. Stelzer, D. Brachman, J. H. Suh, C. J. Schultz, J. P. Bahary, B. J. Fisher, H. Kim, A. D. Murtha, E. H. Bell, M. Won, M. P. Mehta and W. J. Curran, Jr., *The New England journal of medicine*, 2016, **374**, 1344-1355.
78. G. Cairncross, M. Wang, E. Shaw, R. Jenkins, D. Brachman, J. Buckner, K. Fink, L. Souhami, N. Laperriere, W. Curran and M. Mehta, *Journal of clinical oncology : official journal of the American Society of Clinical Oncology*, 2013, **31**, 337-343.
79. J. G. Cairncross, M. Wang, R. B. Jenkins, E. G. Shaw, C. Giannini, D. G. Brachman, J. C. Buckner, K. L. Fink, L. Souhami, N. J. Laperriere, J. T. Huse, M. P. Mehta and W. J. Curran, Jr., *Journal of clinical oncology : official journal of the American Society of Clinical Oncology*, 2014, **32**, 783-790.
80. J. Beiko, D. Suki, K. R. Hess, B. D. Fox, V. Cheung, M. Cabral, N. Shonka, M. R. Gilbert, R. Sawaya, S. S. Prabhu, J. Weinberg, F. F. Lang, K. D. Aldape, E. P. Sulman, G. Rao, I. E. McCutcheon and D. P. Cahill, *Neuro-oncology*, 2014, **16**, 81-91.

81. L. Dang, D. W. White, S. Gross, B. D. Bennett, M. A. Bittinger, E. M. Driggers, V. R. Fantin, H. G. Jang, S. Jin, M. C. Keenan, K. M. Marks, R. M. Prins, P. S. Ward, K. E. Yen, L. M. Liao, J. D. Rabinowitz, L. C. Cantley, C. B. Thompson, M. G. Vander Heiden and S. M. Su, *Nature*, 2009, **462**, 739-744.
82. J. J. Miller, H. A. Shih, O. C. Andronesi and D. P. Cahill, *Cancer*, 2017, **123**, 4535-4546.
83. O. C. Andronesi, G. S. Kim, E. Gerstner, T. Batchelor, A. A. Tzika, V. R. Fantin, M. G. Vander Heiden and A. G. Sorensen, *Science translational medicine*, 2012, **4**, 116ra114.
84. C. Choi, S. K. Ganji, R. J. DeBerardinis, K. J. Hatanpaa, D. Rakheja, Z. Kovacs, X. L. Yang, T. Mashimo, J. M. Raisanen, I. Marin-Valencia, J. M. Pascual, C. J. Madden, B. E. Mickey, C. R. Malloy, R. M. Bachoo and E. A. Maher, *Nature medicine*, 2012, **18**, 624-629.
85. W. B. Pope, R. M. Prins, M. Albert Thomas, R. Nagarajan, K. E. Yen, M. A. Bittinger, N. Salamon, A. P. Chou, W. H. Yong, H. Soto, N. Wilson, E. Driggers, H. G. Jang, S. M. Su, D. P. Schenkein, A. Lai, T. F. Cloughesy, H. I. Kornblum, H. Wu, V. R. Fantin and L. M. Liao, *Journal of neuro-oncology*, 2012, **107**, 197-205.
86. R. B. Cody, J. A. Laramée and H. D. Durst, *Analytical chemistry*, 2005, **77**, 2297-2302.
87. R. M. Alberici, R. C. Simas, G. B. Sanvido, W. Romao, P. M. Lalli, M. Benassi, I. B. Cunha and M. N. Eberlin, *Analytical and bioanalytical chemistry*, 2010, **398**, 265-294.
88. H. Chen, G. Gamez and R. Zenobi, *Journal of the American Society for Mass Spectrometry*, 2009, **20**, 1947-1963.
89. S. Santagata, L. S. Eberlin, I. Norton, D. Calligaris, D. R. Feldman, J. L. Ide, X. Liu, J. S. Wiley, M. L. Vestal, S. H. Ramkissoon, D. A. Orringer, K. K. Gill, I. F. Dunn, D. Dias-Santagata, K. L. Ligon, F. A. Jolesz, A. J. Golby, R. G. Cooks and N. Y. Agar, *Proceedings of the National Academy of Sciences of the United States of America*, 2014, **111**, 11121-11126.
90. K. Margulis, A. S. Chiou, S. Z. Aasi, R. J. Tibshirani, J. Y. Tang and R. N. Zare, *Proceedings of the National Academy of Sciences of the United States of America*, 2018, **115**, 6347-6352.
91. H. Wang, N. E. Manicke, Q. Yang, L. Zheng, R. Shi, R. G. Cooks and Z. Ouyang, *Analytical chemistry*, 2011, **83**, 1197-1201.
92. J. Liu, R. G. Cooks and Z. Ouyang, *Anal Chem*, 2011, **83**, 9221-9225.
93. K. S. Kerian, A. K. Jarmusch and R. G. Cooks, *Analyst*, 2014, **139**, 2714-2720.
94. V. Pirro, R. S. Llor, A. K. Jarmusch, C. M. Alfaro, A. A. Cohen-Gadol, E. M. Hattab and R. G. Cooks, *Analyst*, 2017, **142**, 4058-4066.

95. J. Laskin, B. S. Heath, P. J. Roach, L. Cazares and O. J. Semmes, *Anal Chem*, 2012, **84**, 141-148.
96. F. Tang, C. Guo, X. Ma, J. Zhang, Y. Su, R. Tian, R. Shi, Y. Xia, X. Wang and Z. Ouyang, *Anal Chem*, 2018, **90**, 5612-5619.
97. C. M. Alfaro, V. Pirro, M. F. Keating, E. M. Hattab, R. G. Cooks and A. A. Cohen-Gadol, *Journal of neurosurgery*, 2019, DOI: 10.3171/2018.8.JNS181207, 1-8.
98. R. D. Espy, S. F. Teunissen, N. E. Manicke, Y. Ren, Z. Ouyang, A. van Asten and R. G. Cooks, *Anal Chem*, 2014, **86**, 7712-7718.
99. H. Nagashima, K. Tanaka, T. Sasayama, Y. Irino, N. Sato, Y. Takeuchi, K. Kyotani, A. Mukasa, K. Mizukawa, J. Sakata, Y. Yamamoto, K. Hosoda, T. Itoh, R. Sasaki and E. Kohmura, *Neuro-oncology*, 2016, **18**, 1559-1568.
100. K. E. Yannell, K. Smith, C. M. Alfaro, A. K. Jarmusch, V. Pirro and R. G. Cooks, *Clinical chemistry*, 2017, **63**, 1766-1767.
101. F. Pu, W. Zhang, C. Han and Z. Ouyang, *Analytical methods : advancing methods and applications*, 2017, **9**, 5058-5064.
102. H. Sierotzki and G. Scalliet, *Phytopathology*, 2013, **103**, 880-887.
103. A. Abad-Fuentes, E. Ceballos-Alcantarilla, J. V. Mercader, C. Agullo, A. Abad-Somovilla and F. A. Esteve-Turrillas, *Analytical and bioanalytical chemistry*, 2015, **407**, 4207-4211.
104. W. C. Andersen, S. B. Turnipseed, C. M. Karbiwnyk, S. B. Clark, M. R. Madson, C. A. Gieseke, R. A. Miller, N. G. Rummel and R. Reimschuessel, *J. Agric. Food Chem.*, 2008, **56**, 4340-4347.
105. J. L. M. Vidal, M. D. Aguilera-Luiz, R. Romero-Gonzalez and A. G. Frenich, *J. Agric. Food Chem.*, 2009, **57**, 1760-1767.
106. A. Gulkowska, I. J. Buerge and T. Poiger, *Analytical and bioanalytical chemistry*, 2014, **406**, 6419-6427.
107. H. Wang, J. Liu, R. G. Cooks and Z. Ouyang, *Angewandte Chemie*, 2010, **49**, 877-880.
108. C. Zhang and N. E. Manicke, *Anal. Chem.*, 2015, **87**, 6212-6219.
109. N. E. Manicke, P. Abu-Rabie, N. Spooner, Z. Ouyang and R. G. Cooks, *J. Am. Soc. Mass. Spectrom.*, 2011, **22**, 1501-1507.
110. A. Li, P. Wei, H. C. Hsu and R. G. Cooks, *Analyst*, 2013, **138**, 4624-4630.

111. I. Pereira, S. R. M. Rodrigues, T. C. de Carvalho, V. V. Carvalho, G. S. Lobón, J. F. P. Bassane, E. Domingos, W. Romão, R. Augusti and B. G. Vaz, *Anal. Methods*, 2016, **8**, 6023-6029.
112. T. Guo, P. Fang, J. Jiang, F. Zhang, W. Yong, J. Liu and Y. Dong, *Journal of chromatography. A*, 2016, **1471**, 27-33.
113. S. L. Reeber, S. Gadi, S.-B. Huang and G. L. Glish, *Anal. Methods*, 2015, **7**, 9808-9816.
114. B.-c. Yang, F. Wang, W. Deng, Y. Zou, F.-y. Liu, X.-d. Wan, X. Yang, H. Liu and O.-p. Huang, *Anal. Methods*, 2015, **7**, 5886-5890.
115. C. Shiea, Y. L. Huang, D. L. Liu, C. C. Chou, J. H. Chou, P. Y. Chen, J. Shiea and M. Z. Huang, *Rapid communications in mass spectrometry : RCM*, 2015, **29**, 163-170.
116. S. Gerbig, H. E. Brunn, B. Spengler and S. Schulz, *Anal Bioanal Chem*, 2015, **407**, 7379-7389.
117. M. Beneito-Cambra, P. Pérez-Ortega, A. Molina-Díaz and J. F. García-Reyes, *Anal. Methods*, 2015, **7**, 7345-7351.
118. Y. Ren, S. Chiang, W. Zhang, X. Wang, Z. Lin and Z. Ouyang, *Analytical and bioanalytical chemistry*, 2016, **408**, 1385-1390.
119. L. Li, T. C. Chen, Y. Ren, P. I. Hendricks, R. G. Cooks and Z. Ouyang, *Anal. Chem.*, 2014, **86**, 2909-2916.
120. S. Banerjee and S. Mazumdar, *Int. J. Anal. Chem*, 2012, **2012**.
121. M. Pelajic, G. Pecek, D. Mutavdzic Pavlovic and D. Vitali Cepo, *Food chemistry*, 2016, **200**, 98-106.
122. Y. Shen, Z. Li, Q. Ma, C. Wang, X. Chen, Q. Miao and C. Han, *J. Agric. Food Chem.*, 2016, **64**, 3901-3907.
123. R. Chen, V. M. Ravindra, A. L. Cohen, R. L. Jensen, K. L. Salzman, A. P. Prescott and H. Colman, *Neurosurgical focus*, 2015, **38**, E2.
124. R. M. Grant, J. R. Lama, P. L. Anderson, V. McMahan, A. Y. Liu, L. Vargas, P. Goicochea, M. Casapia, J. V. Guanira-Carranza, M. E. Ramirez-Cardich, O. Montoya-Herrera, T. Fernandez, V. G. Veloso, S. P. Buchbinder, S. Chariyalertsak, M. Schechter, L. G. Bekker, K. H. Mayer, E. G. Kallas, K. R. Amico, K. Mulligan, L. R. Bushman, R. J. Hance, C. Ganoza, P. Defechereux, B. Postle, F. R. Wang, J. J. McConnell, J. H. Zheng, J. Lee, J. F. Rooney, H. S. Jaffe, A. I. Martinez, D. N. Burns, D. V. Glidden and i. S. Team, *New England Journal of Medicine*, 2010, **363**, 2587-2599.
125. K. M. Berg and J. H. Arnsten, *Journal of acquired immune deficiency syndromes*, 2006, **43 Suppl 1**, S79-87.

126. J. R. Castillo-Mancilla, J. H. Zheng, J. E. Rower, A. Meditz, E. M. Gardner, J. Predhomme, C. Fernandez, J. Langness, J. J. Kiser, L. R. Bushman and P. L. Anderson, *AIDS research and human retroviruses*, 2013, **29**, 384-390.
127. J. H. Zheng, C. Rower, K. McAllister, J. Castillo-Mancilla, B. Klein, A. Meditz, L. A. Guida, J. J. Kiser, L. R. Bushman and P. L. Anderson, *Journal of pharmaceutical and biomedical analysis*, 2016, **122**, 16-20.
128. R. S. Jansen, H. Rosing, J. H. Schellens and J. H. Beijnen, *Mass spectrometry reviews*, 2011, **30**, 321-343.

VITA

Fan Pu was born in 1993 to Jian Pu and Haiying Liu in Zibo, Shandong, China. He was admitted to East China University of Science and Technology in 2010 where his major was composite materials and engineering. In his sophomore year, he joined Prof. Shiyou Guan's lab to perform research on energy storage materials for lithium ion batteries and supercapacitors. He was lucky enough to work together with a talented Ph.D. student Dr. Zhou Min and published 4 papers in one year. He came to US in 2013 and began his research on macroions at Dr. Tianbo Liu's lab at University of Akron. He met many more talented researchers in that lab and was convinced to pursue a Ph.D. degree. In 2015 he earned his M.Sc. degree in polymer science and moved to Purdue University. Interested in bringing research advancements to real world applications, he joined Prof. Zheng Ouyang's lab to work on applications development for miniature mass spectrometers. Later he had the great honor to have Prof. R. Graham Cooks jointly advise him on his research. The time he started his research on miniature mass spectrometer is unique, he had the chance to witness the fast growing of Purspec Technologies that Prof. Ouyang founded to commercialize Mini MS. His research work also made him travel between US and China frequently, which had given him unique perspectives of what is going on in this world. Before came to Purdue, he did not really have any hobby. During his free time at Purdue, he developed many hobbies that could accompany him for a lifetime. Of all the hobbies he developed, he devoted most of his passion to photography. He truly had a great time at Purdue.

PUBLICATIONS

1. **Pu, F.**; Zhang, W.P.; Han, C.; Ouyang, Z. Fast Quantitation of Pyrazole Fungicides in Wine by Ambient Ionization Mass Spectrometry. *Anal. Methods* **2017**, 9, 5058.
2. **Pu, F.**; Zhang, W.P.; Bateman, K.P.; Liu, Y.; Helmy, R.; Ouyang, Z. Using miniature MS system with automatic blood sampler for preclinical pharmacokinetics study. *Bioanalysis* **2017**, 9, 1633.
3. **Pu, F.**; Chiang, S.; Zhang, W.P.; Ouyang, Z. Direct sampling mass spectrometry for clinical analysis. *Analyst* **2019**, 144, 1034.
4. **Pu, F.**; Alfaro, C.M.; Pirro, V.; Xie Z.; Ouyang, Z.; Cooks, R.G. Rapid Determination of Isocitrate Dehydrogenase Mutation Status of Human Gliomas by Extraction Nanoelectrospray using a Miniature Mass Spectrometer. *Anal. Bioanal. Chem.* **2019**, 411, 1503.
5. Brown, H.M.; **Pu, F.**; Dey, M.; Miller, J.; Shah, M.V.; Shapiro, S.A.; Ouyang, Z.; Cohen-Gadol, A.A.; Cooks, R.G. Intraoperative Detection of IDH Mutations in Human Gliomas using a Miniature Mass Spectrometer. Submitted.
6. **Pu, F.**; Pandey, S.; Bushman, L.R.; Anderson, P.L.; Ouyang, Z.; Cooks, R.G. Direct quantitation of tenofovir diphosphate in human blood with mass spectrometry for adherence monitoring. In Preparation.